Dissertation zur Erlangung des Doktorgrades
der Fakultät für Chemie und Pharmazie
der Ludwig-Maximilians-Universität München

Towards elucidating the molecular modes of action of two types of antidepressant drugs using proteomics

von

Yu Yan

aus

Yangquan, Shanxi, China

2021

Erklärung

Diese Dissertation wurde im Sinne von § 7 der Promotionsordnung vom 28. November 2011 von Herrn Prof. Dr. Christoph Turck betreut.

Eidesstattliche Versicherung

Diese Dissertation wurde eigenständig und ohne unerlaubte Hilfe erarbeitet.

München, July 5, 2021

Yu Yan

Dissertation eingereicht am

1. Gutachterin / 1. Gutachter: Prof. Dr. Christoph Turck

2. Gutachterin / 2. Gutachter: PD Dietmar Martin

Mündliche Prüfung am

SUMMARY

Major depressive disorder (MDD) is a common mental disorder that globally millions of people of all ages suffer from. Despite the large-scale and long-term research that has been carried out, the etiology of MDD has not been fully elucidated. A number of antidepressants have been developed for pharmacotherapy of MDD with considerable efficacy in many patients. Nevertheless, currently used antidepressants are still limited by their undesirable side effects and other drawbacks, including insufficiency in the therapy of treatment-resistant depression (TRD). A comprehensive mechanistic study of the side effects of clinically used antidepressants and the development of novel antidepressants free from these limitations are of importance and in great demand.

In my PhD work, I have aimed at elucidating the molecular mechanism of action of two drugs that represent different classes of antidepressants. First, in order to investigate side effects caused by chronic treatment with fluoxetine, one of the most widely prescribed selective serotonin reuptake inhibitors (SSRIs), I subjected brain tissue from juvenile macaques that had been treated with fluoxetine for two years to proteome and phosphoproteome profiling using quantitative mass spectrometry. The proteomics data indicate that GABAergic synapse pathways are associated with the increased impulsivity observed in the juvenile macaques after chronic fluoxetine treatment.

In the second study, I attempted to unveil novel protein targets for the fast-acting antidepressant ketamine. Using several mass spectrometry-based strategies to uncover drug-protein interactions, I have identified novel binding partners of ketamine and its metabolites, which includes pyruvate kinase, and implicate the involvement of energy metabolism in ketamine’s mode of action.

In summary, this work reveals that GABAergic synapse pathways are affected by fluoxetine treatment in non-human primate macaques, and suggests new protein targets and associated mechanisms of ketamine as an antidepressant. My project data provide leads for pharmacology, and drug targets for the development of novel antidepressants with greater efficacy and fewer side effects.

Table of Contents

Abbreviations

Abbreviation	Full name
5-HT	5-hydroxytryptamine, serotonin
ABPP	Activity-based protein profiling
AMPAR	α-amino-3-hydroxy-5-methyl-4-isoxazolepropionic acid receptor
ANOVA	Analysis of variance
cAMP	Cyclic adenosine monophosphate
CC	Cingulate cortex
CNS	Central nervous system
DARTS	Drug affinity responsive target stability
DDA	Data-dependent acquisition
DEP	Differentially expressed proteins
DLPFC	Dorsolateral prefrontal cortex
DSM-5	Diagnostic and Statistical Manual of Mental Disorders 5th edition
ESI	Electrospray ionization
FDR	False discovery rate
GABA	Gamma-Aminobutyric acid
HNK	Hydroxynorketamine
HPA	Hypothalamic–pituitary–adrenal
HPLC	High performance liquid chromatography
ITDRF	Isothermal dose-response fingerprint
KET	ketamine
LC-MS/MS	Tandem mass spectrometry
m/z	Mass to charge ratio
MAOA	monoamine oxidase A
MDD	Major depressive disorder
MS	Mass spectrometry
MS1/MS2	Precursor ion/fragment ion
MS-CETSA	Mass spectrometry coupled cellular thermal shift assay
NHP	Nonhuman primate
NMDAR	N-methyl-D-aspartate receptor
PHOTON	Phosphoproteomics dissection using networks
PRM	Parallel Reaction Monitoring
PSM	Peptide-spectrum match
PTM	Posttranslational modification

Abbreviation	Full name
SDS-PAGE	Sodium dodecyl sulfate-polyacrylamide gel electrophoresis
SILAC	Stable isotope labeling with amino acids in cell culture
SIP	Solvent-induced protein precipitation
SSRI	Selective serotonin reuptake inhibitor
TAMPOR	Tunable Approach for Median Polish of Ratio -- Biological Abundance Batch Effect Removal
T_m	Melting temperature
TMT	Tandem mass tag
TPP	Thermal proteome profiling
TRD	Treatment resistant depression
WB	Western blot

1 Introduction

1.1 Major depressive disorder

Major depressive disorder (MDD) is a common mental disorder that more than 264 million people of all ages suffer from worldwide. Characterized by depressed mood, loss of interest, impaired cognitive function and additional symptoms including sleep and appetite disturbance[1], MDD is a leading cause of disability worldwide and a heavy burden to society[2]. The Diagnostic and Statistical Manual of Mental Disorders 5th edition (DSM-5) outlines the current diagnostic criteria and specifiers of MDD to diagnose depression[3]. Potential symptoms of MDD include depressed mood, markedly diminished interest, considerable weight loss (when not dieting), insomnia or hypersomnia, psychomotor agitation or retardation, fatigue or loss of energy, feelings of worthlessness or excessive or inappropriate guilt, diminished ability to think or concentrate, and recurrent thoughts about death. To be diagnosed as MDD, one must be experiencing five or more symptoms mentioned above during the same 2-week period almost every day along with the necessary symptom of depressed mood and/or diminished interest or pleasure.

Patients suffering from MDD usually have a persistent feeling of sadness and hopelessness. It is estimated that MDD occurs about twice as often in women as in men [4]. As one of the most common psychiatric disorders, MDD affects around 6% of the total adult population in the world every year[5]. Associated with other chronic diseases such as diabetes, heart disease and stroke, MDD leads to an extremely heavy burden, not only on patient health but to socioeconomic activity. A previous study revealed that up to 50% of the 800,000 suicides per year worldwide are related to MDD[6] and MDD patients are about 20-fold more likely to commit a suicide than healthy people[7]. According to another study in 2010, approximately 92 billion Euro per year is spent on treating MDD in Europe[8].

1.1.1 Etiology of MDD

Despite the large-scale and long-lasting research that has been carried out, the etiology of MDD has not been fully elucidated. As with many mental disorders, it is believed to be linked to a variety of factors, such as biological, genetic, environmental, and psychosocial factors. The genetic factors are estimated to contribute about 35% to MDD

[1], not via any single gene but via complex genetic features[9]. Early-onset, severe, and recurrent depression may have a higher heritability than other forms of depression[10]. Serotonin transporter-linked polymorphic region (5-HTTLPR) and monoamine oxidase A (MAOA), are genetic segments that influence serotonin and monoamine neurotransmitters. Environmental factors including sexual, physical or emotional abuse during childhood are also associated with the development of MDD. Both genetic and environmental studies of MDD are still far from complete. Therefore, a biological perspective of MDD would provide a better understanding of the etiology of MDD. Several hypotheses have been proposed to explicate it.

1.1.1.1 Monoamine-deficiency hypothesis

One of the leading pathophysiology mechanisms of MDD is the monoamine-deficiency hypothesis, referring to the alteration of levels of monoamine neurotransmitters including serotonin (5-hydroxytryptamine or 5-HT), norepinephrine (NE) and dopamine (DA) in the brain. The monoamine hypothesis postulates that reduced neurotransmitters in the synapse lead to mood alteration in MDD patients. Monoamines were first linked with MDD when lower monoamine levels were found in patients taking the anti-hypertensive drug reserpine, and some of these patients had MDD symptoms[11]. Subsequently more evidence supported the linkage, including the findings that antidepressants such as tricyclic antidepressants (TCAs), monoamine oxidase inhibitors (MAOIs), selective serotonin reuptake inhibitors (SSRIs) and serotonin-norepinephrine reuptake inhibitors (SNRIs) showed robust effects on monoamine neurotransmitters. Almost every compound that has been synthesized for the purpose of inhibiting 5-HT or NE reuptake has been proved to be a clinically effective antidepressant[9].

Monoamine oxidase (MAO) is a family of enzymes involved in the regulation of monoamine neurotransmitters including serotonin, norepinephrine and dopamine. MAO has two isoforms, MAOA and MAOB, differentiated from each other by substrate and inhibitor specificities. Both MAOA and MAOB are responsible for the metabolism of DA. Specifically, mainly expressed in the presynaptic terminals of catecholaminergic neurons, MAOA plays a major role in the metabolism of 5-HT and NE. The signaling pathways modulated by these monoamines are involved in mood, emotion, motor, perceptual and cognitive functions. It has been widely observed that abnormal MAOA activity is associated with psychiatric dysfunction, including MDD[11, 12]. MAOA expression and

function are determined by the interaction between genetic and environmental factors, and elevated MAOA density is the primary monoamine-lowering process in MDD[13, 14]. Significant alterations in the brain architecture and neuronal circuits associated with MAOA and 5-HT were also observed[15]. Therefore, MAOA has been proposed as a candidate of critical genes for MDD and the role of various polymorphisms of the MAOA gene has been investigated.

1.1.1.2 Dysregulation of the stress response systems

Another common pathological mechanism of MDD is the dysregulation of the stress response systems involving the hypothalamic–pituitary–adrenal (HPA) gland axis, through which stress is perceived[16]. The HPA response system, including cortisol and its central releasing factor corticotropin-releasing hormone (CRH), has been widely reported to be associated with depression[17, 18]. Cortisol levels in plasma, CRH levels in cerebrospinal fluid and CRH levels in limbic brain regions were found to be increased[19]. The link between the HPA response system and depression was also verified by the fact that the functional cortisol-suppression response was absent in around half of the patients with serious depression and the suppression could be rescued by antidepressants[20]. Some studies also confirmed the involvement of the HPA response system with an animal behavior test. For example, it was reported that mice with region-specific knockout of the glucocorticoid receptor, and consequently increased activity of the HPA axis, showed significantly increased immobility in the force swim test, which could be reversed by antidepressants[21]. In addition, brain-derived neurotrophic factor (BDNF), well-known for its associated with MDD, is affected by stress and cortisol, which also emphasizes the importance of the HPA response system in the occurrence and development of MDD[22, 23].

1.1.1.3 Other possible mechanisms

Other than the monoamine-deficiency hypothesis or HPA stress response system theory, many relevant mechanisms have been proposed in the pathophysiology of depression. Altered glutamatergic neurotransmission has also become a popular mechanism. Glutamate and glutamine levels in the prefrontal cortex were found to be lower in MDD patients, and ketamine, an NMDA antagonist has shown a rapid and long-lasting antidepressant effect[24, 25]. Reduced GABAergic neurotransmission was also linked to depression in many studies, where levels of gamma-Aminobutyric acid (GABA) in

plasma and cerebrospinal fluid (CSF), as well as GABA neuron immunoreactivity in dorsolateral prefrontal cortex (DLPFC) were found to be reduced, and GABA-modulating agents displayed antidepressant-like effects[26-29]. Inflammation-related theory originates from the fact that the immune system also plays a very important role in physiological stress-sensing pathways, and strongly interacts with the HPA axis and central nervous system (CNS). It has also been found that inflammatory markers are present at higher levels in depressed patients, such as IL-1β, IL-2, IL-6, TNF-α, CRP, and PGE2[30]. Other possible mechanisms include abnormal circadian rhythms[31], deficient neurosteroid synthesis[32], impaired endogenous opioid function[33], monoamine–acetylcholine imbalance[34], thyroxine abnormalities[35], dysfunction of specific brain structures and circuits[36] and others.

1.1.2 Management of MDD

There are currently two main therapy options for MDD, namely psychotherapy and pharmacotherapy. The use of psychotherapy, pharmacotherapy and a combination of both is often determined by depressive episodes in patients.

1.1.2.1 Psychotherapy

Frequently applied psychotherapies of MDD include cognitive–behavioral therapy (CBT), behavioral activation therapy, psychodynamic therapy, problem-solving therapy and interpersonal therapy. Although producing effects that are mostly equivalent to pharmacotherapy, psychotherapy is still limited by time constraints, lack of available services and cost.

1.1.2.2 Pharmacotherapy

The majority of currently available antidepressants are based on the monoamine hypothesis and increase the levels of one or more monoamines (5-HT, NE and DA), including first-generation antidepressants (monoamine oxidase inhibitors and tricyclic antidepressants) and second-generation antidepressants (selective serotonin reuptake inhibitors and serotonin-norepinephrine reuptake inhibitors). Many substances targeting glutamatergic systems, including ketamine, also display the potential to be novel antidepressants.

Monoamine oxidase inhibitors. MAO is an enzyme involved in the metabolisms of biogenic amines located in the presynaptic terminal. MAO inhibitors (MAOIs) inhibit the

activity of MAO and increase the concentration of monoamine neurotransmitters in the presynaptic terminal[37]. Iproniazid, a non-selective irreversible MAO inhibitor, is the first successful pharmacological treatment for depression; however, it was removed from the market due to safety concerns, including hypertensive crises. Reversible inhibitors of monoamine oxidase A (RIMAs, e.g. moclobemide and brofaromine) are safer than irreversible MAOIs. Currently, MAOIs are considered as the second-line antidepressant due to tolerability and safety issues.

Tricyclic antidepressants. The classification of tricyclic antidepressants (TCAs) was based on the three-benzene-ring molecular core. TCAs inhibit presynaptic NE reuptake transporters and 5-HT reuptake transporters, exerting an antidepressant effect by increasing levels of NE and 5-HT in the synaptic cleft. TCAs also block postsynaptic adrenergic α1, α2 receptors, muscarinic receptors and postsynaptic histamine H1 receptors, which is the main cause of side effects such as dizziness and memory impairments. Similar to MAOIs, TCAs are also clinically second-line antidepressant.

Selective serotonin reuptake inhibitors. Since the crucial role of serotonin was discovered, selective serotonin reuptake inhibitors (SSRIs) have been developed for the purpose of increasing serotonin concentrations in the synaptic cleft and stimulating postsynaptic serotonin receptors. SSRIs have 20-1500 times higher selectivity for inhibiting 5-HT over NE, and minimal binding affinity for postsynaptic receptors including postsynaptic 5-HT receptors[37]. Fluoxetine was the first SSRI approved and marketed in the US, and many other SSRIs, including citalopram and paroxetine, are available on the market. Although associated with side effect such as nausea, insomnia, and sexual dysfunction, SSRIs are used as first-line medications because their safety and tolerability may be preferable to patients and clinicians[38].

Serotonin-norepinephrine reuptake inhibitors. Unlike SSRIs acting only upon 5-HT, serotonin-norepinephrine reuptake inhibitors (SNRIs) inhibit the reuptake of both 5-HT and NE at their transporters. Venlafaxine was the first SNRI drug, developed in 1993. SNRIs share many side effects with SSRIs, although to varying degrees.

Novel antidepressants. With the development of the glutamatergic systems-related theory of MDD, many noncompetitive N-methyl-D-aspartate receptor (NMDA receptor) antagonists, low trapping NMDA receptor channel blockers, selective NMDA receptor antagonists and excitatory amino acid transporter 2 (EAAT2) enhancers have been

proposed as novel antidepressants due to their potential antidepressant effects[37]. Among them, ketamine has been widely studied due to its rapid and sustained antidepressant effect. However, the mechanisms involved in the antidepressant effects of these potential novel antidepressants are still not well established.

1.1.2.3 Combined treatment

Meta-analyses indicate that combining pharmacotherapy and CBT leads to better short-term outcomes, with small to medium effects, compared to either treatment alone. A similar pattern is observed for combining any psychotherapy and pharmacotherapy, although the evidence base is not large enough to examine specific psychotherapy treatments other than CBT[38].

1.1.3 Existing challenges in the therapy of MDD

One of the main challenges in the therapy of MDD is treatment resistance. While clinically used antidepressants have shown significant efficacy with many MDD patients, sequenced treatment alternatives to relieve depression (STAR*D) trials demonstrated that approximately 30% of patients meet the criteria for being considered as suffering from treatment resistant depression (TRD)[39]. Statistics revealed that TRD patients have higher normal medical costs and are more likely to be hospitalized, resulting in a 6-fold increase in overall medical costs compared to other MDD patients[40]. TRD exacerbates the symptoms of associated and comorbid physical diseases (e.g. myocardial infarction[41] and diabetes mellitus[42]), further increasing impairment in social functioning and suicidality.

In addition, current antidepressant drugs also have limitations, including modest efficacy, unclear tolerability, delayed onset of therapeutic response, discontinuation symptoms, non-compliance with medication, as well as undesirable side effects[43], which is a hazard for MDD patients. Potential health risks caused by antidepressants include serotonin syndrome, hyponatremia, diabetes and suicidal thoughts[44]. Other common side effects may also occur depending on the drug used, such as feeling agitated, shaky or anxious, feeling and being sick, indigestion and stomach aches, diarrhea or constipation, loss of appetite, dizziness, not sleeping well (insomnia), or feeling very sleepy, headaches, slight blurring of vision, weight gain, heart rhythm problems, etc.[45].

Therapy of MDD still needs to be optimized to tackle these challenges. On the one hand,

not only the combination of current psychotherapy and pharmacotherapy, but also treatments focused on comorbid physical diseases and rehabilitation aimed at restoring social functioning should be more strongly considered. At the same time, unraveling the unknown or obscure mechanisms of both effects and side effects of antidepressants and the development of novel antidepressants that benefit more MDD patients are urgently needed.

1.2 Mass spectrometry-based proteomics

1.2.1 Development of proteomics

Proteomics technologies have great potential for disease diagnosis, prognosis, evaluation of disease development, as well as treatment and drug research and development. The term "proteomics" was created by combining "protein" and "genomics" in 1990s[46]. Being downstream of the genome, proteomics covers, but is not limited to the analysis of protein expression, function, turnover, subcellular location, protein sequencing, protein-protein interactions (PPIs), protein-metabolite interactions, and known/novel post translational modifications (PTMs) [47], which vary within the whole organism and between individual cells form the same organ. Proteomics enables both the identification and quantification of peptides or proteins, including those comprising certain PTMs of interest, providing direct evidence for studies of subsequent biological events at the protein level. Due to the high degree of complexity of a proteome, compared to a genome, resulting from various amino acid compositions, structures, properties, localizations and dynamic range of quantities, the complete investigation of a proteome is very challenging.

The conventional biochemical techniques for protein research make use of ion exchange chromatography (IEC)[48], size exclusion chromatography (SEC)[49] and affinity chromatography (AC)[50] for protein purification, and antibody-based enzyme-linked immunosorbent assay (ELISA) and Western blotting (WB) for protein detection[51]. These techniques are highly dependent on the number of proteins being analyzed, thus incapable of identifying or quantifying proteins on a large scale. Sodium dodecyl sulfate-polyacrylamide gel electrophoresis (SDS-PAGE), two-dimensional gel electrophoresis (2-DE)[52] and two-dimensional differential gel electrophoresis (2D-DIGE)[53] are also commonly used in some proteomic studies, although they have low protein resolution and incomplete separation. Protein microarrays or chips are of a more high throughput nature,

but it is difficult to detect proteins without *in vitro* biological activity[54].

1.2.2 Proteomics with mass spectrometry

The development of technological advances in new mass spectrometers has led to mass spectrometry (MS) becoming the most popular method of choice for large scale proteomic analysis[55]. The mass spectrometer, usually consisting of an ion source, a mass analyzer and a detector, is widely used to measure the mass to charge ratio (m/z) and further determine the molecular weight of the analytes[55]. The most commonly used ionization techniques are Electrospray ionization (ESI) and matrix-assisted laser desorption/ionization (MALDI). Distinguished by their sensitivity, mass accuracy and resolution, different types of analyzer are available, including ion trap (IT), time-of-flight (TOF), quadrupole (Q), Fourier transform ion cyclotron resonance (FT-ICR) and Orbitrap. Hybrid instruments have been developed by combining different analyzers in order to improve the fragmentation efficiency and mass accuracy. High performance liquid chromatography (HPLC)-coupled tandem mass spectrometry (LC-MS/MS) system often prefers ESI as the ion source and triple quadrupole (QQQ)-Orbitrap as the hybrid analyzer, making it possible to separate, fragments and analyze complex proteomic mixtures at both precursor ion (MS1) and fragment ion (MS2) level.

Most proteomic studies undergo “bottom-up” or “shotgun” proteomics processes[56], where all peptides released by proteolysis from protein mixtures (instead of intact proteins) are subjected to LC-MS/MS analysis. In contrast to “top-down” proteomics that directly analyzes intact proteins, “shotgun” proteomics provides indirect information about proteins through the relevant peptides. A typical discovery-based “shotgun” proteomic experiment usually includes protein extraction, digestion, peptide separation and MS spectra generation with LC-MS/MS, peptide identification via database searches against theoretical sequences of protein mixtures, and assignment of peptide sequences to protein sequences. Despite the advantages in PTM analysis and protein isoform identification[57], large scale “top-down” proteomics is still limited by protein separation, ionization and fragmentation. Therefore, “shotgun” proteomics is still being widely used for various proteomic research purposes, such as protein identification, quantification, modifications, PPIs and protein-drug interactions. Traditional shotgun proteomics uses data-dependent acquisition (DDA) for most MS analysis, where the mass spectrometer scans precursor ions and selects the Top N most abundant ions for fragmentation[47]. To overcome the

drawbacks of the DDA mode, including low dynamic ranges of detection and loss of low abundance peptides, data-independent acquisition (DIA) was developed and has been increasingly used. Under DIA mode, data are acquired based on the sequential isolation window and fragmentation of the specific precursor without selection of precursor ions, and thus is capable of identifying low abundance peptides[58].

1.2.3 MS-based quantitative proteomics

MS-based quantitative proteomics more frequently uses relative quantification compared to absolute quantification (e.g. AQUA[59]). In typical shotgun (bottom-up) proteomics, where relative quantification is applied, quantitative data are obtained by either label-free or stable isotope labeling approaches. The isotope labeling approach allows the mixing of multiple samples and thus reduces variability and measurement time. MS1-based and MS2-based methods are two approaches used for both label-free and labeling quantification. MS1-based methods calculate the abundance of peptide precursor ions in MS spectra and MS2-based methods make use of quantities of reporter ions or fragment ions in MS/MS spectra.

1.2.3.1 Label-free quantification

Although suffering from lower quantification accuracy and reproducibility, label-free quantification is still the most frequently used quantification approach due to its simple sample preparation, low cost and flexibility of sample size. Label-free quantification is usually achieved by calculating spectral counts (the frequency of peptide identification for a particular protein)[60] or intensity[61]. The intensity-based approach calculates peptide abundance as an integrated area of peptide peak in the extracted ion chromatogram (XIC) using dedicated tools. In contrast to normal MS1-based label-free quantification, quantification with the DIA workflow uses the intensities of the fragment ions (MS2-based) and leads to an improvement in identified protein numbers and quantification accuracy.

1.2.3.2 Labeling strategy

In an attempt to reduce the technical variability at different stages in sample preparation and measurement and achieve more accurate quantification, isotopic labeling strategies were developed, including chemical isotopic labeling, metabolic isotopic labeling and isobaric tagging. The first chemical labeling methods used for MS-based quantitative

proteomics was the isotope-coded affinity tag (ICAT)[62]. Other commonly used chemical labeling strategies include dimethyl labeling, where dimethyl labels are introduced onto the peptide N-terminus and lysine (K) residues[63] and ^{18}O labeling where the C-terminal carboxyl group is labeled with ^{18}O in the presence of ^{18}O water[64]. For metabolic isotopic labeling, the isotopic atoms are incorporated into the whole proteome through protein synthesis during protein turnover and cell multiplication, such as ^{15}N labeling and stable isotope labeling with amino acids in cell culture (SILAC)[65]. All above-mentioned labeling approaches belong to MS1-based quantification. In contrast, isobaric tagging is an MS2-based labeling strategy. The most widely used isobaric tagging approaches are isobaric tags for relative and absolute quantification (iTRAQ)[66] and tandem mass tags (TMT).

1.2.3.3 Quantification strategy used in the present study

Tandem mass tags (TMT). TMT tags are a series of multiplex tags that have the same total molecular weight, comprising a unique mass reporter, a cleavable linker as a mass balancer, and an amine-reactive group (Figure 1.1). Peptides from different biological samples are labeled with different tags in a set via the chemical reaction between the amine-reactive group of the TMT reagent and N-termini and lysine (K) residues of peptides. After mixing, TMT-labeled peptides are co-eluted and co-isolated during the LC-MS/MS analysis. During the co-fragmentation, the linker is fragmented and the reporter ion is released. The intensity of reporter ions, which represents the relative abundance of the original peptides, is then used for relative quantification. Currently available TMT reagents enable the concurrent quantification of 6 (TMT 6-plex), 10 (TMT 10-plex), 11 (TMT 11-plex), or 16 (TMTpro 16-plex) samples in one LC-MS/MS run, significantly increasing the sample throughput, saving instrument measurement time and reducing variability.

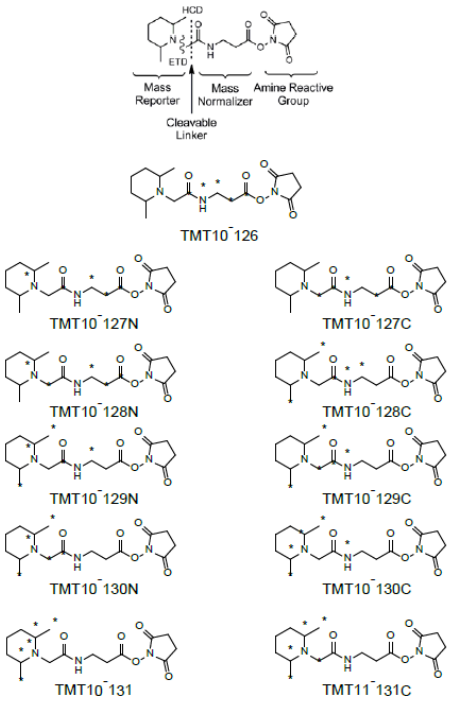

Figure 1.1 Chemical structures of the Thermo Scientific 10 plex TMT Label Reagents. TMT tags have the same total molecular weight but distinct reporter ions after fragmentation in mass spectrometers.

Stable isotope labeling with amino acids in cell culture (SILAC). SILAC labels selected amino acids (usually lysine (K) and/or arginine (R)) in cell culture[65]. Cells are differentially labeled by growing them in medium incorporating normal K/R (K-0 and R-0) or middle labeled K/R (K-4 and R-6) or heavy labeled K/R (K-8 and R-10). Three labeled proteomes are mixed before tryptic digestion, where trypsin cleaves the proteins at K and R residues resulting in tryptic peptides. As a consequence, theoretically all peptides should have labeled C-termini and increased mass. Although initially designed for cell culture, the use of SILAC has already been expanded to the mouse by feeding mice with labeled food. SILAC enables the measurement of a maximum of 3 samples in the same LC-MS/MS run, and more importantly, enables the preparation of 3 samples concurrently from the first step of the whole workflow, further reducing the experimental variability caused by complicated sample preparation procedures. Additionally, the mass change of tryptic peptides is predictable, simplifying the data interpretation process.

1.2.4 Mass spectrometry-based biomarker discovery and MDD

1.2.4.1 MS-based biomarker discovery

A biomarker is a measurable indicator of a specific biological state, particularly one relevant to the risk of contracting or already having a disease, or the stage of the

disease[67]. Biomarkers improve diagnosis, guide molecularly targeted therapy, and monitor activity and therapeutic responses across a wide spectrum of diseases. Therefore, the discovery of biomarkers has been one of the most important and challenging studies in proteomic research. A plethora of technologies and methodologies have been applied to studying and discovering biomarkers, among which mass spectrometry-based proteomics coupled to bioinformatics analysis has been promising and increasingly popular for discovering protein biomarkers. Compared to conventional platforms, mass spectrometry is a powerful and versatile tool with the ability to analyze disease-related candidate biomarkers on a large scale, both qualitatively and quantitatively[68] and with exquisite accuracy and sensitivity.

1.2.4.2 Protein biomarkers and MDD

Extraordinary efforts have been made to identify biomarkers as potential tools for improving prevention, diagnosis, drug response and drug development in MDD. To date, the lack of biomarkers to identify target populations greatly limits the promise of precision medicine for MDD[69]. It was reported that a reduction in acetyl-L-carnitine (LAC) concentrations was associated with abnormal hippocampal glutamatergic function and plasticity. Such alterations suggested that the degree of LAC deficiency was directly proportional to the severity, the age of MDD onset, and the clinical history of treatment-resistant depression (TRD). These findings suggest that LAC may be useful as a diagnostic and prognosis biomarker for MDD. However, no protein biomarker is officially approved for MDD. Thus, prospective studies investigating biomarkers before the onset or relapse/recurrence of MDD are required[70].

2 Investigation of molecular mechanisms involved in the chronic fluoxetine treatment response in juvenile rhesus monkeys by quantitative proteome and phosphoproteome profiling

2.1 Background

2.1.1 Fluoxetine

Fluoxetine (3-(p-trifluoromethylphenoxy)-N-methyl-3-phenylpropylamine HCl; Lilly (LY) 110140, Figure 2.1), with the pharmaceutical tradenames Prozac and Sarafem, is a selective serotonin reuptake inhibitor (SSRI) and the effect of fluoxetine on the metabolism of 5-HT in the rat brain was shown in 1974[71, 72]. As an early member of SSRI antidepressants, the investigational new drug application of fluoxetine was submitted to the U.S. Food and Drug Administration (FDA) in 1977, and finally approved on December 29, 1987. Due to the sustained effectiveness, low side-effect profile, improved risk–benefit ratio, lack of a requirement for dose titration, once-a-day dosing and overdose safety, fluoxetine has been widely prescribed via oral administration for the treatment of MDD, obsessive–compulsive disorder (OCD), bulimia nervosa, panic disorder, and premenstrual dysphoric disorder since its approval[73]. Most importantly, of all the antidepressants, only fluoxetine (Prozac™) has been approved by the FDA to treat pediatric depression in adolescents and children 8 years of age and older[74].

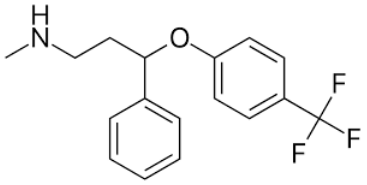

Figure 2.1 Molecular structure of 3-(p-trifluoromethylphenoxy)-N-methyl-3-phenylpropylamine HCl, known as fluoxetine (or Prozac™).

The discovery of fluoxetine was a landmark for illuminating and treating MDD. Firstly, fluoxetine has been widely studied for its effects on 5-HT, which confirmed the crucial role of 5-HT in CNS. The high efficacy and sensitivity of fluoxetine for the 5-HT system has provided the means to clarify the pharmacology of 5-HT in animal models and humans in numerous studies. Secondly, introduction of fluoxetine, the first SSRI to be marketed in the US, has had a profound influence on pharmacotherapy for MDD. It is estimated by Eli Lilly and Company that by the year 2002, more than 40 million patients

had received fluoxetine. The widespread use of fluoxetine and other successful antidepressants has saved numerous patients from MDD torment and made MDD a treatable disease with a response rate of around 60-70%[75].

2.1.2 Major depressive disorders in children

MDD also frequently and recurrently occurs in children and adolescents. In 2003, statistics revealed that around 1-2% of children between 6-12 years old, 2-5% of adolescents between 13-18 years old [76, 77] and 14-25% of young people suffer from MDD before adulthood[78, 79]. With the increasing prevalence of depression, the percentage has risen to 5% in 12-year-olds, 13% in 14-year-olds and 17% in 17-year-olds[80]. Despite the similarity between depression in children and that in adults, there are still some distinct symptoms. Common symptoms of depression in children include fatigue, feeling depressed, sad, irritated, upset, worthlessness or frustrated; loss of interest or pleasure in hobbies or activities, staying away from friends and family, sleep problems, inability to think or concentrate on making decisions, loss of appetite or changes in eating habits, thoughts of death or suicide, and so on.

MDD in often believed to be the result of interactions between environmental and genetic factors. Evidence has shown that children with relatives suffering from depression had a higher risk for depression, indicating that heritability plays a role in children's depression[81-83]. Environmental factors found to be associated with depression in children include perinatal insults, motor skill deficits, and caretaker instability[84]. Considerably fewer studies on depression in children have been reported than those in adults due to greater unavailability of study participants and less funding[85]. As a consequence, fewer studies have led to an incomplete understanding of mechanisms behind depression in children and incomplete assessment of both efficacy and side effects of therapy.

2.1.3 Therapeutic response and side effect of fluoxetine in children

Although tricyclic antidepressants, SSRIs and SNRIs have shown great efficacy in treating depression in adults, there has been little evidence for their significant effect in children due to the limited sample size. Lower efficacy of tricyclic antidepressants has been pointed out in treatment of depression in youths than that in adults. Fluoxetine (Prozac), however, proved to be effective in the pharmacological treatment of depression

in children and adolescents[74, 86, 87]. Other SSRIs failed to present data as reproducible as fluoxetine in therapy. Fluoxetine and escitalopram (Lexapro) are the only two medications approved by the FDA, and only fluoxetine is approved for patients 8 years and older. The therapeutic mode of action of fluoxetine is based on the monoamine deficiency hypothesis, which attributes the cause of depression to a lack of monoamine, such as serotonin or norepinephrine in the synaptic cleft. As an SSRI, fluoxetine selectively inhibits serotonin reuptake into presynaptic serotonin neurons by blocking the reuptake transporter protein located in the presynaptic terminal[88].

There are many common side effects after antidepressant treatment for adults, most of which are also observed in youths. Most importantly, much attention has been drawn to the potential risk of SSRI treatment-emergent suicidality in adolescents, the most well-known side effect of fluoxetine in children. In 2003, the British Medicines and Healthcare Products Regulatory Agency (MHRA) banned the use of several drugs that incorporated SSRIs. In 2004, the U.S. Food and Drug Administration (FDA) stated that all antidepressant drugs must include a warning about dangers when they are sold to children, adolescents and youths.

The first study to investigate the global association between a genetic marker and treatment-emergent suicidal ideation was reported in 2007[89], where it was discovered that some genetic markers in patients taking the drug were associated with a significant increase in suicidality. Since then, researchers have been working on exploring the overall link between antidepressant drugs and suicidality. It was reported that although no suicides occurred in trials, suicidal thoughts and behaviors were significantly increased in children and adolescents taking antidepressants (4%) compared to those taking a placebo (2%)[90].

Given the demonstrated efficacy, drug ineffectiveness is insufficient to explain the association between fluoxetine treatment and suicidality. Several studies on research into the neurobiological mechanism reported an association between fluoxetine treatment and suicidal ideation and behavior in children and youths[91]. A serotonin deficit was proposed to be involved in suicidality in a $5HT_{1A}$/$5HT_2$-dependent manner, thus acute changes in brain serotonin receptor sensitivity might explain the increased suicidality after fluoxetine treatment[92]. Pro-inflammatory cytokines have also been linked with depression and suicidality[93]. It was also reported that susceptibility to SSRI-induced

behavioral side effects may be a function of brain maturation, and varies according to the age of the patient, which could explain more suicidal ideation in children[94]. Several possible mechanisms related to brain-derived neurotropic factor (BDNF) were also reported, including acute reduction of BDNF by fluoxetine treatment, dose-dependent effects of fluoxetine on BDNF levels, and age-related effects of antidepressants on BDNF expression[95]. An increase in IL-6 levels during treatment was found to be a risk factor for the emergence of fluoxetine-associated suicidality[96]. A neuroinflammatory process was suggested to be more pronounced in children under fluoxetine treatment[97]. In contrast to the precise therapeutic mechanism, the exact mechanism whereby fluoxetine increases suicidal ideation and suicidal behavior is not definitely known and needs to be further elucidated.

2.1.4 Impulsivity: a behavioral assessment of suicidality

Impulsivity, broadly defined as behaviors with little or no forethought, reflection, or consideration of the consequences[98], has been widely investigated as a behavioral assessment of suicidality due to the association with etiology and prediction of suicide. The American Association of Suicidology has defined impulsivity as both a chronic and an acute suicide risk factor[99]. It was suggested in a study that impulsivity might act as a more significant indicator of a suicide attempt[100]. Previous studies have noted that a considerable proportion of suicidal behavior is impulsive[101]. Some studies have proposed impulsive behavior as the critical association between family history of suicide and new attempts by probands especially in youths[102, 103]. Although the clear mechanism of relationship between impulsivity and suicide behavior has not been well established[102], both clinical experience and research highlight the involvement of impulsivity in the elucidation of suicidality[104].

Although the precise neurobiological mechanisms underlying the association between impulsivity and MDD are not fully uncovered, the dorsolateral prefrontal cortex (DLPFC) and cingulate cortex (CC) have been widely implicated in MDD and impulsivity[105]. DLPFC is known for its involvement in executive functions and CC is responsible for emotion formation and processing, learning, and memory. Continuous theta burst stimulation in the DLPFC has been found to modulate cortical excitability and thus affects impulsivity in humans[106]. It was also observed that differences in the cortical thickness of DLPFC were predictive of differences in impulsivity and strategic behavior,

irrespective of age[107]. CC is a key brain area for impulse control in that it was found to be essential for the willed control of action[108]. One of the most consistent findings from functional neuroimaging studies is that the CC is involved in error monitoring and detection of conflict among competing responses[109, 110]. Therefore, studying DLPFC and CC brain regions is of importance to uncover the mechanisms underlying increased impulsivity or suicidality.

2.1.5 Nonhuman primate models for MDD

Although hypotheses about interpreting the genetic, neurophysiologic, biochemical and neuroanatomical mechanism of MDD widely exist, experimental investigations in the human population have been arduous due to many confounding factors[111]. At first, many MDD patients also suffer from other mental illnesses or psychopathological disorders, which complicates the process of understanding the mechanism of MDD. In addition, genetic and physiological variation in humans are immeasurable, inducing more random factors in experiments. Moreover, medication, as well as economic and nutritional status also differs from person to person. All these existing problems have been driving researchers to set up various animal models to study MDD.

To serve as an appropriate animal model to study psychopathological disorders, the system should possess many of the traits of the modeled human disease. For instance, the animal model should be activated by the same or similar risk factors or chemical reagents as in the natural condition relevant for the human disease, and exhibit significant pathological changes that can be measured with different assays, including behavior tests or physiological experiments. In addition, the action mode of corresponding therapy for these pathological changes should be comparable to clinical treatments. However, the majority of animal models fail to fulfill all of these requirements. Researches usually apply the animal model when there is enough evidence to prove linkage between typical symptoms of the disease to specific neurobiological or physiologic mechanisms.

The nonhuman primate (NHP) has become one of the best models for translational research of MDD. Firstly, compared to other models such as rodents, NHPs' brain structure resembles a human's and thus offers direct and reliable evidence biochemically or physiologically. Secondly, the experimentally used animal models usually have a clear genetic background and are under controlled environmental conditions, reducing systematic variation. Thirdly, despite the fact that mood or thought-based symptomology

cannot be measured, some symptoms such as psychomotor slowing, and appetitive and sleep disturbances can be directly observed in "depressed" NHPs[112]. Other behaviors including collapsed posture, social withdrawal and impulsivity are also readable from different behavior tests. Lastly, NHPs behave so similarly to humans; they also live in complex social groups and benefit from nutrition supply and phycological development, which makes NHPs mimic and reproduce the behavior of MDD patients very well.

2.1.6 Chronic fluoxetine treatment of nonhuman primates

The tissue specimens I used for my project were from macaques that had been chronically treated with fluoxetine for two years at the University of California, Davis Primate Facility. Several behavioral and biomarker studies had been carried out with the macaques which are elaborated in the following sections[113-116]. Following study completion, brain tissue sections from the macaques were made available to our laboratory and used for my PhD project.

2.1.6.1 Animals

Male rhesus monkeys (Macaca mulatta) at 1 year of age were selected from the colony at the California National Primate Research Center (CNPRC) to form the cohort balanced for age, health history, infant stress responsiveness and genetic polymorphism of monoamine oxidase A (MAOA). These animals were kept in cages and allowed to socialize in pairs. All monkeys were subjected to identical and standardized feeding according to CNPRC protocols. Twelve hours of light and two meals were supplied every day. Cages were cleaned every day and disinfected cages were renewed every two weeks. There were play objects in the cage, mirrors outside the cage and novel food was provided regularly. Animal health was evaluated every day[114].

Subsequently, fluoxetine dosing and behavioral tests were gradually carried out on monkeys around 1 year of age. At the end of the first year of dosing, the monkeys were evaluated by an impulsivity test (reward delay) to assess the side effects of fluoxetine treatment on behavioral levels. Blood and cerebrospinal fluid (CSF) samples were collected for metabonomic analysis. Behavior tests were conducted again after fluoxetine dosing for another year at around 3 years of age. Monkeys lived for 2 years from the age 1-3 and morphometrics was performed at 4 years of age. Monkeys were then sacrificed and brain tissues were collected for proteomic analysis in the present project.

2.1.6.2 Identification of biomarkers of responses to fluoxetine in blood and CSF

Metabolite profiling of plasma and CSF was introduced to assess the long-term effects of fluoxetine dosing in raised juvenile monkeys[114]. The impulsivity of the monkeys was measured as a reward delay behavior and was found to be increased after fluoxetine treatment. Biomarkers for fluoxetine dosing response and biomarkers that correlate with impulsivity were identified separately in plasma and CSF. Two metabolites, 5-aminovaleric acid lactam and hypoxanthine, were significantly changed in both plasma and CSF. 5-aminovaleric acid, a gamma-aminobutyric acid (GABA) homolog known to be a weak GABA agonist, further implied the involvement of regulation of the glutamatergic system by fluoxetine.

2.1.6.3 Metabolic pathway alterations in peripheral fibroblast

Environmental influences are usually confounding in metabolomic analyses of blood and CSF, thus peripheral fibroblasts, a less invasive puncture, were used to analyze pathway alterations by metabolic profiling[115]. Fifteen metabolites were found to be regulated under the fluoxetine treatment, of which 11 metabolites displayed an interaction effect between the MAOA genotype and fluoxetine treatment. Seventeen metabolites were associated with impulsivity without overlap with treatment-effect metabolites. Purine and pyrimidine metabolism, recognized as the most affected pathway, also correlated with impulsive behavior.

2.1.6.4 Regulation of emotional response under fluoxetine treatment in interaction with MAOA

Genetic polymorphisms of MAOA are also considered to be associated with regulation of emotional response in both adolescents and adults. Therefore, high and low transcription-variable number of tandem repeat (VNTR) polymorphisms of MAOA gene were designed as an independent variable to study the emotional response of rhesus monkeys after fluoxetine treatment. Behavioral responses were scored during 30-second exposures to pictures differing in affective content. The results confirmed the effect of fluoxetine in reducing emotional response and revealed that this effect appeared only in monkeys with low MAOA polymorphism, suggesting that MAOA is an important candidate gene for studies of children's response to fluoxetine treatment[116].

2.2 Research aims

The major goal of the project was to elucidate molecular mechanisms involved in the response of juvenile rhesus monkeys towards chronic fluoxetine treatment at the proteome level with LC-MS/MS-based methods.

(1) Establish a complete quantitative proteomics and phosphoproteomics pipeline and deep profiling of the proteome and phosphoproteome of the DLPFC and CC of juvenile rhesus monkeys chronically treated with fluoxetine.

(2) Identify altered protein levels and protein phosphorylation events in the DLPFC and CC of juvenile rhesus monkeys subjected to chronic fluoxetine administration.

(3) Correlate multi-omics data and animal behavior data and identify protein biosignatures associated with animal impulsivity.

(4) Identify cellular signaling pathways altered by fluoxetine treatment associated with side effects of chronic fluoxetine treatment in juvenile rhesus monkeys.

2.3 Material and methods

2.3.1 Reagents and equipment

Table 2.1 Chemicals used in the present study

Reagent	Company
2-Chloroacetamide (CAM)	Sigma
4-(2-hydroxyethyl)-1-piperazineethanesulfonic acid (HEPES)	Sigma
Acetonitile (ACN)	Merck
Ammonia 32%	VWR
BCA protein assay	Thermo Fisher
Deoxycholic acid sodium salt	Carl Roth
Formic acid (FA)	Thermo Fisher
Hydroxylamine 50%	Thermo Fisher
Isopropanol	Merck
Potassium dihydrogen phosphate	Sigma
Potassium hydroxide (KOH)	Sigma
rLys-C (mass spec grade)	Promega
Sodium chloride (NaCl)	Sigma
Titansphere 5µm	GL Sciences Inc
TMT10plex Isobaric Label Reagent Set	Thermo Fisher
Trifluoroacetic acid (TFA)	Sigma
Tris (2-carboxyethyl) phosphine (TCEP)	Sigma
Trypsin	Serva
Water (mass spec grade)	Honeywell
Zirconium Oxide Beads	Biostep GmbH

Table 2.2 Consumables used in the present study

Consumable	Company
96 well cell culture plate	Greiner bio-one
Capillary analytical column	New Objective Inc
C18 precolumn	Thermo Fisher
C18 ReproSil particles 1.9µm	Dr. Maisch GmbH
Empore C8	3M
epT.I.P.S. Reloads	Eppendorf

Pierce C18 tips	Thermo Fisher
Pierce™ High pH Reversed-Phase Peptide Fractionation Kit	Thermo Fisher
Safe-Lock Tubes	Eppendorf

Table 2.3 Equipment used in the present study

Equipment	**Company**
Bullet Blender Storm	Next Advance
Centrifuge 5804 R	Eppendorf
Centrifuge tubes 15/50 mL	Fisher Scientific
Galaxy mini centrifuge	VWR
Mechanical Pipette	Eppendorf
Q-Exactive-Plus mass spectrometer	Thermo Fisher
Reax top Shakers & Mixers	Heidolph
SpeedVac Plus SC210A	SAVANT Instruments Inc
Thermomixer 5436	Eppendorf
Ultimate 3000 UHPLC system	Thermo Fisher

Table 2.4 Software and tools used in the present study

Software/Tools	**Source**
BatchServer	https://lifeinfo.shinyapps.io/batchserver/
Cytoscape 3.8.2	https://cytoscape.org/
Gene Ontology Resource	http://geneontology.org/
Kyoto Encyclopedia of Genes and Genomes	https://www.genome.jp/kegg/
Perseus 1.6.14.10	https://maxquant.net/perseus/
PhosphoSite Plus	https://www.phosphosite.org
Proteome Discoverer 2.4	Thermo Fisher
R 64-bit version 4.0.4	https://www.r-project.org/
Reactome	https://reactome.org/
STRING database	https://string-db.org/
UniprotKB	https://www.uniprot.org/
WikiPathways	https://www.wikipathways.org/
Xcalibur v4.2.47	Thermo Fisher

2.3.2 Study design

Twenty-four juvenile male rhesus monkeys with high- and low-activity MAOA polymorphism genotypes (n = 12/MAOA genotype) were randomized within groups to receive either fluoxetine or an equivalent volume of vehicle control (n= 6 per treatment group) at 1 year of age, as shown in Figure 2.2. After 1 year of dosing, the monkeys' behavior was evaluated by impulsivity tests to assess the effect of fluoxetine. Blood and cerebrospinal fluid (CSF) samples were collected for metabolomic analysis. Daily fluoxetine dosing lasted for 2 years and ended with additional behavioral tests. After brain morphometrics at 4 year of age, monkeys were sacrificed and tissue punches from different brain regions were collected and used for proteomics and RNA-seq analysis.

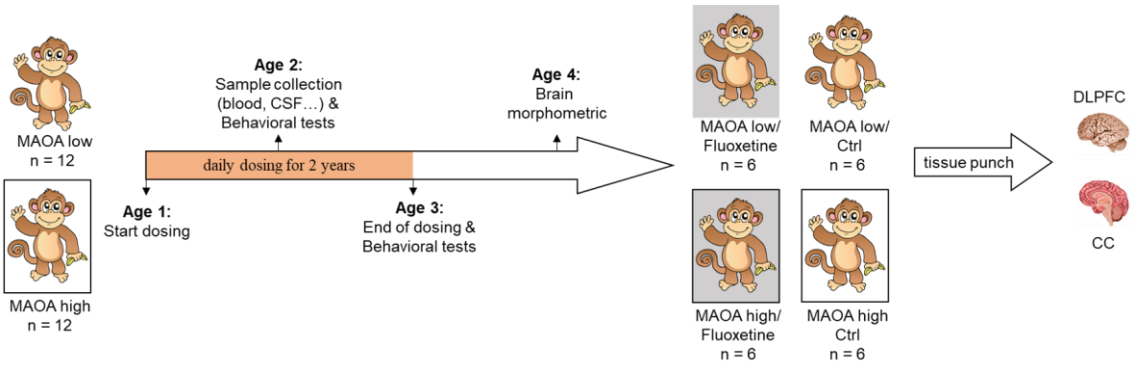

Figure 2.2 Timetable of the study design. 24 juvenile male rhesus monkeys were administrated with flavored syrup (vehicle control) or fluoxetine over 2 years and subjected to different analyses. DLPFC and CC tissue punches were used in the present study.

Tissue punches (Figure 2.2) were weighted and then homogenized in lysis buffer to extract proteins. The concentration of extracted proteins was determined by a BCA assay before the proteins were digested by trypsin. Phosphopeptide enrichment was performed for phosphoproteome profiling. Subsequently, peptides or enriched phosphopeptides were subjected to TMT labeling, yielding sample-specific TMT-labeled peptides. A pool of all samples was also prepared in parallel to serve as an internal standard. Samples were randomized and every 8 samples comprising 2 replicates of each of 4 different experimental groups (MAOA high/Fluoxetine, MAOA high/Ctrl, MAOA low/Fluoxetine and MAOA low/Ctrl) as well as 2 internal standard samples were mixed. Mixtures were pre-fractionated at basic pH to reduce the complexity. Fractions were analyzed by nano LC-MS/MS analysis with a TMT quantification strategy. Raw mass spectrum files were processed with proteomics software by searching against protein sequences from public

databases. Result files containing protein identification and quantification information were exported and further analyzed with statistics and bioinformatics tools.

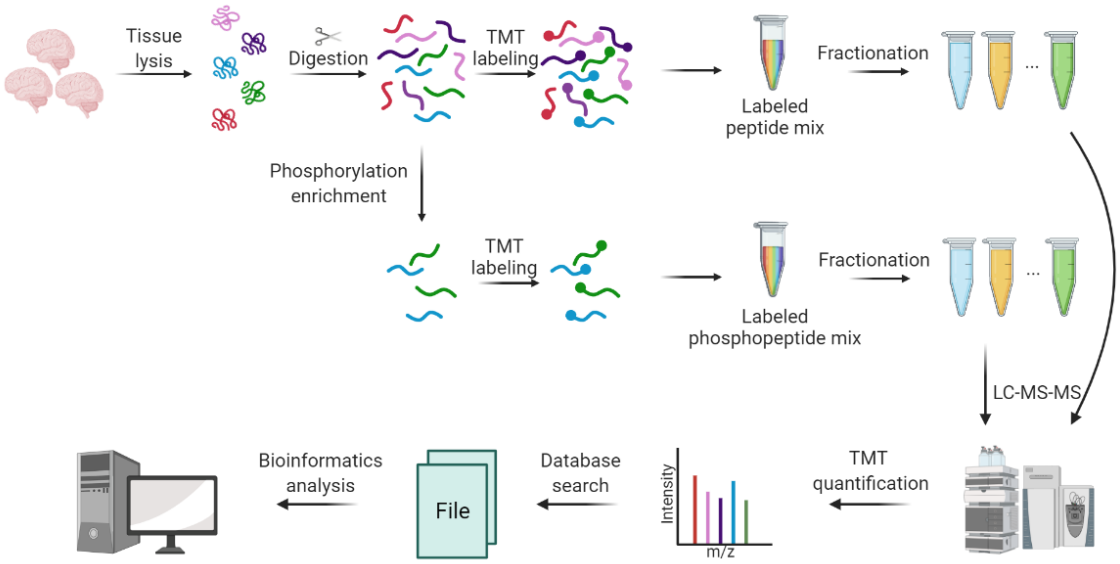

Figure 2.3 Scheme of mass spectrometry sample preparation and raw data analysis for proteome or phosphoproteome profiling of macaque DLPFC and CC.

Due to the potential existence of interactions between two independent biological factors (treatment and MAOA polymorphisms), in the data analysis strategy (Figure 2.4), two-way ANOVA was first applied to discover interactors, followed by Tukey's Test for Post-Hoc analysis. Subsequently, one-way ANOVA was used to determine significantly changed proteins or phosphopeptides considering both treatment and MAOA genotype. For phosphoproteomic data, phosphoproteomics dissection using networks (PHOTON) was performed to convert site information into proteins level information and obtain annotated protein-protein interactions. All regulated proteins, phosphoproteins and PHOTON functional proteins were correlated with impulsive behavior data to obtain a list of proteins associated with both an increase in impulsivity and fluoxetine treatment. Biomarker candidates were identified with high correlation with impulsivity. Subsequently, all correlated proteins were subjected to Gene Ontology (GO) annotation and pathway analysis to reveal the underlying mechanistic mode of action of fluoxetine.

Figure 2.4 Data analysis strategy for identifying altered proteins or phosphorylation events, discovering biomarkers and bioinformatics analyses.

2.3.3 Methods

2.3.3.1 Buffer preparation

All buffers or solutions used in mass spectrometry sample preparation were prepared freshly according to the following recipes. SDC lysis buffer: 4% SDC (wt/vol), 25 mM HEPES, 125 mM NaCl (pH 8.5); reduction/alkylation buffer: 100 mM TCEP, 400 mM CAM pH 7-8; EP loading buffer: 6% TFA, 80% ACN; enrichment buffer: 48% TFA, 8 mM KH_2PO_4; wash buffer: 5% TFA, 60% isopropanol; transfer buffer: 0.1% TFA, 60% isopropanol; elution buffer: 200 µl ammonia in 800 µl of 40% ACN.

2.3.3.2 Animal impulsivity test

A reward delay test adapted for monkeys from similar tests in children was performed by our collaborators at UC Davis to measure impulsivity[114]. Briefly, monkeys were relocated individually to a separate test room. The impulsivity test was hand administered in the Wisconsin General Test Apparatus in one session of 40 trials, which were blinded and randomized for each group. Each monkey was moved to a separate room. In each experiment, an opaque door would open, to expose an opaque movable screen and a test

board covered with a transparent plastic box behind the screen, with some preferred food on it (raisins, miniature marshmallows). The screen moved backwards by 1 inch every 2 seconds. After a total of 7 intervals, the food box would be fully exposed. At this time, the monkey could move the box and get the food rewards. If the monkey touched the box before the box was fully exposed, the experiment stopped immediately. Measurements for calculating impulsivity were the average number of screen intervals to complete the trial (Ave. screen), average latency time and number of trials for the monkeys to get the rewards (Ave. lat and Ave. trial)[114].

2.3.3.3 Isolation of macaque brain tissue sections

Isolation of macaque DLPFC and CC tissue sections was conducted by project co-workers. Briefly, monkeys were anesthetized with ketamine (10 mg/kg i.m.) and excess pentobarbital (120 mg/kg i.v.), followed by perfusion with 1 liter of warm heparinized saline, then 3 liters of cold heparinized saline and a final flush with 500 ml cold saline. Subsequently, brains were quickly removed and stored in saline for 10 min on ice. Then brains were first cut into 5 mm slices and further into right and left halves along the midsagittal line. Frozen slices were placed on pre-chilled glass plates and DLPFC and CC punches were taken according to the stereotaxic atlas of Rhesus monkey brain[117]. All tissue punches were immediately frozen in liquid nitrogen and stored in -80^{o}C for future use.

2.3.3.4 Tissue lysis and protein concentration determination

Dorsolateral prefrontal cortex and cingulate cortex tissue punches from 24 macaques were lysed with a bullet blender (speed 4/6, 1 min) in lysis buffer containing 4% SDC, 25 mM HEPES and 150 mM NaCl (pH 8.5). Homogenized tissue suspension was heat-treated for 5 min at 95^{o}C followed by sonication (35% power, 1 s pulse) for 1 min at 4^{o}C. Samples were centrifuged (20 min, 18,000 g, 4^{o}C) and the supernatants were retrieved. Subsequently, protein concentrations in the supernatants were determined with a BCA assay according to the manufacturer's instruction. Lysates were snap-frozen in liquid nitrogen and stored at -80°C for further use and long-term storage.

2.3.3.5 Protein digestion

Aliquots of each sample lysate were diluted with lysis buffer to equal protein concentrations based on BCA assay results to achieve the desired starting amount (1 mg)

in a final volume of 270 µl. Samples were then reduced and alkylated with 100 mM TCEP and 400 mM 2-chloroacetamide (pH 7-8) at 1:10 volume (30 µl) for 15 min at 45°C in a thermal shaker. After cooling down to room temperature, samples were subjected to protein digestion at 37°C overnight with addition of Lys-C and trypsin (1:100).

2.3.3.6 Peptide preparation for proteomic analysis

From each sample, 5% of digests were aliquoted and acidified with 100% formic acid to a final concentration of 5%. Samples were fully vortexed then centrifuged at 10,000 g for 20 min. Supernatants (peptides) were transferred into a new 1.5 ml Eppendorf tube and pellets (SDC) were washed twice with 30 µl of 25 mM HEPES buffer before being discarded. Supernatants were all combined and adjusted to pH 7.5-8 with 5 M KOH.

2.3.3.7 Phosphopeptides enrichment for phosphoproteomic analysis

Phosphopeptide enrichment was carried out based on the Easy-Phos protocol with modified steps. Briefly, 95% of digests for each sample were added to 400 µl of isopropanol, followed by 30 s of complete mixing under vortexing at maximal speed. Subsequently, 100 µl of enrichment buffer (see buffer recipes) was added before another complete mixing. TiO_2 beads were weighted out, resuspended in EP loading buffer (see recipes) at a concentration of 1 mg/µl and then added into samples at a beads-to-protein ratio of 12:1 (w/w). After 5 min incubation at 40°C under vortexing at maximal speed, beads were pelleted by centrifugation at 2000 g for 1min. Supernatants containing non-phosphorylated peptides were removed and 1ml wash buffer (see recipes) was added to beads bound to phosphorylated peptides. Samples were vortexed at room temperature for 30 s and then centrifuged at 200 g for 1 min to remove the wash buffer. Wash steps were repeated for another 4 times to completely removed non-phosphorylated peptides. Beads were then resuspended in 75 µl EP transfer buffer (see recipes) and then loaded onto in-house packed C8 tips in 200 µl pipette tips. Samples were centrifuged to dryness at 3,000 g for 10 min. Phosphopeptides on beads in C8 tips were eluted with 50 µl EP elution buffer by centrifugation at 3,000 g for 10 min. Elution was repeated one more time and elutes were combined before dying down in a vacuum centrifuge. Dried samples were reconstituted in 30 µl HEPES buffer.

2.3.3.8 TMT labeling

Peptides and phosphopeptides after enrichment were subjected to TMT labeling

separately using the TMT 10-plex workflow according to manufacturer's protocol. Samples in different MAOA genotypes and treatments were first evenly distributed into 3 TMT datasets. For each TMT dataset, 10 channels (from 126 to 131N) were used to label 8 samples as well as 2 internal standards (an aliquot from the pool of all samples) used for data normalization. Generally, 0.8 mg of TMT reagents were sufficient to label 200 µg of peptides. To guarantee the labeling efficiency, TMT reagents used for phosphopeptides were doubled due to potential remaining ammonia. TMT10-plex reagents were solubilized in anhydrous acetonitrile and added into samples to trigger a labeling reaction. After 1 h incubation at room temperature, reactions were quenched using 1µl of 5% hydroxylamine solution and incubated for another 15 min. For every TMT dataset, small aliquots with equal volumes were taken from each sample to create a QC sample, a mixture of these aliquots across 10 labeled samples. QC samples were then acidified with 2% formic acid (final concentration) and desalted with C18 Tips. Peptides were eluted with elution buffer containing 70% ACN and 0.1% formic acid for MS measurement in a short gradient. Raw files were quantified with Proteome discoverer 2.4 (see data processing). Mean abundances of each channel in every QC sample were calculated to obtain the mixing ratio of labeled samples; labeling efficiencies were also checked. Labeled peptides were mixed at the calculated mixing ratio based on the results of QCs to bring equal mean abundance to each channel in one dataset. Mixed peptides were dried down by vacuum centrifugation and stored immediately at -20°C for further use.

2.3.3.9 Peptide fractionation

Peptides and enriched phosphopeptides were fractionated using a Thermo High pH Reversed-Phase Peptide Fractionation Kit according to the manufacturer's protocol. Dried peptides or phosphopeptides were reconstituted in 300 µl of 0.1% formic acid and loaded onto a fractionation column preconditioned with ACN and 0.1% triethylamine. Elution solutions were a series of 0.1% formic acid mixed with various percentages of ACN (from 5% to 50%). In-gradient elution solutions were used to elute peptides or phosphopeptides to separate fractions. 8 fractions for peptides and 10 fractions for phosphopeptides for each TMT experiment were collected before being evaporated in vacuum centrifuge. Peptides/phosphopeptides were ready for MS analysis and were stored in -80^{o}C for long-term storage.

2.3.3.10 Nano-LC-MS/MS analysis

The analysis of fractionated TMT-labeled peptides or phosphopeptides was performed on an Ultimate 3000 UHPLC system (Thermo) coupled with a Q-Exative-Plus mass spectrometer, controlled by Xcalibur software v4.2.47 (Thermo Fisher Scientific, Waltham, MA, USA). Briefly, 1 µg of the 0.1% formic acid (FA)-resuspended peptides from each fraction was automatically loaded onto a C18 pre-column (300 µm i.d., Thermo) at a flow rate of 10 µl/min (2% ACN/0.1% FA). The 15 cm capillary analytical column (75 µm i.d., New Objective, Inc.) was packed in-house with 1.9 µm of C18 ReproSil particles (Dr. Maisch GmbH). The mobile phases used to elute the peptides comprised 0.1% FA as phase A and 95% ACN/0.1% FA as phase B with a flow rate of 300 nl/min. The 160 min gradient was developed as follows: a pre-equilibration phase with 95% A for 5 min; 5% - 30% B for 110 min; 30% - 60% B for 20 min; 98% B for 5 min and a post-equilibration with 96% A for 20 min.

The liquid chromatography-tandem mass spectrometry (LC-MS/MS) system was operated in a data-dependent acquisition (DDA) mode. The full mass scans were acquired in the Orbitrap mass analyzer under the profile mode at a resolution of 70,000 over a range of 375 to 1400 m/z. The top 10 precursor ions were selected for HCD fragmentation with a normalized collision energy (NCE) of 32% and a dynamic exclusion time of 30 s. The MS/MS scans were also acquired in the Orbitrap under the centroid mode with a resolution of 35,000. The AGC targets for full scan and MS/MS were set to 3×10^6 and 1×10^5, respectively. The spray voltage of the ESI ion source was 1.85 kV and the temperature of the ion transfer capillary was 250°C.

2.3.3.11 Raw data processing

Protein database searches of all raw LC-MS/MS data were performed with Thermo Proteome Discoverer 2.4 (Thermo Fisher Scientific) using the SequestHT search engine against the complete Macaca mulatta (Rhesus macaque) sequence database including all Uniprot entries (download 20201103). Spectra selection and most other parameters were set at default settings. Trypsin was specified as the protease. Mass tolerance for precursor and fragment ions was set to 10 ppm and 0.02 Da, respectively. Fixed modifications were set as TMT6 at the N-termini and lysine (K) residues, and carbamidomethyl at cysteine (C) residues. Methionine (M) oxidation was set as a variable modification in both proteomic and phosphoproteomic data analysis. Variable modification of phosphorylation

on serine (S), threonine (T) and tyrosine (Y) was only enabled for phosphoproteomic analysis. Posterior error probabilities (PEPs) were calculated and peptide spectrum matches (PSMs) were filtered using Percolator. False discovery rate (FDR) was estimated with a q-value and controlled under 0.05. The IMP-ptmRS algorithm was introduced to localize phosphorylation sites sensitively in the phosphoproteomic analysis. For reporter ion quantification in a consensus workflow, raw intensity of unique and razor peptides without normalization and data imputation were extracted for following processing and statistical analysis.

2.3.3.12 Bioinformatics analysis

Processing and bioinformatics analysis of raw quantified data exported from Proteome Discoverer 2.4 were performed using Microsoft Excel, Perseus (1.6.14.10), custom scripts in R (64-bit version 4.0.4) or Cytoscape 3.8.2.

2.3.3.13 Outlier identification and missing value imputation

Raw quantified data were filtered to retain proteins or phosphopeptides identified in at least 2 TMT datasets and then log2 transformed. Hierarchical cluster analysis with a "complete" agglomeration method was performed with R to identify the existence of outliers. After removal of outliers, low abundance resampling was applied to in-set missing values, which belong to Missing at Random (MAR). Missing values generated by merging different TMT datasets belonging to Missing Completely at Random (MCAR) were imputed with the package ImputeLCMD in Perseus. The KNN mode with the number of neighbors set as 15 was used. Histogram plots were used to visualize the distribution of imputed values after imputation.

2.3.3.14 Batch effect removal

Imputed data were first quantile normalized with Perseus. Hybrid mode of R package TAMPOR, which uses both internal standards and total channel intensity, was applied to batch effect removal. Principal Component Analysis (PCA) from R base package Principal Variance Component Analysis (PVCA) from BatchServer was performed on data before and after the batch effect removal to evaluate the removal efficiency. R package factoextra was used to visualize the PCA results.

2.3.3.15 Statistical analysis

Two-way ANOVA with treatment as the first factor and genotype as the second factor

was performed with R on global proteomic and phosphoproteomic data to differentiate between proteins or phosphopeptides with changed expression profiles. Significance was determined by p-values corrected for multiple hypothetic comparisons using the Benjamini-Hochberg method (adjusted p-value). Significant comparison pairs were determined by p-value following the Tukey's Test for Post-Hoc Analysis. Unless stated otherwise, the cut-off of a p-value or adjusted p-value was set as 0.05. Fold-change cut-off varied in different analyses.

Unpaired two-sided Student's t-tests were performed with R package Limma on specific comparisons between two groups. Unless stated otherwise, the cut-off of a p-value or adjusted p-value was set at 0.05-Fold change cut-off varied in different analyses.

2.3.3.16 Hierarchical clustering

Hierarchical cluster analysis for significantly changed proteins and phosphopeptides was performed and a heatmap was created with R package. "Euclidean" distance and "average" method were selected for both row and column clustering on Z-scored data.

2.3.3.17 Human homologous proteins and phosphosite conversion

Identified macaque proteins were converted to gene symbol and human homologous proteins to follow pathway analysis using R package clusterProfiler and org.Hs.eg.db. Evolutionally conserved phosphorylation site information in humans was downloaded from PhosphoSite Plus.

2.3.3.18 PHOTON

Data preprocessing for PHOTON was performed with Perseus 1.6.10.43 on log2-transformed normalized phosphopeptide quantities. Uniprot accession numbers of macaque proteins were first mapped to gene names and further annotated to human homologous uniprot accessions and ESNPs. Phosphopeptides not able to be mapped to any ESNPs were discarded. Human genetic networks were downloaded from the STRING database and created with Perseus 1.6.0.2078, and high confident interactions with combined scores greater that 900 were selected. Phosphopeptide quantification information was used to annotate nodes in the established protein network, during which protein functionality scores were calculated.

2.3.3.19 Behavior data correlation

Behavior data were processed with R. Significance of hypothetic analysis and impulsivity tests data were calculated with the Scheirer-Ray-Hare test due to the non-normality of the data. P-value < 0.05 was used as a threshold for a significant effect.

Data correlation between behavior tests and between behavior data and omics data were performed using R package Hmisc. Spearman correlation coefficients and significance p-values were calculated with a linear model due to the non-normality of the behavior data. A harsh R^2 cutoff of 0.6 (both positive and negative) and adjusting p-values by the Benjamini-Hochberg method of 0.05 was used as a threshold unless stated otherwise in order to filter potential biomarkers that strongly indicate the behavior-related side effect. A relaxed R^2 cutoff of 0.1 was applied on differentially expressed proteins to select those associated with behavior data.

2.3.3.20 GO and pathway enrichment analysis

GO and pathway enrichment analysis were applied to assign functional annotation to selected (sub)sets or pairs of correlating human homologous genes. GO enrichment and pathway analyses were performed with either R package clusterProfiler or the ClueGO plugin of Cytoscape 3.8.2. Gene Ontology enrichment was performed for cellular component (CC), Molecular Function (MF) and Biological Process (BP). The annotated pathway database used in the analysis was a combination of Kyoto Encyclopedia of Genes and Genomes (KEGG), Reacteome and WikiPathways. A cut-off of adjusted p-values by Benjamini-Hochberg method was set at 0.05 unless stated otherwise. Removal of redundant GO or pathway terms was achieved by enabling “Use GO term fusion” in CluoGO or by clusterProfilier. Visualization of GO and pathway enrichment analysis was performed by either R package ggplot2 or network construction in Cytoscape. GO or pathway terms with low enrichment scores or low significance were removed from the visualized results.

2.3.3.21 Network analysis

Functional protein-protein interaction networks were established based on the knowledge in the STRING or imported from the KEGG database with the KEGGparser plugin using Cytoscape 3.8.2. Confident score cut-off for protein-protein interaction was set to 0.4 to exclude low confident interactions. MCODE and CentiScape plugins were used for generating a subnetwork with calculation of Maximal Clique Centrality (MCC) and Degree. yFiles Layout Algorithms were used to modify the network layout.

2.4 Results

2.4.1 Multiplexed quantitative analysis of macaque DLPFC and CC proteomes and phosphoproteomes

To generate a deep macaque DLPFC and CC proteome and phosphoproteome profile, I used a mass spectrometry-based quantitative proteomic pipeline coupled with a tandem mass tag (TMT) labeling strategy and basic pH peptide pre-fractionation to achieve extensive peptide separation, high mass resolution and better quantification accuracy (see Section 2.3.2 for more details).

As a result, 4939 proteins and 8459 phosphopeptides were identified and quantified in DLPFC, among which 3656 proteins and 3674 phosphopeptides were found in all 3 TMT datasets (<1% FDR). In CC, 4984 proteins and 8083 phosphopeptides were identified and quantified, among which 3143 proteins and 3894 phosphopeptides were found in all 3 TMT datasets (<1% FDR, Figure 2.5).

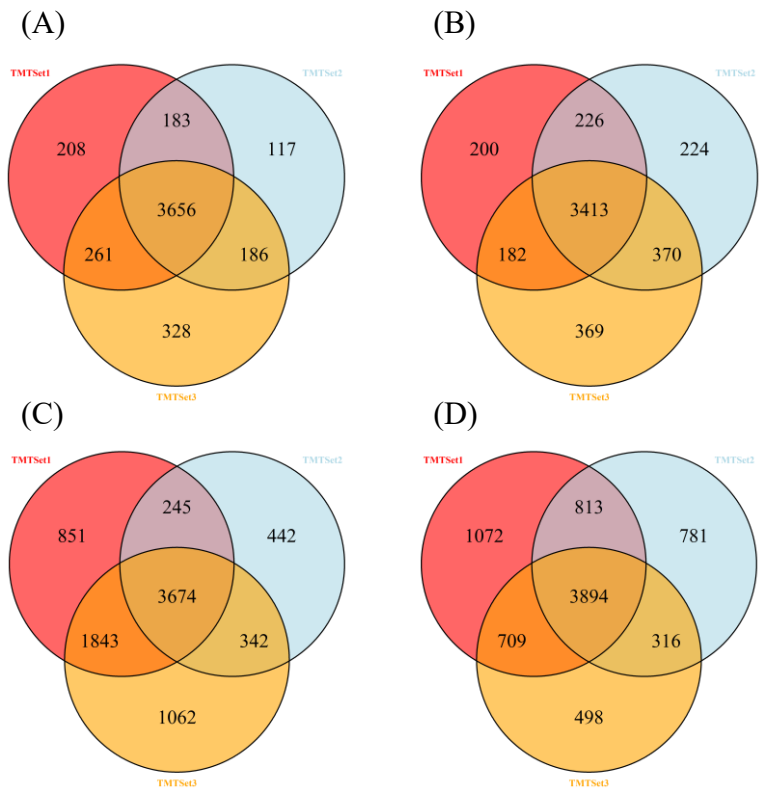

Figure 2.5 Proteins and phosphopeptides identified. (A) Proteins in DLPFC; (B) proteins in CC; (C) phosphopeptides in DLPFC; (D) phosphopeptides in CC.

10229 phosphorylation sites were identified in DLPFC, among which 8452 sites had phosphorylation site probability greater than 75% (Class I site). 9819 phosphorylation sites were identified in CC, among which 8099 sites were a Class I site. For all Class I sites, the distribution of phosphorylation targeting residues was: 90% on serine, ~10% on threonine and <1% on tyrosine for DLPFC, and 90.2% on serine, 9.7% on threonine and <1% on tyrosine for CC, similar to reported distributions (Figure 2.6).

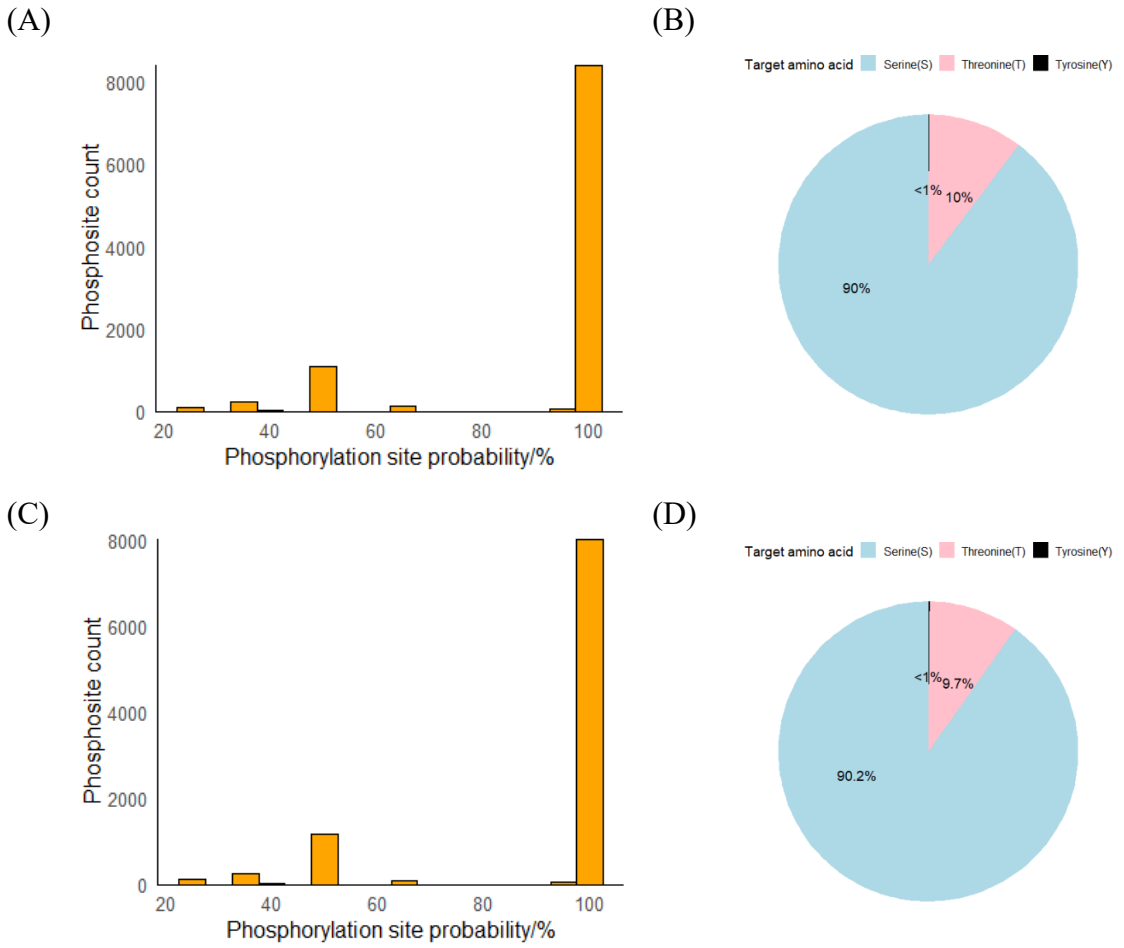

Figure 2.6 Distribution of phosphorylation site probability and target amino acids. (A-B) for PFC; (C-D) for CC.

All together 6054 proteins, 10428 phosphopeptides and 12647 phosphorylation sites were quantified. Although the numbers of proteins and phosphoproteins of DLPFC and CC were comparable (Figure 2.7), 1978 proteins, 4198 phosphopeptides and 5446 phosphorylation sites were unique for a given specific tissue, which is probably due to different cell type distribution.

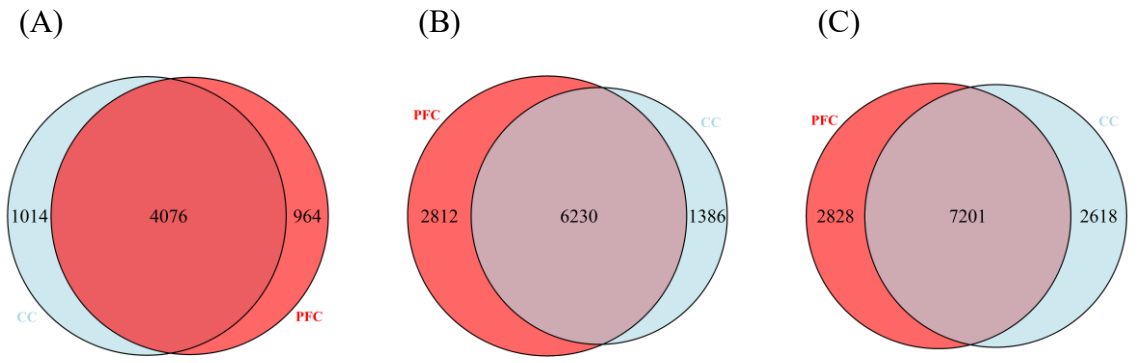

Figure 2.7 Overall proteins (A), phosphopeptides (B) and phosphosites (C) identified in PFC (red) and CC (blue).

Data quality was evaluated as described in Section 2.3, followed by removal of outliers and data normalization. Normalized DLPFC datasets contain 4251 proteins and 7673 phosphopeptide isoforms (13201 quantified in total) and normalized CC datasets contain 4186 proteins and 7348 phosphopeptide isoforms (12834 quantified in total) without missing values. PCA plots showed that normalized data were grouped by the biological treatment rather than the TMT batch (Figure 2.8). Normalized data were used for further differential expression analysis.

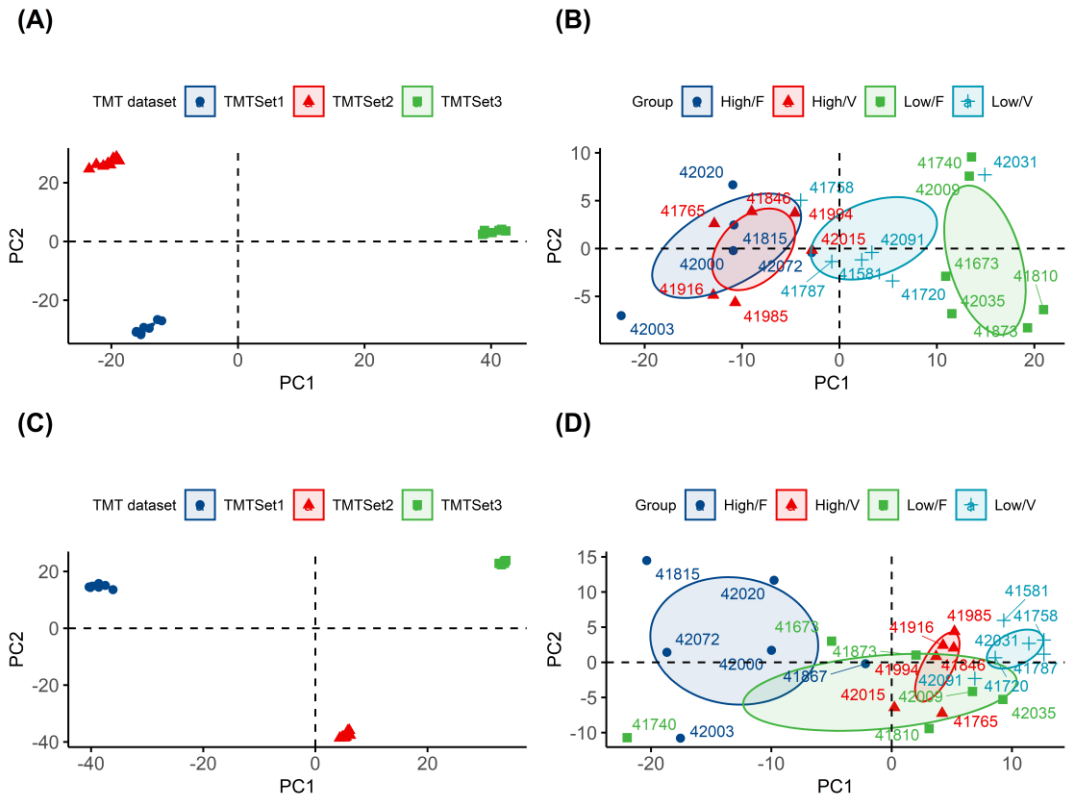

Figure 2.8 PCA plots of all measured samples. (A) DLPFC raw data; (B) DLPFC normalized data; (C) CC raw data; (D) CC normalized data. Different colors represent the groups indicated above each plot.

2.4.2 Identification of altered proteins and phosphopeptides under fluoxetine treatment

To explore the tissue specific molecular changes caused by fluoxetine treatment, differential expression analysis was performed with both proteomic and phosphoproteomic data from DLPFC and CC. Two-way ANOVA followed by Tukey's Test for Post-Hoc Analysis was performed first to identify proteins or phosphorylation sites that were significantly affected by fluoxetine in interaction with MAOA polymorphism. Subsequent multiple sample tests (one-way ANOVA) followed by Tukey's Test for Post-Hoc Analysis was applied to identify proteins or phosphorylation sites whose expression level was altered by fluoxetine treatment. Specifically, for phosphopeptides, phosphoproteomics dissection using networks (PHOTON) was performed to convert phosphopeptides and site information to protein level information that can be used in the following analyses.

2.4.2.1 Fluoxetine induces proteome-wide perturbation in DLPFC

In DLPFC a total of 87 proteins were identified as significant interactors between fluoxetine treatment and MAOA polymorphism (adjusted p-value < 0.05). Tukey's Test for Post-Hoc Analysis further revealed 79 comparison-pairs with a significant expression difference (p-value < 0.05, protein expression fold change > 1.5) derived from 39 proteins (Figure 2.9 A). The heatmap of the 39 interactors showed the fingerprint profile after hierarchical clustering on both samples and proteins. These proteins formed 2 main clusters and samples were grouped based on their MAOA polymorphism and drug treatment. The group in low MAOA polymorphism under Fluoxetine treatment (called Low_Fluoxetine hereafter) showed a significant down-regulation of proteins in Cluster C1 but up-regulation of proteins in Cluster C2. In contrast to the Low_Fluoxetine group, the High_Fluoxetine group has up-regulated C1 proteins but down-regulated C2 proteins.

For the other two groups (High_Vehicle and Low_Vehicle), expression of the majority of interactors was slightly up-regulated. The expression profile of these interacting proteins was highly correlated to their biological traits (drug treatment and MAOA type) and represent animals with different MAOA polymorphism in response to fluoxetine treatment (Figure 2.9 B). Multiple sample tests performed on proteins showing no interaction effect demonstrated that 907 comparison pairs from 482 proteins were found differentially expressed (fold change > 1.5 and adjusted p-value < 0.05, Figure 2.9 C).

The summarized statistics of differentially expressed proteins (DEPs) shown in Figure 2.9 includes 986 comparison-pairs from 521 unique proteins with or without interaction effects (Figure 2.9 D). The most proteome changes were observed for the comparison between High_Fluoxetine and Low_Fluoxetine groups, indicating that the two MAOA genotypes respond differently to fluoxetine treatment. In contrast, few changed proteins were observed between the two MAOA genotypes for vehicle control, emphasizing that the MAOA genotype may play an important role in the DLPFC proteome in response to fluoxetine treatment. In total, proteins affected by fluoxetine treatment from 3 comparisons (High_Fluoxetine vs Low_Fluoxetine, High_Fluoxetine vs High_Vehicle and Low_Fluoxetine vs Low_Vehicle) were merged and this yielded 471 fluoxetine-regulated proteins.

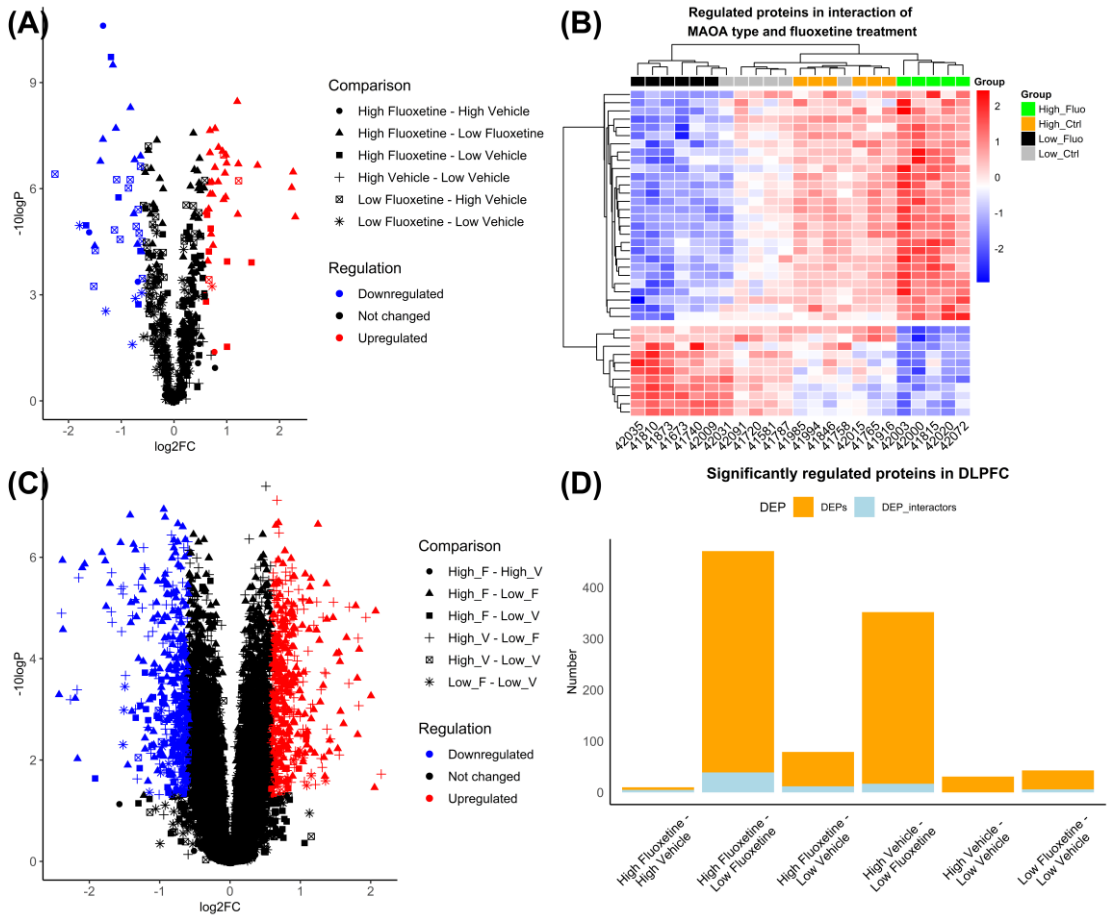

Figure 2.9 Proteomic perturbation induced by fluoxetine in DLPFC. (A) Volcano plot of interactors in paired comparison. Different comparisons are labeled with different point symbols and colors as indicated in the figure: red, blue and black spots represent proteins upregulated, downregulated and not regulated, respectively. (B) heatmap of expression of 39 interactors. Sample group nodes are labeled in different colors. Protein quantities are shown in Z-scored values. (C) volcano plot of non-interactors in paired comparison; (D) the number of all DEPs in different comparisons; light blue and orange bars indicate DEPs with and without interaction effect, respectively.

For phosphorylation sites regulated by fluoxetine treatment in DLPFC, differential expression analysis was performed on phosphopeptides using the same strategy as described above. As a result, 117 phosphopeptides showed significant interaction effects between drug treatment and MAOA polymorphism. Compared to the more drastic perturbation found for the proteome, the phosphoproteome underwent a relatively mild change and thus a smaller threshold of 1.3-fold change was applied for significantly regulated phosphopeptides. Thirteen pair-comparisons across 10 phosphopeptides comprising 10 phosphorylation sites were discovered. However, the phosphorylation profile of these phosphopeptides showed weak correlation to their experimental group (Figure 2.10 A-B). Subsequent analysis identified 44 significant comparison pairs with 37 phosphopeptides of 36 proteins that were affected by fluoxetine without interaction with the MAOA type. Summarized statistics of differentially expressed phosphopeptides revealed that most phosphoproteome changes were also found in the "High_Fluoxetine vs Low_Fluoxetine" comparison, consistent with findings in the proteomic data (Figure 2.10 C-D). Overall, 19 unique phosphopeptides in distinct phosphoproteins were found to be significantly affected by fluoxetine treatment in different comparisons.

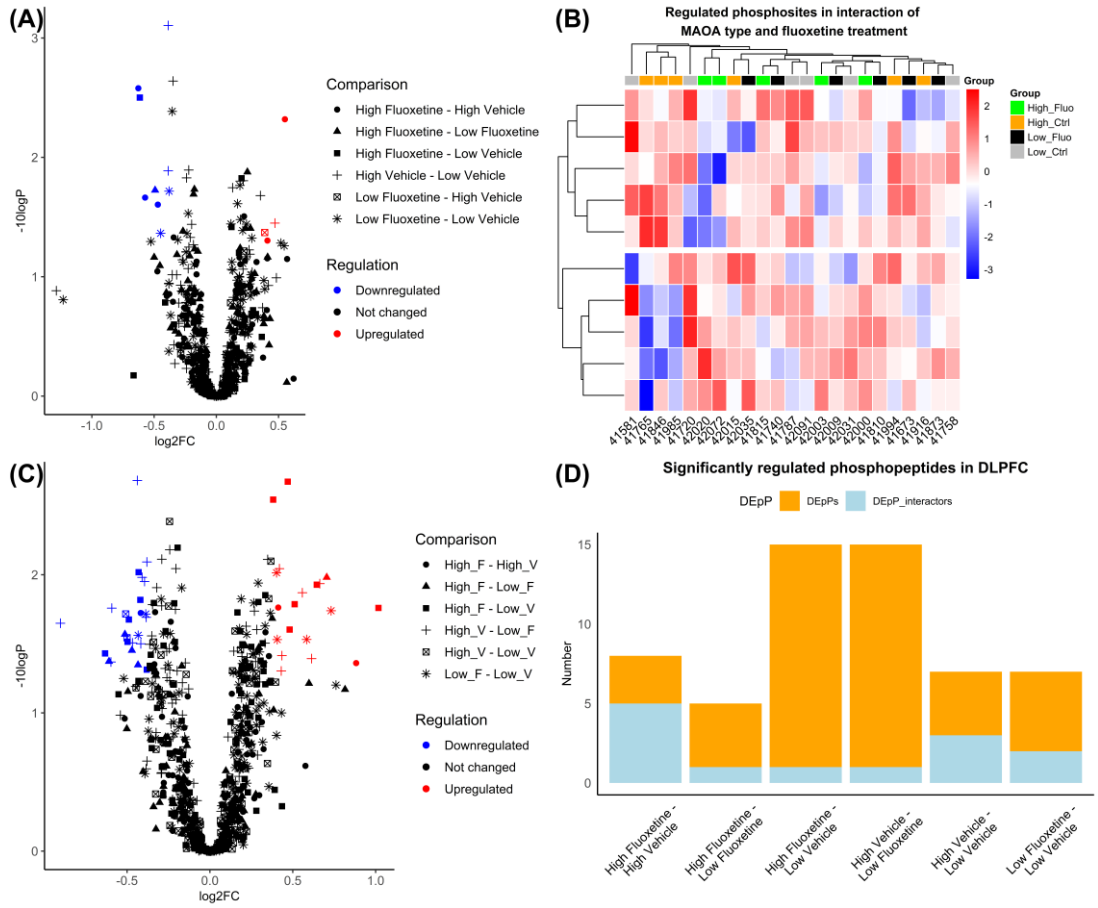

Figure 2.10 Phosphoproteomic perturbation induced by fluoxetine in DLPFC. (A) Volcano plot of interactors in paired comparison. Different comparisons are labeled with different point symbols and colors as indicated in the figure: red, blue and black spots represent proteins upregulated, downregulated and not regulated, respectively; (B) heatmap of expression of 10 interactors. Sample group nodes are labeled in different colors. Protein quantities are shown in Z-scored values; (C) volcano plot of non-interactors in paired comparison; (D) the number of all differentially expressed phosphopeotides (DEpPs) in different comparisons; light blue and orange bars indicate DEpPs with and without interaction effect, respectively.

2.4.2.2 Fluoxetine affects phosphoproteome stability in CC

Altogether 4186 high-confident CC proteins showed no interaction between fluoxetine treatment and the MAOA type. 450 comparison pairs out of 248 proteins were found to be differentially expressed (1.5-fold change and p-value 0.05), among which 194 comparison pairs corresponding to 134 uniquely regulated proteins were related to fluoxetine treatment, suggesting that fluoxetine induced weaker proteome perturbation in CC than in DLPFC.

In total 981 phosphopeptides displayed a significant interaction effect between fluoxetine treatment and MAOA polymorphisms, and among them 216 comparison pairs from 172 phosphopeptides of 115 proteins were regulated by at least 30% (fold change > 1.3, Figure 2.11). One-way ANOVA identified 44 phosphopeptides from 35 phosphoproteins that were significantly changed by at least 30%. 181 pairs from 159 phosphopeptides were found to be relevant for fluoxetine, indicating that the CC phosphoproteome is affected more under fluoxetine treatment than DLPFC.

In summary, fluoxetine effects were more pronounced at the proteome level in DLPFC, but at the phosphoproteome level in CC. In order to translate phosphopeptide information into global maps of active proteins and signaling networks, phosphoproteomics dissection using networks (PHOTON) was performed to identify all proteins that are part of possible kinase-substrate complexes, including their adaptor proteins, but not limited by phosphoproteins identified in phosphoproteomic dataset (see Section 2.3). After PHOTON analysis, 324 and 599 functional proteins were found from phosphoproteomic data in DLPFC and CC, respectively.

Overall, profiling of the proteome and phosphoproteome, and subsequent differential analysis yielded 471 regulated proteins and 19 phosphopeptides in DLPFC, as well as 134 proteins and 159 phosphopeptides in CC. PHOTON analysis yielded 324 functional

regulated proteins in DLPFC and 599 in CC.

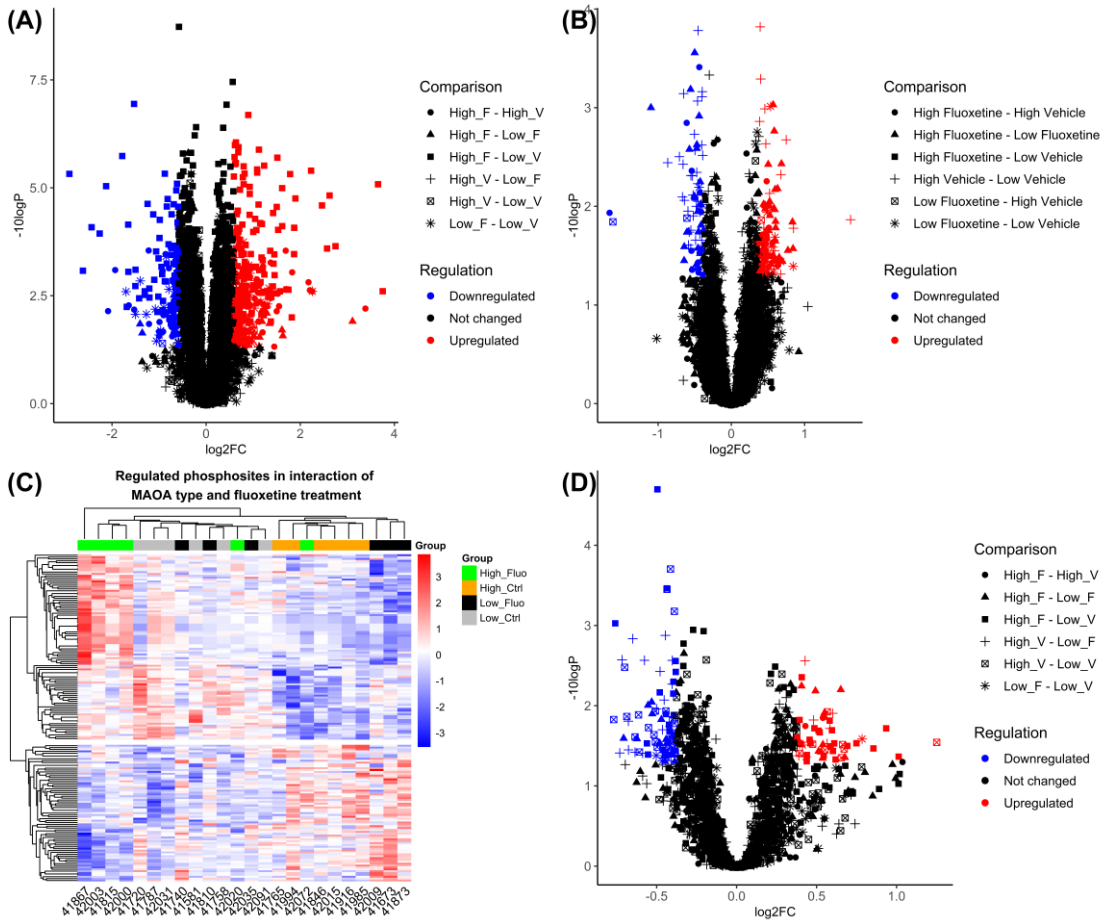

Figure 2.11 Proteomic and phosphoproteomic perturbation by fluoxetine in CC. (A) Volcano plot of proteins affected by fluoxetine without interaction effect; (B) volcano plot of phosphopeptides displaying an interaction effect; (C) heatmap of expression of interacting phosphopeptides. Sample group nodes are labeled in different colors. Phosphopeptides quantities are shown in Z-scored values; (D) volcano plot of phosphopeptides affected by fluoxetine without an interaction effect. Different comparisons are labeled with different point symbols and colors as indicated in the figure: red, blue and black spots represent proteins upregulated, downregulated and not regulated, respectively.

2.4.3 Macaque impulsivity-associated biomarkers

The impulsivity test was carried out at the UC Davis Primate Facility[114]. It measures how long the monkey can wait to receive the food reward by counting 3 different measurements, including the screen intervals (Ave. screen), latency time (Ave. lat) and number of trials (Ave. trial) as described in Section 2.3. A Scheirer-Ray-Hare test was performed on three different measurements of impulsivity to assess the effect of fluoxetine and MAOA polymorphism on the impulsivity of the monkeys. It was demonstrated that Ave. screen, Ave. lat and Ave. trials were all significantly affected by fluoxetine treatment (p-values 0.049, 0.049 and 0.025, respectively) but not MAOA

polymorphism. Moreover, the Pearson correlation among these 3 measurements revealed that they were highly correlated with each other (R = 1, -0.85 and -0.86), indicating that more screen intervals, longer latency time and fewer trials times (negatively correlated) represented increasing impulsivity. The impulsivity test suggested that fluoxetine increased juvenile rhesus monkeys' impulsivity (Figure 2.12). In contrast, MAOA genotypes showed no significant effect on monkeys' impulsivity[114].

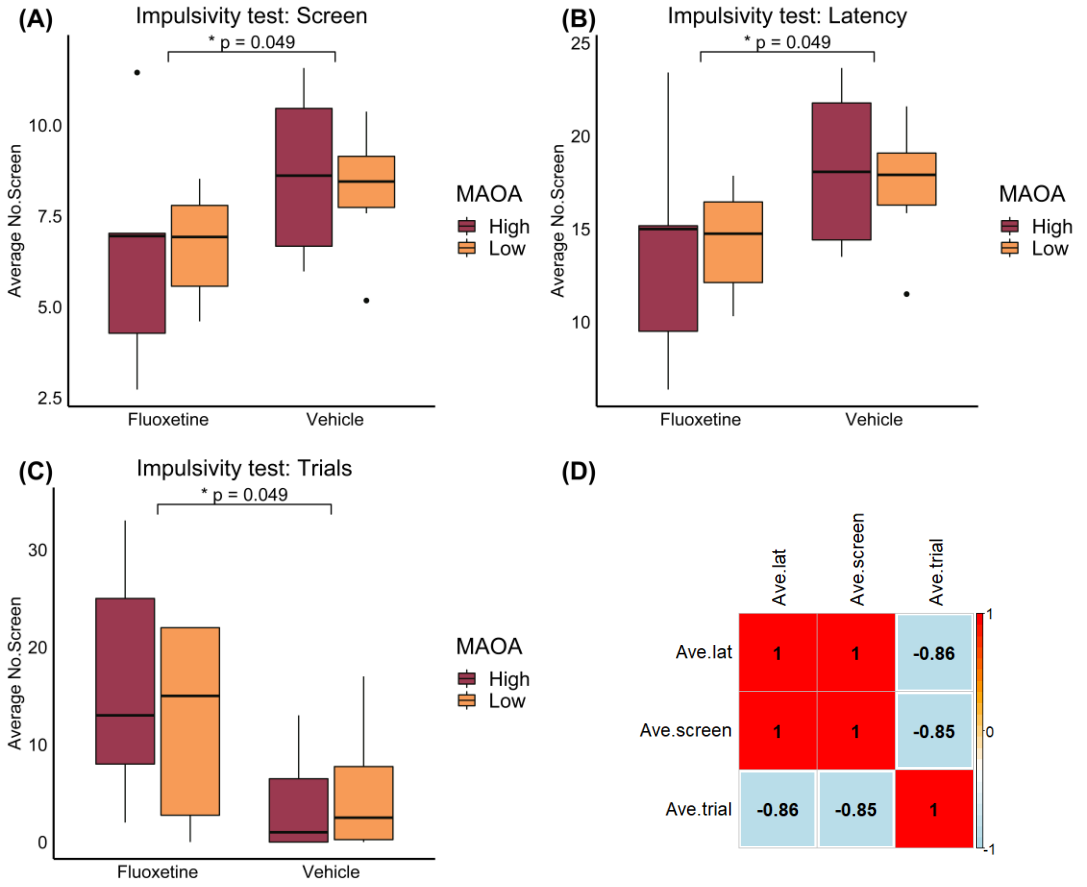

Figure 2.12 Measurements from impulsivity tests conducted at UC Davis by Mari Golub[114]. (A) Average number of screens; the effect of fluoxetine but not MAOA polymorphism on screen interval was significant (p = 0.049); (B) average latency time; the effect of fluoxetine but not MAOA polymorphism on screen interval was significant (p = 0.049); (C) average number of trials; the effect of fluoxetine but not MAOA polymorphism on screen interval is significant (p = 0.025); (D) Pearson correlation of the screen intervals, the latency time and the number of trials (red nodes refer to positive correlation and blue nodes refer to negative correlation).

To identify protein biomarkers in DLPFC and CC that can reflect the behavior-related side effect of fluoxetine, linear regression between omics data and impulsivity test data was performed. The expression level of 21 proteins in DLPFC were found to be associated with impulsivity behavior, among which 7 proteins were linked with the average screen interval, 10 proteins were linked with average latency time and 17 proteins were linked

with average number of trials (|correlation coefficient| > 0.6 and adjusted p-value < 0.05). Consistent with behavior data correlation, all proteins that negatively correlated with the average number of trials (n = 12) correlated positively with average screen interval and latency time, and *vice versa*, all proteins that positively correlated with the average number of trials (n = 9) correlated negatively with average screen interval and latency time (Figure 2.13).

Altogether 21 proteins, FECH (Ferrochelatase), RAB12 (Ras-related protein Rab-12) and NFIA (Nuclear factor 1 A-type) were found to be highly associated with all three impulsivity test measurements. FECH negatively correlated with the average number of trials (R = -0.67) and positively correlated with average screen interval and latency time (R = 0.67 and 0.7). In contrast, RAB12 and NFIA demonstrated positive correlation with the average number of trials (R = 0.69 and 0.63) and negative correlation with average screen interval (R = -0.66 and -0.6) and latency time (R = -0.66 and -0.61).

A total of 23 proteins were identified in association with impulsivity in CC, of which 14 proteins were linked with the average screen interval, 13 with average latency time and 11 with average number of trials. LOC720791 (Ribonuclease inhibitor) and CFL2 (Cofilin-2) were significantly correlated with all impulsivity tests, both showing positive correlation with the average number of trials (R = 0.65 and 0.62) and negative correlation with average screen interval (R = -0.7 and -0.63) and latency time (R = -0.7 and -0.63).

No protein was found to be correlated with impulsivity in both DLPFC and CC. Protein annotation of all the above-mentioned biomarkers are listed in Appendixes.

A number of phosphorylation events were also found linked with impulsivity. In DLPFC, phosphorylation levels of 25 sites correlated significantly with impulsivity, of which 15 sites were linked with the average screen interval, 16 sites with average latency time and 20 sites with average number of trials (|correlation coefficient| > 0.6 and adjusted p-value < 0.05). 11 sites correlated negatively with the average number of trials and 14 sites correlated positively (Figure 2.14). Phosphorylation of T331 and S333 of LOC719082 (WASH complex subunit 2C), S1876, S1878 and S1880 of SRRM2 (Serine/arginine repetitive matrix protein 2) and T303, S308 and S310 of SPP1 (Osteopontin) were found to be significantly positively associated with the average number of trials (R = 0.62, 0.6 and 0.61) and negatively correlated with average screen interval (R = -0.69, -0.62 and -0.63) and latency time (R = -0.72, -0.63 and -0.63). And

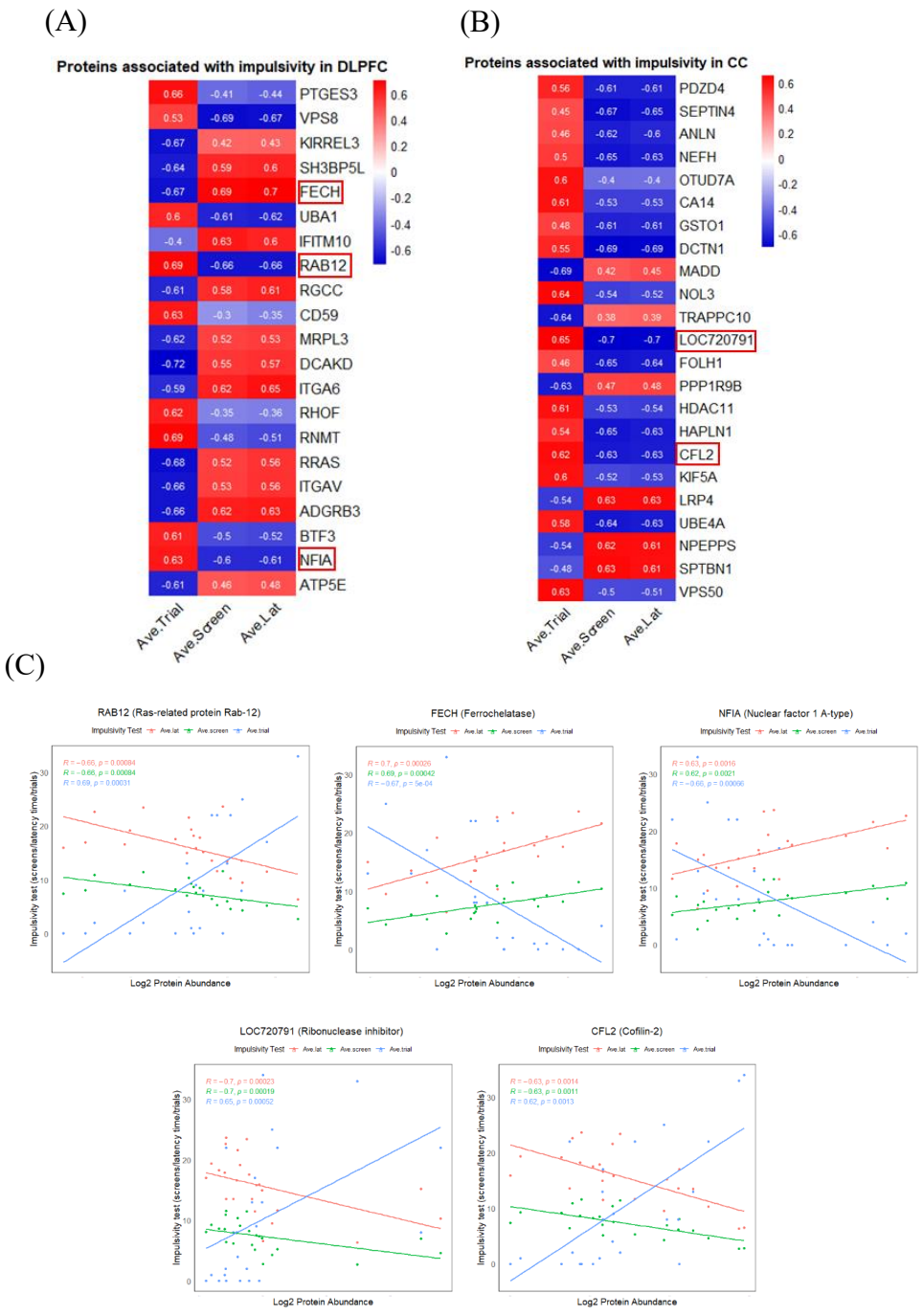

Figure 2.13 Proteins associated with impulsivity. Correlation coefficients were calculated by Spearman correlation. Blue nodes refer to negative correlation and red nodes refer to positive correlation. Color density represents the absolute value of correlation coefficients. (A) Proteins biomarkers in DLPFC; (B) proteins biomarkers in CC. (C) Proteins associated with all 3 impulsivity test measurements. RAB12, FECH and NFIA in DLPFC; LOC720791 and CLF2 in CC.

phosphorylation of S1455 of ANK2 (Ankyrin-2), S39 of SLC7A11 (Cystine/glutamate transporter) and S61 of MAPT (Microtubule-associated protein tau) displayed strong negative correlation with the average number of trials (R = -0.71, -0.65 and -0.69) and positive correlation with average screen interval (R = 0.64, 0.64 and 0.6) and latency time

(R = 0.65, 0.66 and 0.6).

In contrast to DLPFC, a total of 127 phosphorylation sites were linked with impulsivity in CC (|correlation coefficient| > 0.6 and adjusted p-value < 0.05) and 41 of them demonstrated high correlation with impulsivity (|correlation coefficient| > 0.65). The number of phosphorylation sites correlating with the average numbers of trials, average screen interval and latency time are 10, 36 and 29, respectively. 5 phosphorylation events were significantly associated (R > 0.65) with all of the three impulsivity tests, namely S608 of SLC29A1 (Equilibrative nucleoside transporter 1), S2578 and S2851 of BSN (Protein bassoon), S293 and S300 PDHA1 (Pyruvate dehydrogenase E1 component subunit alpha), S292 of CHGB (Secretogranin-1) and S312 on CNP (2',3'-cyclic-nucleotide 3'-phosphodiesterase).

(A)

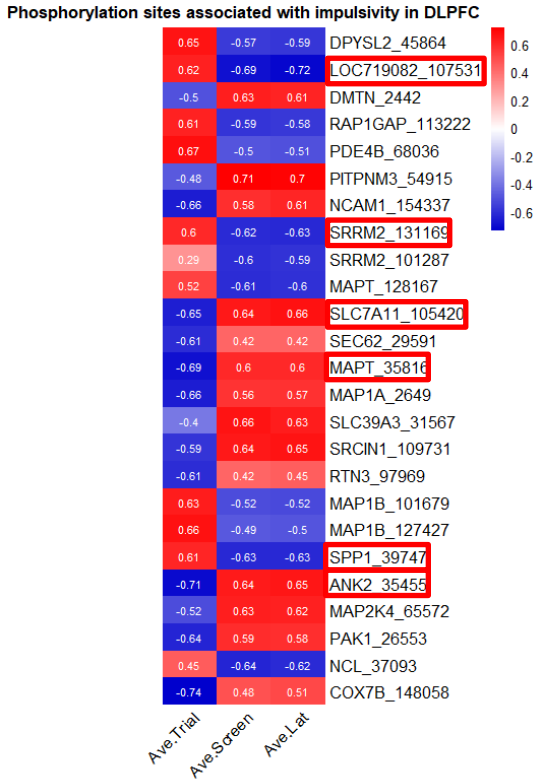

(B)

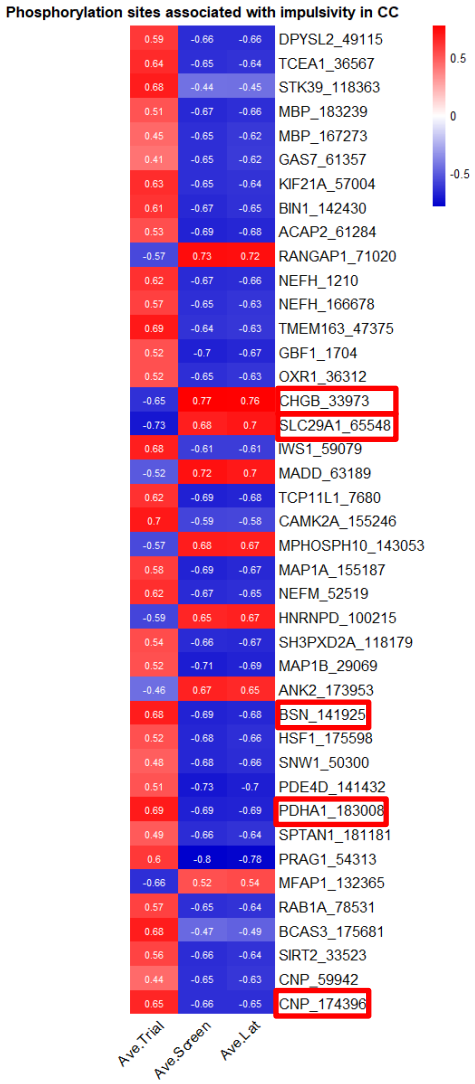

(C)

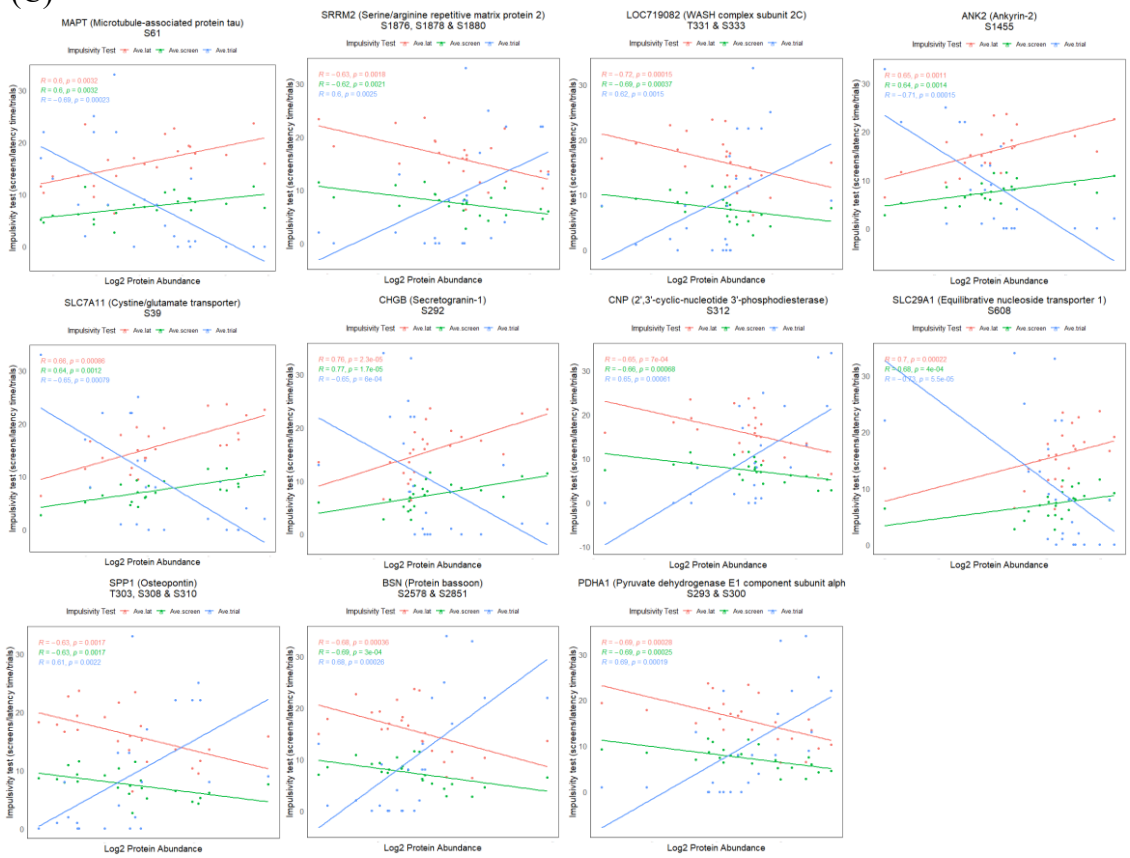

Figure 2.14 Phosphorylation events associated with impulsivity. Correlation coefficients were calculated by Spearman correlations. Blue nodes refer to negative correlation and red nodes refer to positive correlation. Color density represents the absolute value of correlation coefficients. (A) Phosphorylation biomarkers in DLPFC; (B) phosphorylation biomarkers in CC (R > 0.65). (C) Proteins associated with all 3 impulsivity test measurements: p-SRRM2, p-LOC719082, p-ANK2 and p-SPP1, p-SLC7A11 and p-MAPT in DLPFC; p-SLC29A1, p-BSN, p-PDHA1, p-CHGB and p-CNP in CC.

Interestingly, phosphorylation of S507 and T509 in DPYSL2 (Dihydropyrimidinase-related protein 2) was found to be correlated with impulsivity in both DLPFC and CC (Figure 2.15), suggesting that S507 and T509 phosphorylation may represent a phosphorylation biomarker for impulsivity. Annotation of all the above-mentioned phosphoproteins and phosphorylation sites are listed in Appendixes.

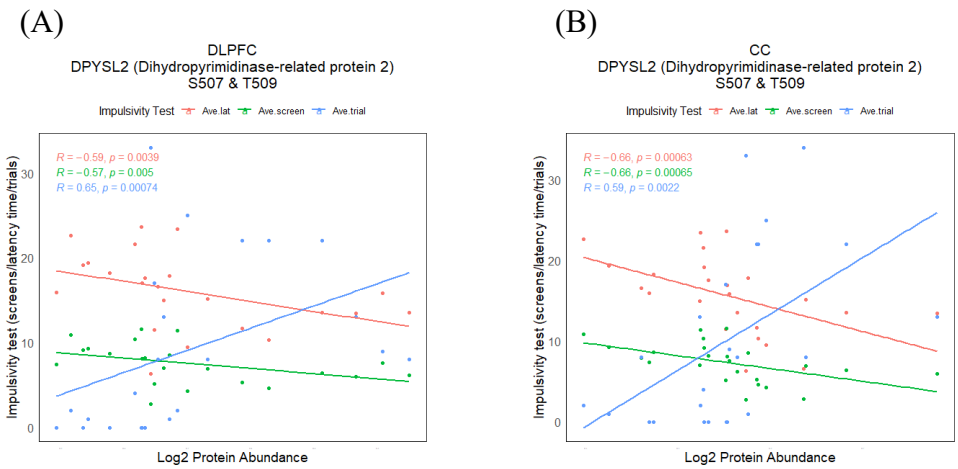

Figure 2.15 Phosphorylation biomarker p-DPYSL2. Phosphorylation of S507 and T509 is highly associated with impulsivity in both DLPFC and CC.

2.4.4 Biological pathways affected by fluoxetine

2.4.4.1 Pathways regulated by fluoxetine

To explore the biological functions that were affected by fluoxetine and the potential mechanisms underlying the increased impulsivity in macaque, GO annotation and pathway analysis of proteins and phosphoproteins was performed on those correlating with the impulsivity test. First, proteins that had at least a weak correlation of R > 0.1 with one of the 3 impulsivity measurements were selected. Next, all regulated proteins and PHOTON functional proteins from omics-data profiling were mapped to impulsivity-related proteins, generating a list of proteins that were associated with both impulsivity and fluoxetine treatment. Subsequently, all selected proteins were subjected to GO annotation and pathway analysis to investigate the pathways regulated by fluoxetine in connection with the impulsivity of macaques.

In GO enrichment analysis of cellular components, terms enriched from PHOTON functional proteins showed higher overall significance than those from differentially altered proteins. The most enriched cellular component terms in the CC phosphoproteome were “endoplasmic reticulum lumen” and glutamatergic synapses. “G-protein beta/gamma-subunit complex” was the most significant term in the DLPFC phosphoproteome, which was also one of the top hits in the enriched terms of the CC and DLPFC proteomes. Most GO terms enriched by proteins from proteomic data were found in multiple datasets. “Cytoplasmic side of membrane” and “inner mitochondrial membrane protein complex” were significantly enriched in both CC and DLPFC (Figure

2.16).

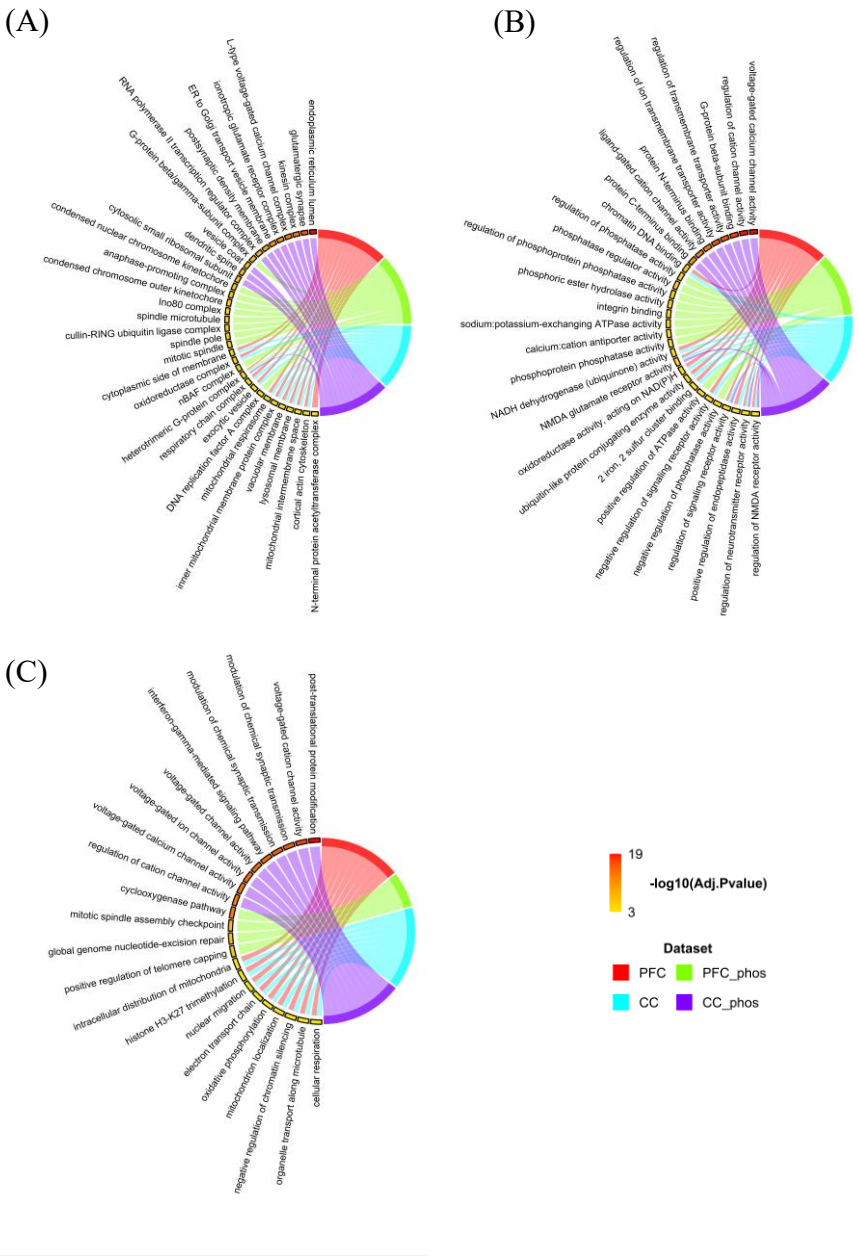

Figure 2.16 GO enrichment analysis of differentially expressed proteins associated with impulsivity. (A) GO cellular component (GOCC); (B) GO molecular function (GOMF); (C) GO biological processes (GOBP). GO terms were sorted accordingly to adjusted p values. Node color represents the dataset, as indicated.

A similar distribution pattern of GO terms was also observed in molecular function analysis, where the CC phosphoproteome displayed high activity in “voltage-gated calcium channel activity”, “G-protein beta-subunit binding” and “regulation of transmembrane transporter activity”. Many terms related to enzyme activities were enriched in the DLPFC phosphoproteome, such as “Regulation of phosphatase activity” and “sodium: potassium-exchanging ATPase activity”. More specific terms linked to

receptor activities enriched in proteomic and phosphoproteomic data include "NMDA glutamate receptor activity" and "regulation of neurotransmitter receptor activity" (Figure 2.16).

GO analysis also offered an insight into general biological processes affected by fluoxetine. "Post-translational protein modification" was the most enriched process from the CC phosphoproteome, followed by "voltage-gated cation channel activity" and "modulation of chemical synaptic transmission". "Cyclooxygenase pathway" was the most significant process in response to fluoxetine in the DLPFC phosphoproteome. In proteomic data, most enriched terms were found in both CC and DLPFC, including "electron transport chain" and "negative regulation of chromatin silencing" (Figure 2.16).

GO annotation provided a glimpse into the macro changes at proteome and phosphoproteome levels for fluoxetine treatment. In order to investigate the specific pathways in relation to increased impulsivity affected by fluoxetine, pathway enrichment was performed against a pool of KEGG, Reacteome and Wikipathway databases. "Nuclear Envelope (NE) Reassembly" and "Neurotransmitter receptors and postsynaptic signal transmission" showed the best correlation with fluoxetine treatment-related impulsivity increase in DLPFC proteome (Figure 2.17). "Amplification of signal from the kinetochores" was the most significantly affected pathway in the DLFPC phosphoproteome and "Nicotinate metabolism" was also linked to fluoxetine treatment. "GABAergic synapse" was the most relevant pathway in response to fluoxetine in the CC proteome, followed by "Signaling by ERBB2" and "Gap junction trafficking and regulation". "Neurotransmitter receptors and postsynaptic signal transmission" and "Ras signaling pathway" were drastically enriched in the CC phosphoproteome.

To better interpret the pathway enrichment result, redundant pathways were removed and the 20 most relevant pathways were selected for further investigation. Heatmaps revealed that enriched pathways from phosphoproteomic data were generally more significant than from proteomic data, consistent with the outcome of the GO annotation. A number of pathways were enriched in multiple datasets, although with varying significance. "GABA synapse" was the only pathway enriched in all 4 datasets, suggesting that the GABA synapse related signaling pathway plays an important role in increasing impulsivity after chronic fluoxetine treatment in macaques.

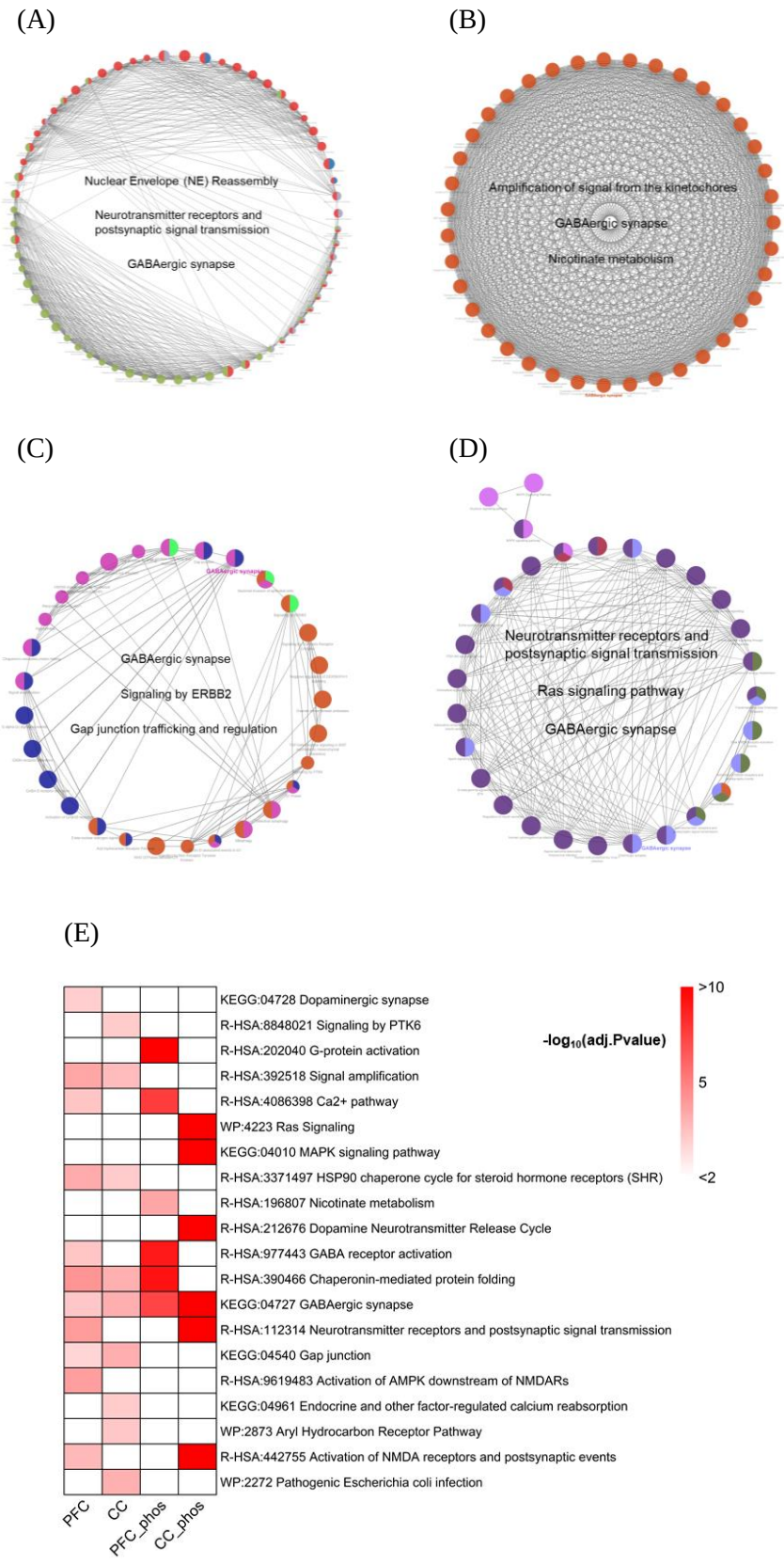

Figure 2.17 Pathway enrichment analysis of differentially expressed proteins associated with impulsivity. (A) DLPFC proteins; (B) DLPFC phosphoproteins; (C) CC proteins; (D) CC phosphoproteins. (E) A summary of significantly regulated pathways in the different datasets. Color density represents adjusted p values from the enrichment analysis.

2.4.4.2 Impulsivity-related GABA signaling pathway alteration associated with chronic fluoxetine treatment

Integrative analysis of proteome and phosphoproteome data in both DLPFC and CC suggested that the GABAergic synapse signaling pathway was associated with increased impulsivity of macaques and was significantly affected by fluoxetine treatment. To uncover the potential mechanistic mode of action of fluoxetine on the GABAergic synapse signaling pathway, all proteins, PHOTON functional proteins and corresponding phosphoproteins were integrated and used to construct a protein-protein interaction-based signaling network underlying the measured responses.

In DLFPC, a total of 60 proteins in the GABAergic signaling pathway associated with increased impulsivity under fluoxetine treatment were part of a protein-protein interaction network annotated in the STRING database (Figure 2.18). To find clusters where proteins were highly interconnected, MCODE analysis was applied to original complex networks, yielding one cluster consisting of distinct G proteins, G proteins' upstream receptors GABA B receptor (GABBR1, GABBR2) and metabotropic glutamate receptor 2 (GRM2), some G proteins modulators (GNGT2, GPSM1) and downstream protein kinase C (PRKCA, PRKCB, PRKCG), all involved in the subnetwork. Several topological algorithms including Maximal Clique Centrality (MCC) and Degree were applied to this subnetwork to investigate the core of the subnetwork. Both MCC and Degree analyses revealed 10 G-proteins as being the most dominant proteins for the whole network.

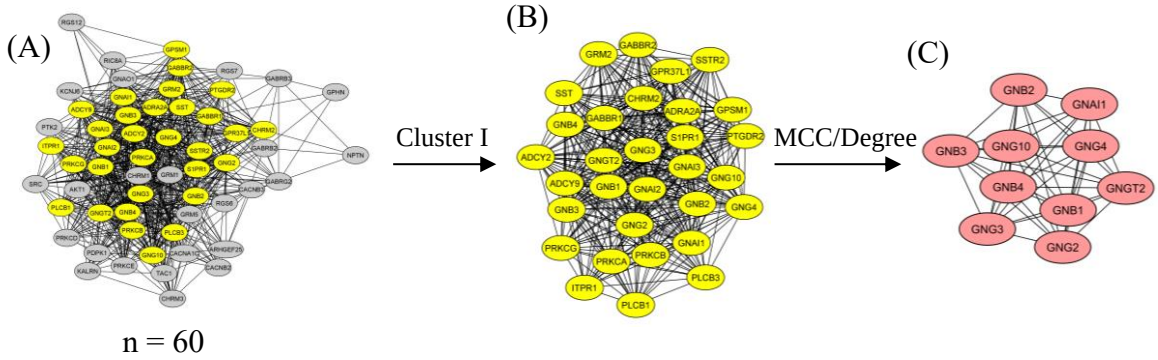

Figure 2.18 Reconstructed protein-protein interaction network with all altered DLPFC proteins involved in the GABAergic synapse pathway. (A) Complete reconstructed network consisting of 60 proteins; (B) highly interactive subnetwork extracted with MCODE analysis; (C) the core of the interaction network further extracted with MCC/Degree analysis.

The initial network in CC comprising 143 proteins related to impulsivity and fluoxetine

treatment was further clustered into 2 subnetworks by MCODE analysis (Figure 2.19). Consistent with the cluster in DLPFC, cluster I of CC also involved many G-proteins and their receptors or modulators both up- and downstream. Interestingly, cluster II consisted of GABA receptor binding-related proteins, including 3 potential biomarkers identified in previous analyses, namely, Ras-related protein Rab-1A (RAB1A), Spectrin alpha chain (SPTAN1) and Ankyrin-2 (ANK2). To further simplify the complex subnetwork cluster I, topological algorithms were carried out. Although both MCC and Degree calculation yielded a group of G-proteins, a network based on the calculation of Degree showed the involvement of several downstream kinases including protein kinase A (PRKACA, PRKACG), protein kinase C (PRKCA, PRKCB) and RAC-alpha serine/threonine-protein kinase AKT1.

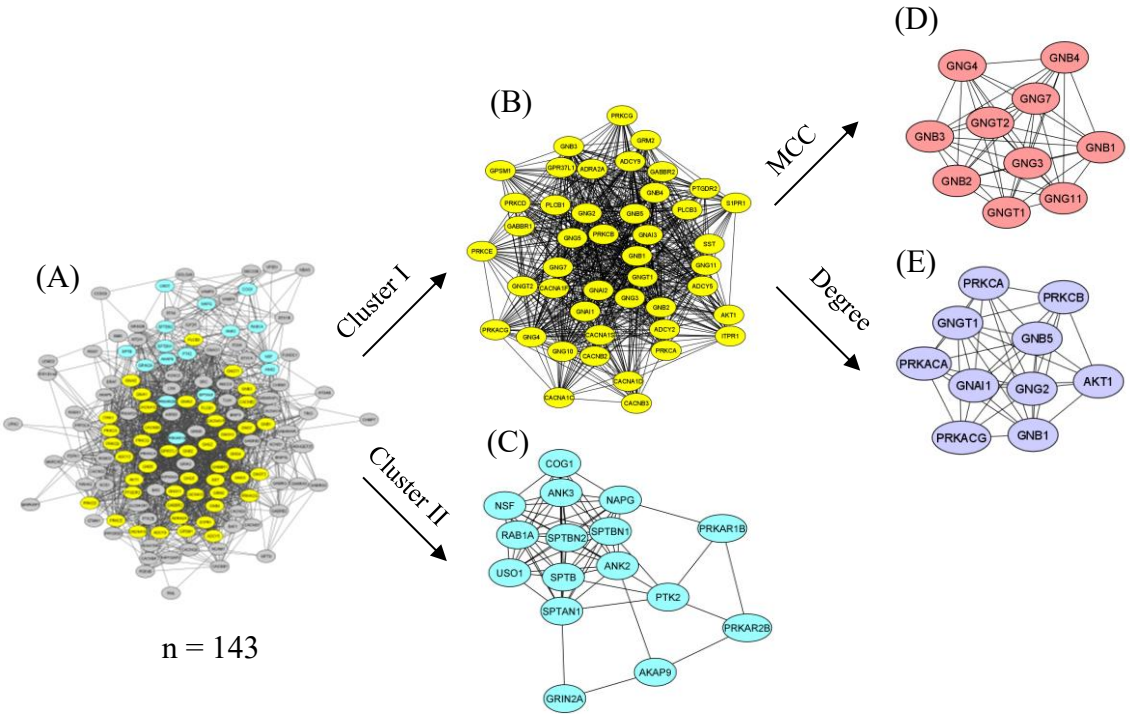

Figure 2.19 Reconstructed protein-protein interaction network with all altered CC proteins involved in the GABAergic synapse pathway. (A) Complete reconstructed network consisting of 143 proteins; (B) highly interactive subnetwork cluster I extracted with MCODE analysis; (C) highly interactive subnetwork cluster II extracted with MCODE analysis. (D) The core of interaction network cluster I further extracted with MCC analysis; (E) the core of interaction network cluster I further extracted with Degree analysis.

G-proteins and their receptors and modulators changed to a small extent in DLPFC and CC with fluoxetine treatment, indicating that G-protein signaling pathways, part of the GABAergic pathway, play an important role in the mechanism underlying fluoxetine-

induced impulsivity increase in macaque. Subsequently a reconstructed network consisting of G-protein signaling and its main downstream effector, the cAMP signaling pathway was analyzed. 95 proteins were involved in the reconstructed network, 44 of which were identified and quantified in our datasets (non-grey nodes). Although most of the identified proteins in the network were not regulated (green nodes), some key regulators in these two signaling pathways were found to be significantly affected at either the proteomic or phosphoproteomic level (red nodes), including GABA receptor (GABRA1, GABBR1, GABBR3), G protein family (Ga,i,o,s), adenylate cyclase (ADCY1), protein kinase A (PRKACA) and Bcl2-associated agonist of cell death (BAD), suggesting that fluoxetine-induced increased impulsivity might be associated with G-protein coupled-cAMP signaling pathways (Figure 2.20).

As part of the cAMP signaling pathway, G-protein coupled activation of cAMP and PKA was previously reported to be regulated in suicidal ideation and behavior[93]. Consistent with the reported results, the pathway was also found to be less active in our dataset, as reflected by downregulation of key protein expression levels or phosphorylation levels (PHOTON functional score). Under fluoxetine treatment, downregulation of GABA B receptor contributed to overexpression of Gαi (GNAI1, GNAI2 and GNAI3), i-form α subunits of G proteins that are known to inhibit the activity of adenylyl cyclases (ADCY1), resulting in the further inhibition of ADCY1 and subsequent decrease in PKA activity. Inhibited PKA suppresses the activity of Bcl2-associated agonist of cell death, possibly leading to cell death. All these results indicate that the cAMP-PKA signaling pathway might be the effector of fluoxetine-induced increase of impulsivity in macaques.

(A)

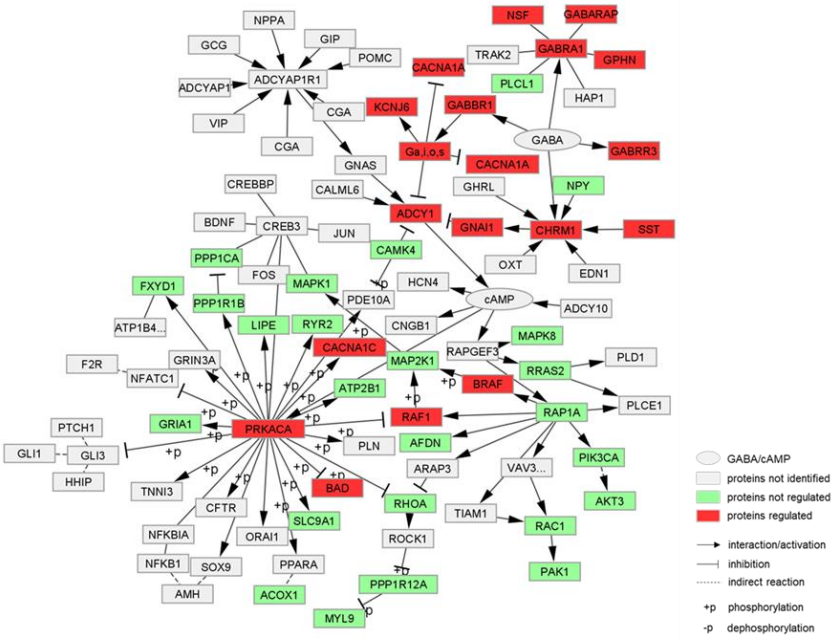

(B)

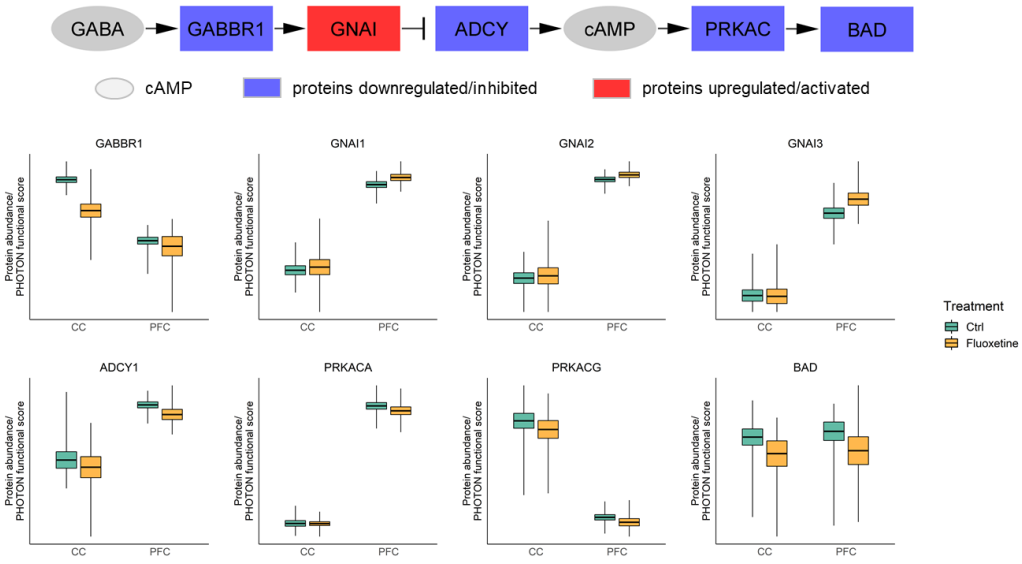

Figure 2.20 cAMP pathways are involved in fluoxetine-induced increase of impulsivity. (A) cAMP signaling pathway; red nodes represent proteins that were found to be regulated in our data; green nodes represent proteins that were not regulated in our data; grey nodes represent proteins not identified in our data. (B) Proteins that were found to be regulated in the GABA-cAMP-PKA pathway. Red node represents the protein (GNAI) upregulated; blue nodes represent proteins downregulated; boxplots show the differences in expression between individual proteins or subunits in controls versus fluoxetine treatment.

2.5 Discussion

Major depressive disorder (MDD) is a common mental disorder that represents a great burden for patients and society. Although numerous studies have attempted to investigate the etiology and therapy of MDD, the biological and neurological mechanisms underlying MDD are still obscure. In addition, clinically administered antidepressants for treating MDD are limited by insufficient efficacy in treatment resistant depression (TRD), unclear tolerability, delayed onset of a therapeutic response and undesirable side effects. As the only antidepressant approved by the FDA for treatment of depression in adolescents and children, fluoxetine (Prozac™) has been shown to induce suicidal ideation and behavior in a subset of adolescents due to unknown mechanisms.

Macaque mulatta, a nonhuman primate (NHP), is one of the best models for translational research on MDD due to its similarity with humans in brain structure and social behavior. Mass spectrometry (MS)-based quantitative proteomics has become one of the leading techniques in mechanistic studies, biomarker discovery, drug development and translational research. Aiming to elucidate mechanisms underlying the effects and side effects in children treated by fluoxetine, we took advantage of an established reproducible quantitative proteomic platform and conducted a system-level analysis of the proteome and phosphoproteome of 24 macaques under chronic fluoxetine treatment in the dorsolateral prefrontal cortex (DLPFC) and the cingulate cortex (CC). Subsequent bioinformatic analyses of the omics data identified a series of potential biomarkers and revealed significantly altered biological pathways in response to fluoxetine treatment.

2.5.1 Deep proteome and phosphoproteome profiling of macaque brain sections

One of the critical steps in quantitative proteomic analysis is sample preparation, which determines the quality of the proteomic datasets generated, especially for phosphoproteomics, which suffers from under-sampling and consequently poor reproducibility. We established a complete labeling quantitative proteomics and phosphoproteomics pipeline. Sample preparation procedure was optimized for compatibility with a large batch of tissue samples. TMT labeling of peptides and phosphorylation-enriched peptides was performed at high efficiency but low expense with an in-house protocol.

We have successfully identified and quantified a total of 6054 proteins, 10428

phosphopeptides and 12647 phosphorylation sites in macaque DLPFC and CC with an FDR of 1%, of which 32.7% of proteins, 40.3% of phosphopeptides and 43.0% of phosphorylation sites were unique in only one specific tissue. This indicates the existence of a global proteome and phosphoproteome difference between these two brain regions, probably resulting from different cell types. A considerable proportion of proteins and phosphorylation sites in the present study were identified for the first time due to the limited preexisting research. The comprehensive profiling yielded an integrated insight into the tissue-specific proteome and phosphoproteome of macaque brain, which is, to our knowledge, the largest proteome profiling of specific macaque brain regions to date. This provides a context to understanding biological signaling of nonhuman primates in psychiatric disorders and other diseases.

Mass spectrometry data in this study were acquired using the data-dependent acquisition (DDA) mode, where precursors from several of the most abundant ions are selected for fragmentation. As a consequence, the randomness in precursor ion selection led to increased numbers of missing values and thus lower reproducibility among different mass spectrometry runs, especially for large-scale proteomic analysis of a large batch of samples. We tackled this problem by coupling TMT isobaric labeling, a powerful quantification strategy for multiplexed deep proteome profiling, with high throughput and subsequent bioinformatic analysis. First, peptides and phosphopeptides were distributed into 3 groups and labeled with TMT tags, enabling the concurrent LC-MS/MC analysis of 10 samples including 2 internal standard samples for each MS run. Next, missing values that appeared upon dataset merging were imputed (MAR or MCAR, see Section 2.3). Subsequently, after comparison and evaluation of various bioinformatic algorithms, including internal reference scaling (IRS)[118], combat[119] and limma[120], batch effects caused by separate MS runs were eventually removed by a median polish algorithm TAMPOR[121]. PVCA analysis on normalized data verified the efficiency of removing the batch effect by TAMPOR. Our combined strategy managed to minimize the system error in DDA and obtain more accurate normalized quantification data free of batch specific variation, which can be subjected to bioinformatic analysis.

In particular, phosphoproteomic data are generally more heterogeneous than proteomic data. Protein phosphorylation is one of the major protein posttranslational modifications (PTMs) regulating protein function and signal transduction. The development of mass spectrometry has remarkably facilitated the study of phosphoproteomics, focusing on

phosphorylation on a large scale. Similar to genes, proteins and metabolites, dysregulated phosphorylation has also been demonstrated to be a hallmark of many diseases in many large-scale phosphoroteomic studies, including a variety of cancers[122-124], Alzheimer's disease[125] and diabetes[126]. However, very few investigations at the phosphoproteomic level have been carried out in the study of psychiatric disorders.

Despite the deep phosphoproteome profiling, and both the known and novel phosphorylation sites we have identified, the acquired phosphoproteomic data have several limitations: (1) the majority of phosphorylation sites in our macaque datasets lack functional annotation in public knowledge databases, especially for those with poor conservation between human and macaque. Follow up analysis or validation can be performed to verify the biological function of these phosphorylation sites. (2) Phosphoproteomics takes advantage of enrichment and measurement of phosphorylated peptides from phosphoproteins, one small subset of the total proteome, and thus interpretation of only phosphopeptide information does not offer an overview of the entire signaling pathway alteration. (3) Phosphoproteomics is characterized by under-sampling and the availability of tools in bioinformatics. A very limited number of phosphopeptides and phosphorylation sites are typically identified in a normal phosphoproteomic dataset.

In this project, I took advantage of phosphoproteomics dissection using networks (PHOTON) to overcome the shortcomings mentioned above. First, macaque/human homologous proteins were retrieved after gene annotation and sequence similarity comparison, which facilitates the subsequent analysis due to more annotation and better availability of human data in the database. Next, I established a robust, high-confidence (interaction score > 900) human protein-protein interaction (PPI) network using PPI information downloaded from the STRING database. Then the phosphopeptide changes in the original dataset were mapped with the established PPI network in a weighted manner to transform the raw phosphopeptide quantification data into functionality scores of proteins in the signaling network. Since proteins in the network are not limited to enzymes, e.g. kinases or phosphates, all biologically relevant proteins in the whole network are annotated by raw phosphoproteomic data, largely expanding the scale of the proteome. Finally, a p-value for each protein in every sample was estimated to represent its up- or down-regulated functionality. Phosphoproteomic data processed with PHOTON rendered more biologically meaningful outcomes at the protein level and thus were accessible to more common bioinformatics tools.

2.5.2 Protein and phosphorylation biomarkers associated with increased impulsivity of macaques in response to chronic fluoxetine treatment

In the present study, we examined the long-term effects of fluoxetine treatment on juvenile monkeys. Behavior tests (see Section 2.3) performed to assess the impulsivity of monkeys involved a reward delay behavior test designed to measure average screen intervals, average latency times and the number of trials[114]. Behavior tests confirmed that fluoxetine treatment increased the impulsivity of monkeys in both MAOA high and low genotypes; correlation was significantly negative with average screen intervals and average latency time, but positive with the number of trials. Linear regression between omics data and impulsivity test measurements was performed to investigate potential biomarkers that reflect the behavior-related side effect of fluoxetine. Using a stringent cut-off of the correlation coefficient ($R > 0.6$ unless stated otherwise), 21 proteins were identified as being highly correlated with fluoxetine treatment in DLPFC, and 23 proteins in CC. Among them, 3 proteins, FECH (Ferrochelatase), RAB12 (Ras-related protein Rab-12) and NFIA (Nuclear factor 1 A-type) in DLPFC, and 2 proteins, LOC720791 (Ribonuclease inhibitor) and CFL2 (Cofilin-2) in CC, showed significant association with all 3 readouts of the impulsivity test. The phosphorylation level of 25 sites in DLPFC and 41 in CC ($R > 0.65$) showed high correlation with impulsivity outcomes, of which S507 and T509 phosphorylation of DPYSL2 (Dihydropyrimidinase-related protein 2) correlated with impulsivity in both DLPFC and CC.

Ferrochelatase (FECH) is the terminal enzyme of the heme biosynthetic pathway in all cells. Evidence from translational research has shown that FECH is associated with MDD and anxiety disorder; FECH was identified as one of the 26 biomarkers by genome-wide transcriptomic profiling of the blood from two animal models of depression and validated by unbiased analyses of the 26 transcriptomic markers in blood samples of 15–19-year-old adolescents ($N = 14$) with MDD[127].

The Ras superfamily is an evolutionarily conserved protein superfamily of small GTPases. As a subfamily of Ras, Rab was reported to be linked with psychiatric disorders. Rab gene mutations were found in patients suffering from psychiatric and neurodevelopmental disorders[128]. In a study where a 2-DE proteome profiling approach was used to examine changes occurring in rat brain proteins after treatment with fluoxetine, Rab proteins were found to be modulated, indicating an increase in neuronal

vesicular cell trafficking and synaptic plasticity after chronic fluoxetine treatment[129]. Other Ras proteins were also demonstrated to be involved in depressed suicide[130]. However, Rab-12 was found in the context of depression and impulsivity for the first time in this current study.

NFIA, a member of the Nuclear Factor I family of transcription factors, is critical for normal brain development and function, and was reported in association with behavioral abnormalities such as bipolar disorder and depression [131-133].

As the major ADF/cofilin isoform in mammalian neurons, CFL (cofilin) influences the dynamics of actin assembly by severing or stabilizing actin filaments, and plays a central role in regulating actin filament dynamics[134]. A previous study showed that repeated treatment with the selective serotonin reuptake inhibitor (SSRI) sertraline altered the expression of lysophosphatidic acid (LPA)-downstream genes in rodent brain, including cofilin[135].

We also compared our phosphorylation site candidates to a published phosphoproteomic analysis of major depressive disorder postmortem brains, where 90 phosphoproteins showed different levels of phosphorylation in postmortem brain tissues from MDD subjects compared to controls. Three phosphoproteins with distinct phosphorylation sites were reproduced in our datasets. Whereas S415 and S542 on DPYSL2, S721 in MAPT and S409 in CNP were found to be linked with depressed suicide in the reported study, we discovered that S507 and T509 on DPYSL2, S61 on MAPT and S312 in CNP were closely associated with increased impulsivity caused by chronic fluoxetine treatment.

DPYSL2 (or CRMP2, dihydropyrimidinase-related protein 2) acts in the regulation of axon guidance, vesicle trafficking and synaptic function, and has been shown to bind and be modulated by antidepressants and neuroactive molecules[136]. DPYSL2 has been associated with several neuropathologic or psychiatric conditions at the level of genetic polymorphisms, protein expression, post-translational modifications, and protein/protein interactions. Although widely reported to play an important role mainly in schizophrenia, DPYSL2 has also been identified as a marker for escitalopram resistance in a stress model of depression[137]. A meta-analysis of the neurobiology of suicidal behavior, and a functional protein network analysis of post mortem tissue samples from the prefrontal cortex[138] and amygdala of suicide victims, as well as a chronic unpredictable mild

stress rat model also demonstrated the potential of DPYSL2/p-DPYSL2 as a biomarkers of depressed suicide[139, 140].

Here, we propose that phosphorylation of DPYSL2 on Ser507 and Thr509 could be biomarkers in depression-related suicidal ideation and behavior under long-term fluoxetine treatment due to its significant association with impulsivity changes in juvenile monkeys. While Thr509 phosphorylation of DPYSL2 has been widely linked to cancer in numerous studies[141], there is no published data directly correlating phosphorylated DPYSL2 with MDD and suicide to date.

The Tau protein, one of the microtubule-associated proteins (MAPs) encoded by the MAPT gene, plays an important role in maintaining neuron morphology and promoting axonal development in the cytoskeleton system[142]. Tau proteins are the transport channels of axons and dendrites, and phosphorylated Tau regulates this function during normal neuron maturation[143]. It has been found in previous studies that chronic unpredictable mild stress (CUMS) can induce hyperphosphorylation of Tau protein at Ser202, Thr231, Ser262, and Ser396/404 sites of hippocampal neurons, and fluoxetine reduced the levels of hyperphosphorylated Tau protein[144, 145]. S61 phosphorylation of MAPT was only reported in a breast cancer research[146]. In the current study, we report for the first time that phosphorylation of MAPT on S61 correlates with monkey impulsivity.

The CNP gene encodes the enzyme 2',3'-cyclic nucleotide 3'-phosphodiesterase (CNP), which is expressed in the development of oligodendrocytes (OLs) and increases with the onset of myelination, remaining detectable throughout life[147]. A microarray analysis of postmortem tissue from depressive individuals showed that myelination or OL-lineage-related transcriptional genes, including CNP, were involved and differentially regulated[148]. A significant reduction in CNP was also observed at both transcriptome and proteome levels in the postmortem brains of patients with MDD[147]. Another study also reported that CNP loss-of-function genotypes were causative in MDD[149]. The phosphorylation of S312 presented here is a novel phosphorylation site that was poorly investigated in preexisting studies.

Our correlation between animal impulsivity tests and proteomic/phosphoproteomic data reproduced several pre-reported MDD/suicide relevant biomarker candidates (as discussed above) at both protein and posttranslational modification (phosphorylation)

levels. We also discovered a few novel potential biomarkers, including RNH1 and S61 phosphorylation of MAPT. The biological functions of all of these biomarker candidates are highly relevant to MDD and suicidal ideation/behavior and are worthy of follow-up validation to provide hallmarks of depression-related suicide.

2.5.3 GABAergic signaling is involved in the response to fluoxetine treatment

Although monoamine deficiency is the most well-studied hypothesis for MDD, some emerging evidence has implicated a Gamma-amino butyric acid (GABA) deficit in a hypothetical model of MDD[150]. GABA is the major inhibitory neurotransmitter in the mammalian central nervous system. In some genomic studies, several genes related to the glutamate/GABA system have been reported to be associated with MDD and suicidal behavior[151-153]. Some preliminary studies have revealed a negative correlation between GABAergic function and impulsivity, consistent with a simple model of GABAergic function playing an inhibitory role on affectively driven impulsivity behavior including suicidality[154]. Several pharmacological treatments that decrease impulsivity-related symptoms were found to be linked with pro-GABAergic mechanisms[155]. Studies of peripheral GABAergic function have found evidence of decreased plasma GABA levels associated with impulsivity[156]. Postmortem microarray studies of suicide and/or MDD also reported differential expression of GABA receptor subunits[157-160]. In addition, our previous metabolomic study revealed that 5-aminovaleric acid lactam, a GABA homolog shown to be a weak GABA agonist[161], was significantly altered in both plasma and CSF of fluoxetine-treated juvenile monkeys[114]. The metabolism of nicotinamide, an endogenous GABA receptor ligand, was also found to be affected by fluoxetine treatment in previous data[114], suggesting the involvement of the GABAergic system in MDD and/or suicidal ideation and behavior.

Consistent with the previous metabolomic profiling study mentioned above [114], in my current proteomic study I discovered that both protein and phosphorylation events related to GABAergic synapses were involved in the response to fluoxetine treatment in juvenile monkeys. Fluoxetine treatment induced downregulation of GABA B receptor, a key regulator of membrane excitability and synaptic transmission in the brain, in both DLPFC and CC. The GABA B receptor is a G-protein coupled receptor (GPCR) that associates with a subset of G-proteins (pertussis toxin sensitive Gi/o family), which in

turn regulate specific ion channels and trigger cAMP cascades. Overexpression of $G\alpha_i$ proteins (GNAI1, GNAI2 and GNAI3), which are expected to inhibit adenylate cyclase (ADCY), caused by downregulation of GABA B receptor was also observed. This further induces the inhibition of ADCY, a family of proteins that synthesize cAMP from ATP. Consequently, inhibition of ADCY affects the activation of downstream cAMP-PKA signaling pathway-associated biological processes, probably via gene transcription.

However, my study has two limitations. Firstly, no direct evidence was found in my data suggesting how fluoxetine diminished the expression of GABA B receptors. As a selective serotonin reuptake inhibitor, fluoxetine has been known to augment serotonin concentrations within the synapse by inhibiting the serotonin transporter. Although an association between fluoxetine and brain GABA levels was reported, the mechanism of the indirect action mode was not elucidated in that study[162]. The role of GABA or GABAergic function and/or fluoxetine in suicide should also be further investigated.

Secondly, how inhibition of the cAMP-PKA pathway regulates the downstream signaling pathway to exert its action is not explained by my data. In a typical cAMP-PKA pathway, the association of cAMP with the regulatory components of PKA causes dissociation of the tetramer, allowing the free, active catalytic subunits of the kinase to phosphorylate target proteins including CREB, which binds the cAMP response element (CRE) and alters gene transcription, as well as phosphorylating a variety of other proteins, such as BAD, PLCγ1 and histone H3. Although suppression of BAD was also found in our data, other downstream substrates of PKA were not identified. Further investigation is required to confirm the change in PKA activity.

In conclusion, in my project focusing on the impulsivity-related side effect of fluoxetine on juvenile macaque monkeys, I identified several biomarkers that are associated with increased impulsivity. My data also indicate a downregulation of GABA B receptor-mediated GABAergic synapse function, which might play a role in the chronic side effects of fluoxetine in children.

3 Novel antidepressant drug target identification

3.1 Background

3.1.1 Drug repurposing and target deconvolution

It is estimated that bringing one entirely new drug to the market currently requires 13–15 years and costs $2–3 billion on average[163]. Therefore, repurposing (also known as repositioning or reprofiling) of "old" drugs is becoming increasingly popular in drug research and development (R&D). Drug repurposing is a strategy in the drug industry that attempts to discover novel uses for approved drugs beyond their conventional medical indication [164]. The advantages of this strategy over developing completely new drugs include better drug safety, shorter development periods and lower R&D costs, which ensures higher success rates.

So far, the majority of known drugs are small molecule compounds and they mostly take effect through binding or interacting with cellular proteins. Some natural products or currently used drugs have been repurposed as strongly potent novel drugs with good biological activity in relevant diseases, but the protein target and mechanism of action are usually unclear. Therefore, drug target deconvolution is one of the crucial steps in drug discovery, shedding light on the mechanism of the action of a drug. Identification of targets and potential off-targets of a drug is very important for understanding its mode of action and potential adverse effects.

Distinct and complementary methods are available for discovering the protein target of a small molecule, including indirect methods such as genetic and computational approaches and direct methods, which will be mentioned in later sections.

3.1.2 Ketamine as an antidepressant

Glutamate is the anion of glutamic acid and plays a very important role in neurotransmission. As the major excitatory neurotransmitter in the brain, glutamate is thought to be widely present in synapses. Biochemical receptors of glutamate are mainly divided into two classes, the ionotropic glutamate receptor including the α-amino-3-hydroxy-5-methyl-4-isoxazolepropionic acid receptor (AMPA receptor or AMPAR), the N-methyl-D-aspartate receptor (NMDA receptor or NMDAR), the kainic acid receptor (KAR) and the metabotropic glutamate receptor (mGlu receptor or mGluR).

Ketamine, or (R, S)-ketamine, is a racemic mixture that consists of equal parts of (R)-ketamine (or arketamine) and (S)-ketamine (or esketamine). As an NMDAR antagonist often used in starting and maintaining anesthesia, it was discovered in 1962 and approved for anesthetic use by the US Food Drug Administration (FDA) in 1970 after another general anesthetic phencyclidine (PCP) was terminated in medical use due to its serious side effects, such as hallucinations, postoperative delirium, and confusion[165]. Later in 1983, ketamine was confirmed to be NMDAR antagonist (Ki = 0.53 μM)[166]. Consistent with its higher binding affinity to NMDAR, (S)-ketamine (Ki = 0.30 μM) shows ~3-4 fold greater anesthetic potency as well as psychotomimetic side effects than (R)-ketamine (Ki = 1.4 μM)[167, 168]. So far, ketamine has been used widely despite some psychotomimetic and dissociative effects, and abuse potential.

The antidepressant-like effects of ketamine were first reported in 1975 in animal models. In this study, ketamine was found to possess antidepressant activity over a wide range of oral doses in different animal models including reversal of tetrabenazine-induced ptosis in mice, reversal of reserpine-induced hypothermia in rats, enhancement of yohimbine toxicity in mice and inhibition of oxotremorine-induced tremors in mice, although the activity was less than that of imipramine[169]. After confirmation of ketamine's inhibiting effect on NMDAR, the potential antidepressant effect of other NMDAR antagonists was also investigated in many studies. AP-7 and (+)-MK-801 were found to have antidepressant-like effects in rodents, followed by the discovery that CGP-37849 and eliprodil also had antidepressant-like effects in depressed animal models[170-176]. Therefore, NMDAR antagonists have drawn much attention in the discovery of novel antidepressants.

In 2000, the antidepressant effect of ketamine in humans was first investigated in a double-blind, placebo-controlled study, where Berman et al. showed that a single intravenous (i.v) infusion of ketamine (0.5 mg/kg) produced a rapid acting and sustained antidepressant response in MDD patients[177], which was similarly confirmed in patients suffering from TRD [178]. Subsequently, a series of studies demonstrated that ketamine also has robust effects in patients with not only MDD but also bipolar depression (BD) including those with suicidal ideation [179-183].

As mentioned above, ketamine is a racemic mixture of (R)-ketamine and (S)-ketamine. Despite lower binding affinity to NMDAR, in 2014 (R)-ketamine was found to have better

potency and longer lasting antidepressant effects than (S)-ketamine in a neonatal dexamethasone-treated model of depression [184]. The following study reported the same result in neonatal dexamethasone-treated, chronic social defeat stress (CSDS), and learned helplessness (LH) models of depression in rodents [184-187]. Moreover, the detrimental side effects of (R)-ketamine were found to be lower than those of ketamine and (S)-ketamine in rodents and monkeys [188-190]. Some other studies also verified that (S)-ketamine contributes more to the acute side effects of ketamine than (R)-ketamine [191]. All these findings, together with the fact that some non-ketamine NMDAR antagonists (i.e., memantine, traxoprodil, lanicemine, rapastinel and AV-101) did not exhibit robust ketamine-like antidepressant effects [181, 182], have suggested that NMDAR inhibition may not play a key role in the antidepressant actions of ketamine. Despite several concerns about its efficacy and side effects, (S)-ketamine has been approved in both the USA and Europe as a nasal spray in the treatment of TRD, and clinical trials of (R)-ketamine in humans are currently under study. Given the evidence from previous studies that (R)-ketamine has greater potency and fewer side effects than (S)-ketamine, it is promising that (R)-ketamine may become a safer antidepressant [192].

3.1.3 (2R,6R)-hydroxynorketamine (HNK) as an antidepressant

Ketamine undergoes extensive metabolism initially via nitrogen demethylation to norketamine, and is then further metabolized to the hydroxynorketamines (HNKs) and dehydronorketamine (DHNK), or in some minor cases, metabolized to other products[191] (Figure 3.1). In 2016, it was reported that the derivative (2R,6R)-HNK (Ki > 10 μM for NMDAR), the metabolite of (R)-ketamine, exerted antidepressant effects in rodent models without exerting the undesirable side effects of (R,S)-ketamine (i.e. hyperlocomotion, pre-pulse inhibition deficits, motor incoordination, and abuse liability), generating a new hypothesis that (2R,6R)-HNK is essential for the antidepressant effect of ketamine, and AMPAR but not NMDAR is involved in the antidepressant-like effects of ketamine/HNK [186]. This result was replicated later in research in rodents [193-195]. However, (2R,6R)-HNK was demonstrated not to bind directly to functionally activated AMPARs. Furthermore, (2R,6R)HNK failed to evoke AMPAR-centric changes in any electrophysiological endpoint from adult rodent hippocampal sections[196]. It was further confirmed in another study where the AMPAR potentiator Org 26576 did not show antidepressant effects in depressed patients, suggesting that (2R,6R)-HNK is not involved in AMPAR functioning[197].

In another study (2R,6R)-HNK was demonstrated to inhibit synaptic NMDARs, indicating that (2R,6R)-HNK indeed acts in an NMDAR-dependent but not NMDAR-independent manner [198]. Regarding other mechanisms of action of (2R,6R)-HNK, it is also suggested that the group II metabotropic glutamate receptor subtypes 2 (mGlu2) are involved, since the antidepressant effect of (2R,6R)-HNK was blocked in mice lacking the Grm2 gene but not the Grm3gene[199]. It was also reported that astrocytic cyclic adenosine monophosphate (cAMP)-dependent brain-derived neurotrophic factor (BDNF) may be involved in the antidepressant actions of ketamine and (2R,6R)-HNK[200].

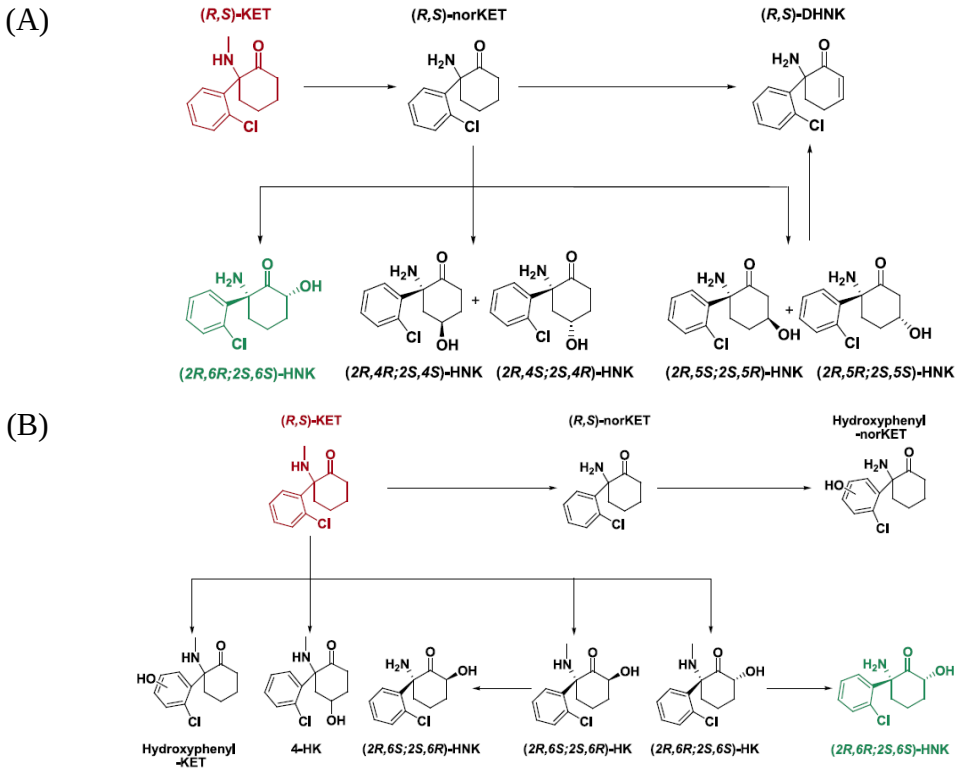

Figure 3.1 Metabolic pathways of ketamine. (A) major metabolic pathway where ketamine is metabolized into HNKs or DHNKs; (B) minor metabolic pathway where ketamine is metabolized into other products[191].

In contrast, some studies showed that (R)-ketamine, but not (2R,6R)-HNK, exhibits rapid and long-lasting antidepressant effects in three different rodent models, indicating that (2R,6R)-HNK does not possess an antidepressant effect [201, 202]. Pretreated by two cytochrome P450 (CYP) enzymes inhibitors (ticlopidine hydrochloride and 1-aminobenzotriazole), the metabolism of (R)-ketamine to (2R,6R)-HNK was blocked but the antidepressant effects after (R)-ketamine (3 mg/kg) injection were retained. However, these effects disappeared in the absence of CYP inhibitors when treating with the same dose of (R)-ketamine, suggesting that the conversion of (R)-ketamine to (2R,6R)-HNK was unnecessary for its antidepressant effects[203]. Thus while (R)-ketamine was shown

to exert antidepressant-like effects partly via conversion to (2R,6R)-HNK[204], more studies indicated that (R)-ketamine itself is responsible for its antidepressant effect[205, 206].

3.1.4 Proteomics-based protein-drug interaction identification

Two different strategies are commonly used in proteomics-based protein-drug interaction identification: a labeling strategy and label-free strategy.

The most developed and widely used labeling strategy is activity-based protein profiling (ABPP). ABPP is one of the most commonly used chemical proteomic approaches that uses small-molecule probes to identify the interaction between compounds and protein targets and to understand the mechanisms of compounds in terms of their action mode[207]. Small-molecule probes are first designed and synthesized before the ABPP process begins. In principle, a probe consists of a reactive group, a linker and a reporter group. The reactive group of the drug interacts directly with target proteins and the reporter group helps fish these proteins out, such as fluorescent groups, biotin, alkynes or azide, which can be used in target protein enrichment via "click chemistry" reactions. A typical ABPP workflow (Figure 3.2) goes as follows: (i) incubation of the probe with the proteome of interest (cell, tissue or lysate); (ii) (for highly active reporter groups like "clickable" groups) perform copper (I)-catalyzed azide-alkyne cycloaddition (CuAAC, the most widely used click chemistry reaction) to label the drug-protein complex with a detectable label; (iii) run quantitative proteomics or fluorescence scanning after pull-down of target proteins according to the detectable labels used[208, 209].

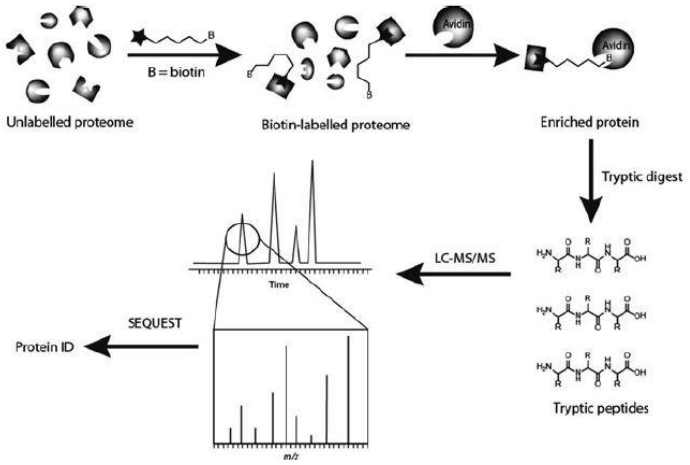

Figure 3.2 LC-MS-based ABPP platforms[207]. Proteomes are labeled with a biotinylated ABPP probe. The labeled proteome is then incubated directly with (strept)avidin beads to pull down target proteins. Enriched proteins are then

subjected to gel-based analysis or to on-bead tryptic digestion followed by analysis with LC-MS/MS. Proteins identified after database searches are potential protein targets[210].

Chemical modifications require expertise in organic or synthetic chemistry and knowledge about the activity of modified drugs. In some cases, the drug of interest does not contain any suitable site for chemical modification or loses biological activity after modification. Consequently, a series of label-free strategies have emerged and been used to investigate protein-drug interactions on a proteomic scale for a number of small molecule compounds.

3.1.4.1 Drug affinity responsive target stability (DARTS)

DARTS is a label-free proteomic method used to identify protein-drug interaction, first developed by the Huang lab [211]. The basic principle of DATRS is that binding of drugs stabilizes target proteins, thereby reducing their sensitivity to proteases and thus proteolysis efficiency (Figure 3.3). Upon exposure to experimentally determined proteases, target proteins behave more conservatively than non-target proteins, which can be monitored by detecting non-/less-digested proteins by SDS-PAGE[212] or LC-MS/MS[213].

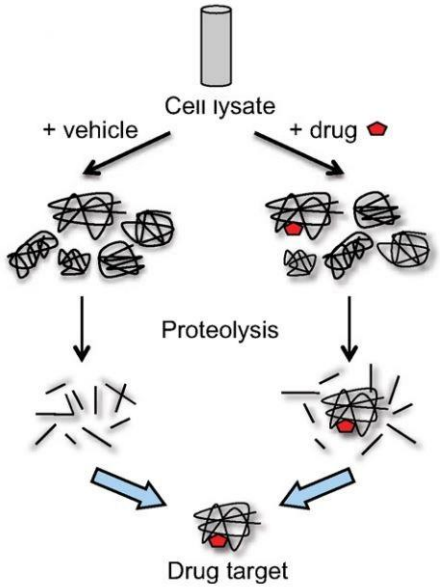

Figure 3.3 Scheme of DARTS [211]. After incubation, binding of drugs is proposed to stabilize target proteins. Decreased protease susceptibility of the target protein leads to less complete digestion by non-specific proteases. Remaining proteins after partial digestion are enriched through centrifugal filters and then subjected to complete digestion followed by LC-MS/MS analysis.

DARTS enables direct protein target identification that is especially suitable for low-affinity bindings between protein and drug due to the absence of wash steps in sample preparation[214]. However, DARTS is limited in some studies in terms of identifying low-abundance proteins or smaller proteins. Proteins with low abundance are likely to be missing in DARTS after proteolysis on a proteome scale, resulting in false negative results. Small proteins (<5 kDa) close in size to the proteolytic fragment of larger proteins might be wrongly excluded from potential target protein lists.

3.1.4.2 Stability of proteins from rates of oxidation (SPROX)

SPROX is a method similar to DARTS, also based on protein stabilization upon drug binding[215]. Unlike DARTS, SPROX measures methionine oxidation under chemical denaturation as the readout of stabilization. A typical SPROX workflow is shown in Figure 3.4. Briefly, target protein stability is increased by drug binding after incubation. Then hydrogen peroxide oxidizes methionine different degrees in the presence of a gradient of guanidinium hydrochloride (GdmCl). After the oxidation reaction is quenched, proteins are subjected to trypsin digestion and LC-MS/MS to calculate the oxidation level on methionine. Compared to non-target proteins, target proteins are more stable and less sensitive to denaturation, and in principle show different oxidation curves.

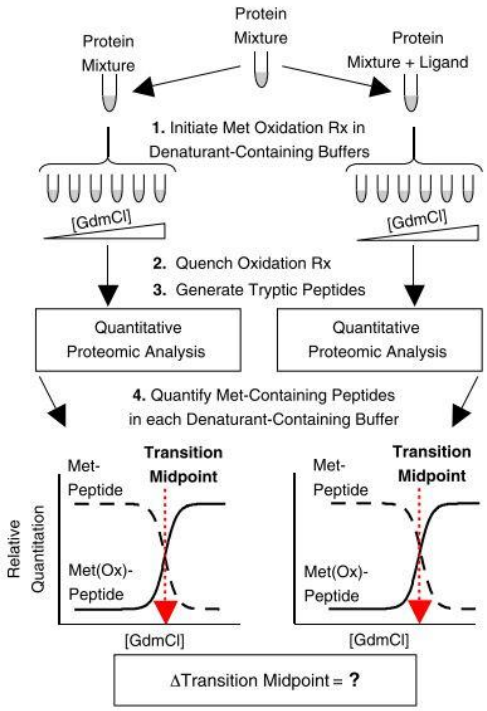

Figure 3.4 Schematic representation of SPROX [215]. In both control and drug-treated group, aliquots of the protein mixture are distributed into a series of samples with increasing concentrations of a chemical denaturant (GdmCl). Each

aliquot is then treated with the same amount of hydrogen peroxide for a certain time to reach selective oxidization on the thioether groups in the side chain of methionine residues. Then oxidization is quenched and samples are subjected to LC-MS/MS sample preparation and analysis. Oxidized methionine-containing peptides are quantified as a function of the SPROX buffer denaturant concentration, which can be used to recognize target proteins.

However, one of the major disadvantages of SPROX is the dependence on methionine, since quantification by LC-MS/MS strongly depends on the number of identified methionine-containing peptides, which leads to limited proteomic coverage.

3.1.4.3 Chemical denaturation and protein precipitation (CPP)

CPP is also a newly developed approach to protein-drug interaction analysis[216]. Similar to SPROX, CPP is also amenable to the detection of drug targets on the basis of chemical denaturation of the protein. Moreover, CPP is highly preferred when larger proteomic coverage is required. The CPP protocol developed involves incubating the drug or vehicle with cell lysates, followed by chemical denaturation of proteins with increasing concentrations of GdmCl, protein aggregation after GdmCl dilution, centrifugation of precipitates and LC-MS/MS analysis of supernatants or pellets (Figure 3.5). Sample pre-conditioning in CPP is similar to that of SPROX, but incorporated protein precipitation is performed instead of methionine oxidation, thus greatly improving proteomic coverage. In a CPP experiment, proteins in the soluble fraction decrease with the increase in GdmCl concentrations, while proteins in the pellet increase. If direct binding between a protein and a drug is present, the curve representing the protein folding equilibrium will be shifted towards higher GdmCl concentrations.

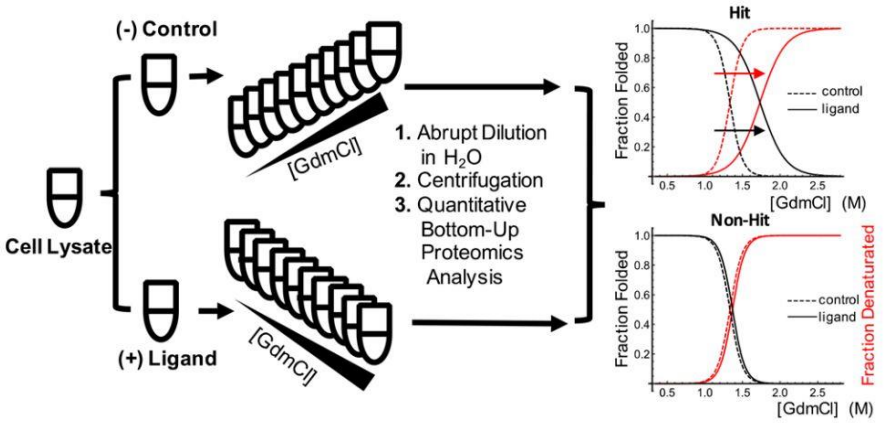

Figure 3.5 Workflow of CPP [216]. Necessary steps include: incubation with the drug (ligand), denaturation with GdmCl, abrupt dilution in H_2O, removal of aggregates and precipitations, and LC-MS/MS analysis of the supernatant-containing

target proteins. WHY on the left "Control" is at the top, yet on the right "Hit" is on the top…. Not logical. Also do not use all capital letters, e.g. Abrupt dilution…

One of the advantages of CPP is that the extent to which the curve is shifted can be used to quantify the affinity of the corresponding protein-drug interactions. In addition, indirect binding may also result in a change in folding equilibrium, indicating that CPP may also act as a useful tool in the discovery of potential protein-protein interactions upon drug binding.

3.1.4.4 Solvent-induced protein precipitation (SIP)

SIP was recently established by the Ye lab[217]. Proteins are denatured and precipitated by the addition of organic solvents, which decreases their dielectric constant and causes competition for protein hydration; thus it could also be developed to screen drug targets or off-targets based on a similar principle to SPROX and CPP. Briefly, the cell lysate is incubated with a drug or vehicle control and treated with a particular percentage of organic solvent mixtures to precipitate the proteins (Figure 3.6). Soluble fractions are collected after centrifugation and subjected to MS sample preparation and analysis. A change in protein quantification results indicates potential drug binding to a target.

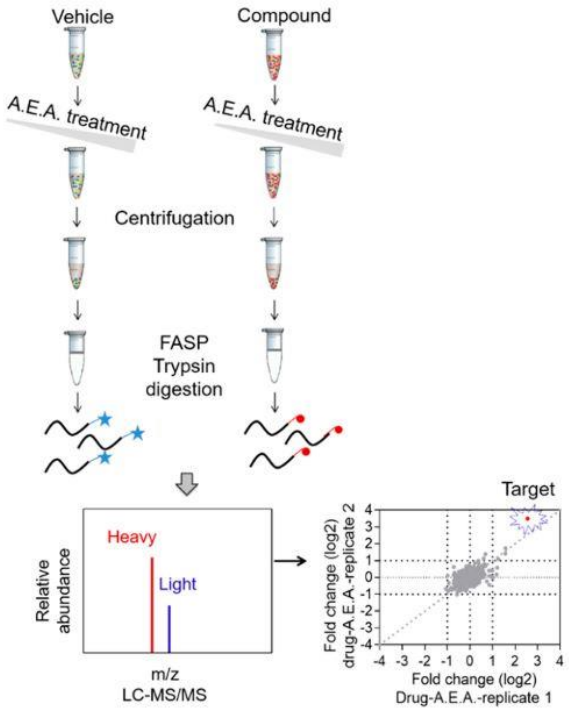

Figure 3.6 Schematic representation of SIP for screening drug targets[217]. A cell lysate is incubated with (or without) drugs and treated with a particular percentage of an organic solvent mixture to precipitate the proteins. Soluble proteins are then separated and subjected to LC-MS/MS sample preparation and analysis.

3.1.4.5 Cellular thermal shift assay (CETSA)

CETSA is an emerging and powerful methodology to identify drug targets in non-labeled manner [218]. The principle of CETSA lies in the altered thermodynamic stability of target proteins when bound to a drug. In a CESTA experiment, compound or vehicle control-treated cell lysates or intact cells are heated under different temperatures to cause protein aggregation and precipitation. Due to protection by the drug, target proteins remain in soluble fractions, and are then separated by centrifugation and visualized by Western blots (WB). The shift in melting temperature (Tm, the temperature where 50% of one protein remains in the soluble fraction) indirectly indicates potential binding between a drug and a protein. Moreover, a complementary method called isothermal dose-response fingerprint (ITDRF) can be applied to confirm the results from CETSA. In contrast to CETSA, in ITDRF cell lysates or cells are treated with different doses of drugs and then heated at a fixed temperature in order to assess whether the drug concentration affects a potential binding event.

Thermal proteome profiling (TPP) is mass spectrometry coupled to CETSA (MS-CETSA), and is capable of identifying protein-drug binding on a large scale [219]. As a combined workflow of CETSA and quantitative mass spectrometry, TPP enables proteome-scale profiling of protein thermal stability and unbiased measurements of protein-drug interactions. In a TPP experiment (Figure 3.7), after CETSA treatment, instead of using WB, all soluble proteins obtained at different temperatures are subjected to proteolysis, and the resulting peptides are further labeled by a tandem mass tag (TMT) reagent to be quantified using the isobaric labeling strategy of LC-MS/MS. This usually results in a thermal shift curve and the shifted Tm for each protein, which are later used as the criteria for selecting target or off-target proteins. Similarly, ITDRF can also be coupled with multiplexed quantitative mass spectrometry to trace protein stability at the proteome level.

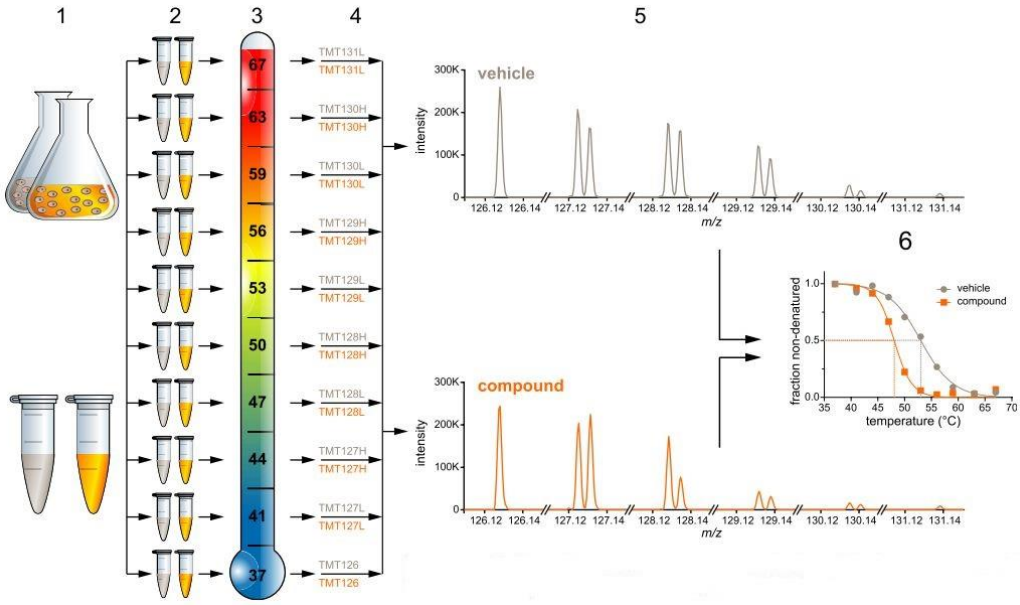

Figure 3.7 Quantitative proteome-wide profiling of protein thermal stability[219]. (1) Cells or lysates are treated with a drug or vehicle. (2) For each condition, cells or lysates are divided into 10 aliquots. (3) Aliquots are subjected to heating at the indicated temperatures. (4) Cells are lysed (if applied to living cells), and after centrifugation supernatants are digested with trypsin, and peptides are labeled with TMT10. (5) All aliquots belonging to the same single condition are merged and analyzed by LC-MS/MS. (6) Thermal melting curves are fitted based on the quantitative results.

A complete MS-CETSA experiment involves a huge number of samples that incur high costs for isobaric labeling, and take up to months to finish sample preparation and MS measurements for only a very few compounds or doses of interest. Most recently, a simplified CETSA workflow called an isothermal shift assay (iTSA) has been developed to increase throughput using TPP and statistical power to detect proteome-wide thermal stability shifts upon drug binding [220]. In contrast to the Tm in TPP, the shift of thermal stability in iTSA is detected by quantifying the difference in the soluble protein fraction at only one temperature with reduced sample scale. This simplified principle allows more biological replicates in sample preparations, which strengthens the statistical power to discover more confident hits.

An alternative to TPP (or MS-CETSA), called 2D difference gel electrophoresis based CETSA (2D-CETSA) has been developed, also aiming at unbiased profiling of thermal stability-shifted proteins[221]. In brief, cell lysates are similarly treated with a drug or vehicle control and subjected to thermal denaturation under different temperatures (Figure 3.8). After centrifugation, each soluble fraction is labeled with Cy3 or Cy5, and combined samples including an internal standard labeled with Cy2 are separated by Two-

Dimensional Difference Gel Electrophoresis analysis. Normalization is performed between gels based on a Cy2 stained standard. As a result, target proteins with changed stability due to drug binding are visualized as red spots (stabilized) or green spots (destabilized). Subsequent identification of these proteins is performed by LC-MS/MS after in-gel digestion.

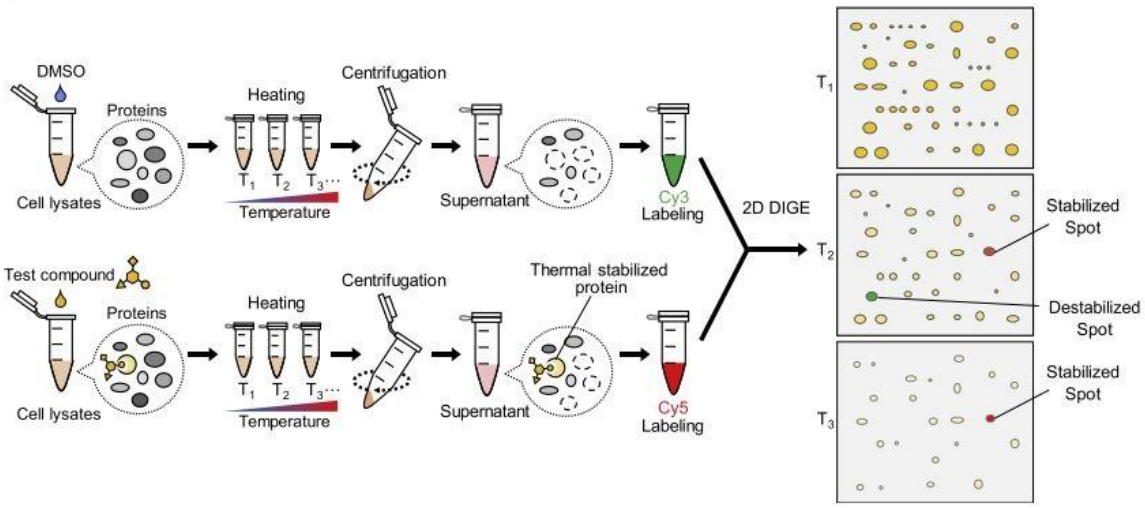

Figure 3.8 Scheme of 2DE-CETSA. Cell lysates are treated with a vehicle control or the test compound and then heated over a range of temperatures. After centrifugation the supernatants are labeled with Cy3 or Cy5, mixed, and then analyzed by 2D DIGE. Targets proteins with shifted stability are detected as red or green spots on the 2D gel.

TPP also has some significant drawbacks. For example, TPP requires multiplexed samples to be measured with TMT in the same MS run, incurring high costs and labor in sample preparation, and severely challenging the reproducibility of the results. Besides, like many non-denatured protein-ligand interaction methods, in most cases TPP is not compatible with membrane proteins due to their low stability and solubility even although they are “druggable”. Efforts are being made to resolve these obstacles.

3.1.4.6 Limitied proteolysis (LiP)

LiP monitors protein conformation or structure changes and also indicates potential drug binding at a global scale in cells [222]. Conventionally, the structure of a purified protein has been analyzed by X-ray crystallography, nuclear magnetic resonance (NMR) and other spectroscopic techniques. However, LiP investigates protein structure changes upon drug binding in a proteome-wide manner. The LiP workflow includes lysate extraction, drug incubation, native proteolysis, complete proteolysis and mass spectrometry analysis (Figure 3.9). Briefly, a total proteome is extracted from various biological sources

including cells or animal tissues under non-denatured condition, followed by drug or vehicle treatment. Then lysates are first digested with a broad-specificity protease for short time to achieve partial degradation, generating large protein fragments with random termini. Subsequently, a second-round digestion is performed under completely denaturing conditions, generating peptides with tryptic termini suitable for LC-MS/MS analysis. A control experiment is performed on an aliquot of the same proteome but with only one-step full trypsinization. The binding event or the potential binding sites can be discovered by comparing peptides with tryptic termini between the LiP sample and control sample. Full-length tryptic peptides containing LiP sites (possible drug binding sites) should to be more abundant than those without LiP sites upon drug binding (condition 2). In contrast, shorter tryptic peptides of target proteins will be more abundant without drug binding (condition 1).

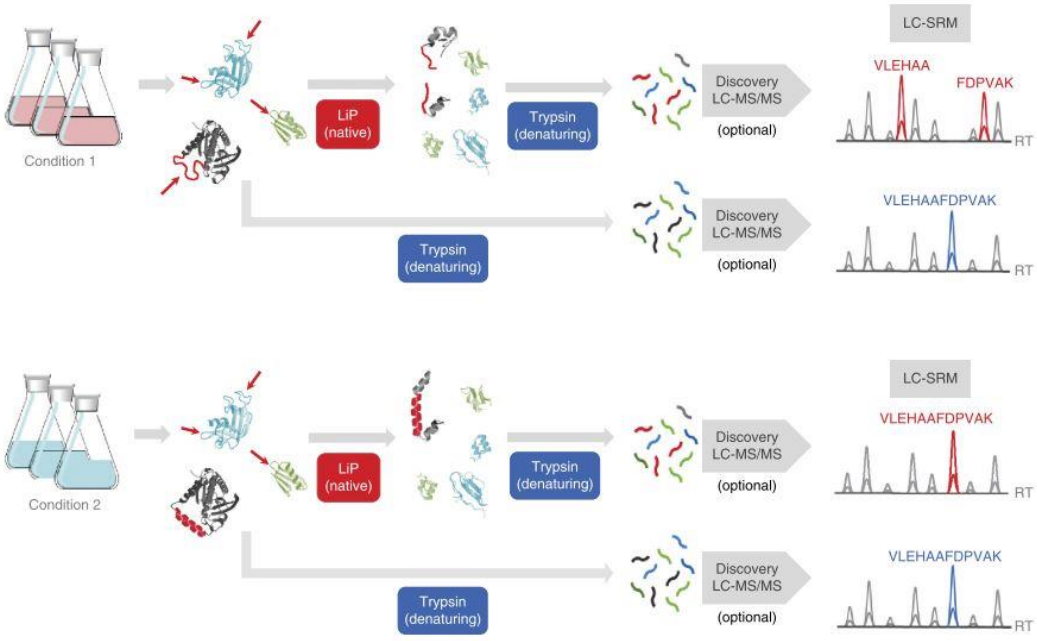

Figure 3.9 LiP workflow. Lysates obtained from cells or tissues under nondenaturing conditions are incubated with a drug or vehicle. Limited proteolysis is conducted with a broad-specificity protease (e.g. proteinase K) for a short time, followed by a complete digestion with trypsin under denaturing conditions. As a control, a fraction of the same sample is only subjected to the trypsin step under denaturing conditions. Samples are subjected to LC-MS/MS analysis and in-pair comparison. A full-length tryptic peptide containing a LiP cleavage site (possible drug binding site) will be detected in the trypsin control and replaced by two shorter tryptic halves in the sample subjected to LiP.

3.2 Research Aims

The antidepressant effects of ketamine are now well documented by several clinical studies with patients suffering from MDD. However, the mechanisms underlying the antidepressant effects remain unclear despite almost 20 years of investigation. Elucidation of the precise molecular and cellular mechanisms relies on identifying the functional protein targets of ketamine and/or its metabolites.

The aim of my PhD project was to identify and verify binding proteins of ketamine and its metabolite HNK that may represent drug targets using a series of mass spectrometry-based proteomic techniques. Specifically, the following topics were addressed:

1. Establishing a mass spectrometry platform in combination with different methodologies aimed at identifying protein-ligand interactions. Labeling/label-free quantitative proteomics was to be applied to screen potential binding targets of ketamine and HNK. These included both MS1 (SILAC) and MS2 (TMT) labeling strategies for accurate protein quantification of the protein target(s) (discovery phase).

2. Applying bioinformatic analysis to all potential target proteins originating from the discovery phase to narrow down the protein list, resulting in a few high-confidence protein targets biologically relevant for the mechanism of the ketamine/HNK antidepressant effect.

3. Functionally validating selected protein targets with different biochemical or electrophysiological methodologies to verify the biologically effective binding events between ketamine/HNK and proteins. On the basis of these findings, potential mechanisms of the action of ketamine/HNK should result in a better understanding of ketamine's antidepressants effects and support the discovery of novel antidepressants with a similar mode of action.

3.3 Material and methods

3.3.1 Reagents and instruments

Table 3.1 Chemicals used in the present study

Reagent	Company
(±)-Ketamine hydrochloride	Sigma
(2R,6R)-Hydroxynorketamine hydrochloride (R-HNK)	Sigma
(2S,6S)-Hydroxynorketamine hydrochloride (S-HNK)	Sigma
2-Iodoacetamide (IAM)	Sigma
4-(2-hydroxyethyl)-1-piperazineethanesulfonic acid (HEPES)	Sigma
Acetic acid	Merck
Acetone	Merck
Acetonitrile (ACN)	Merck
Acrylamide/Bis 30%	Serva
Ammonium Persulfate (APS)	Sigma
anti-COMT antibody	Santa Cruz
Anti-mouse IgG HRP-linked Antibody	Cell signaling Technology
anti-PKLR antibody	Thermo Fisher
Anti-rabbit IgG HRP-linked Antibody	Cell signaling Technology
anti-STXBP1 antibody	Thermo Fisher
BCA protein assay	Thermo Fisher
Coomassie brilliant blue R250	Biorad
Dulbecco's Modified Eagle's Medium (DMEM)	Gibco
Ethanol	Merck
Fetal bovine serum (FBS)	Gibco
Formic acid (FA)	Thermo Fisher
Heavy L-arginine/L-lysine	Silantes
hydroxylamine 50%	Thermo Fisher
Immobilon Forte Western HRP Substrate	Merck
Immobilon polyvinylidene difluoride (PVDF) membrane	Merck
L-glutamine	Sigma
Light L-arginine/L-lysine	Silantes
L-proline	Silantes
Medium L-arginine/L-lysine	Silantes

MTase-Glo™ Methyltransferase Assay	Promega
NP-40	US Biological
PBS pH 7.4	Gibco
Penicillin-Streptomycin (10,000 U/mL)	Gibco
Precision Plus Protein All Blue Standard	Biorad
Pronase	Roche
Protease inhibitor	Roche
Pyruvate Kinase Activity Assay Kit	Sigma
Resolving/Stacking gel buffer	Biorad
SILAC FBS (dialyzed)	Silantes
Sodium dodecyl phosphate (SDS)	Sigma
Tetramethylethylenediamine (TEMED)	Biorad
TMT10plex Isobaric Label Reagent Set	Thermo Fisher
Tris base	Sigma
tris(2-carboxyethyl) phosphine (TCEP)	Sigma
Trypsin	Serva
Urea	Merck

Table 3.2 Consumables used in the present study

Consumable	**Company**
Cell culture dish	TPP
C18 precolumn	Thermo Fisher
C18 ReproSil particles 1.9µm	Dr. Maisch GmbH
Capillary analytical column	New Objective Inc
epT.I.P.S. Reloads	Eppendorf
Microcon Centrifugal Filters 30K	Merck
PCR Tubes 0.2 mL	Thermo Fisher
Pierce C18 tips	Thermo Fisher
Pierce™ High pH Reversed-Phase Peptide Fractionation Kit	Thermo Fisher
Safe-Lock Tubes	Eppendorf
Serological pipette	Greiner bio-one

Table 3.3 Equipment used in the present study

Equipment	Company
Centrifuge 5804 R	Eppendorf
Centrifuge tubes 15/50 mL	Fisher Scientific
Galaxy mini centrifuge	VWR
iMark Microplate reader	Biorad
Mechanical Pipette	Eppendorf
Q-Exactive-Plus mass spectrometer	Thermo Fisher
Reax top Shakers & Mixers	Heidolph
Sonifier 250	Branson
SpeedVac Plus SC210A	SAVANT Instruments Inc
Thermomixer 5436	Eppendorf
TProfessional Basic Thermocycler	Biometra
Trans-Blot Turbo	Biorad
Ultimate 3000 UHPLC system	Thermo Fisher

Table 3.4 Software and tools used in the present study

Software/Tools	Source
Proteome Discoverer 2.4	Thermo Fisher
Gene Ontology Resource	http://geneontology.org/
MaxQuant	https://www.maxquant.org/
Perseus 1.6.14.10	https://maxquant.net/perseus/
Skyline	MacCoss Lab Software
Xcalibur v4.2.47	Thermo Fisher

3.3.2 Study design

Three different label-free mass spectrometry-based protein-ligand interaction methodologies for identifying protein targets of ketamine and HNKs were applied to samples from the mouse hippocampal cell line HT-22. TMT and SILAC mass spectrometry quantification strategies were used in order to improve quantification accuracy for multiple samples. Test compounds were incubated with extracted cell lysates or intact living cells to form a protein-drug complex. Subsequently, the cellular proteome

was subjected to CETSA, DARTS or SIP treatment to allow partial protein degradation or denaturation. The non-denatured fraction of the proteome containing potential target proteins was then digested into tryptic peptides. Labeled peptides were from either labeled proteins in SILAC cell culture or TMT labeling after digestion. Samples from different conditions were multiplexed and analyzed using LC-MS/MS. MS raw data were processed with bioinformatic tools for determining potential protein drug targets.

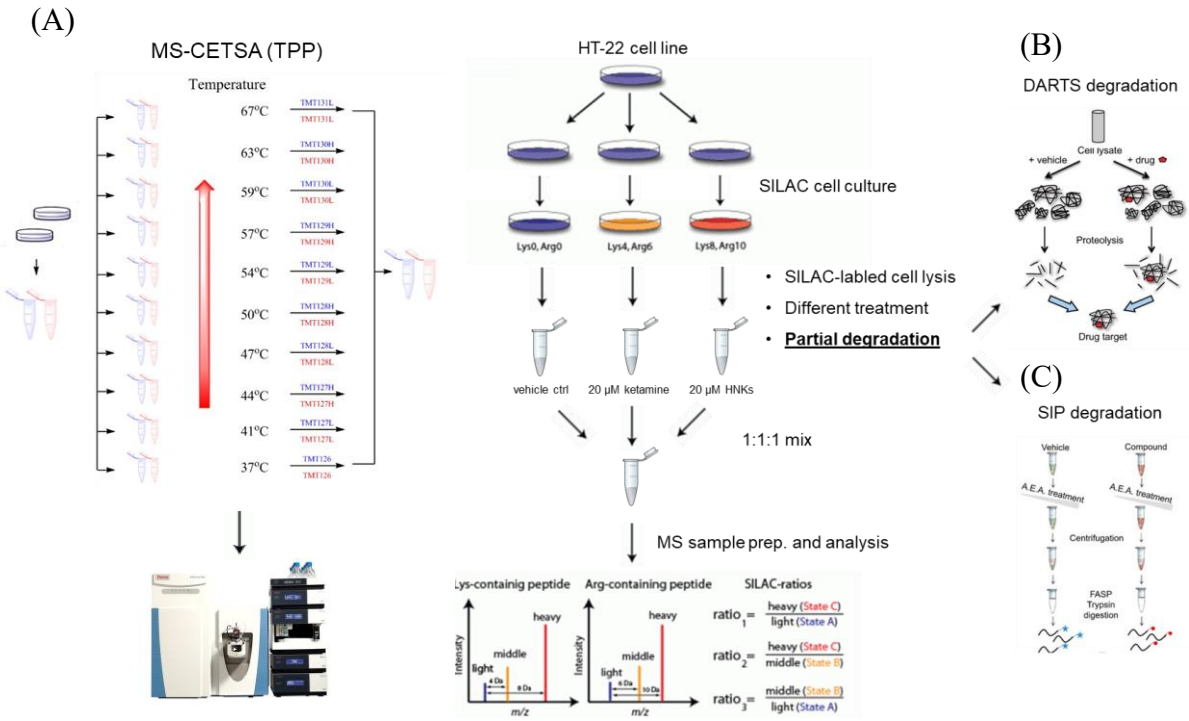

Figure 3.10 Experimental design of ketamine/HNK drug target identification. HT-22 cell lysate or living cells were partially degraded or denatured with (A) heat conditioning (MS-CETSA or TPP), (B) pronase digestion (DARTS) or (C) A.E.A.(SIP). MS-CETSA (TPP) was coupled with TMT 10-plex quantification and DATRS and SIP were coupled with SILAC 3-plex quantification. Samples were subjected to LC-MS/MS analysis and relative quantification.

3.3.3 Methods

3.3.3.1 Cell culture

Unless otherwise stated, HT-22 cells were cultured in DMEM supplemented with 10% FBS and 1% Penicillin-Streptomycin in a cell incubator at 37ºC with 5% CO_2. Cell passaging was conducted whenever cell confluency reached around 80%.

For SILAC cell culture, SILAC-DMEM (Silantes) containing 10% dialyzed FBS and 1% Penicillin-Streptomycin was incorporated with unlabeled L-lysine/L-arginine or $^{2}H_4$ L-lysine/$^{13}C_6$ L-arginine or $^{13}C_6{}^{15}N_2$ L-lysine/$^{13}C_6{}^{15}N_4$ L-arginine to form complete light, medium or heavy labeled culture media at final concentrations of 0.798 mM lysine and

0.398 mM arginine. 2 mM final concentration of L-glutamine and 250 mg/ml L-proline were also added to the culture media. Frozen HT-22 cells were revived in 3 different SILAC media to generate stable isotopic labeled HT-22 cell lines. Cells were cultured in a cell incubator at 37°C with 5% CO2. Cell passaging was conducted whenever cell confluency reached around 80%. SILAC-labeled cells were cultured for several generations until a quality control mass spectrometry sample showed labeling efficiency had reached > 99%.

3.3.3.2 Cell lysate preparation

Cultured HT-22 cells or SILAC-labeled HT-22 cells were washed 3 times with ice-cold PBS and resuspended with PBS containing 0.4% NP-40 and 1× protease inhibitor cocktail. Suspended cells were snap frozen in liquid nitrogen and thawed at 37°C in a water bath. Freeze-thaw cycles were repeated twice to lyse cells completely. Cell debris was removed by centrifugation at 4°C for 20 min. A BCA assay was used to determine the protein concentration of the supernatant.

3.3.3.3 Cellular thermal shift assay (CETSA)

For *in vitro* CETSA on cell lysates, HT-22 cell lysates were incubated with 20 µM ketamine, 20 µM R-HNK, 20 µM S-HNK (final concentrations) or H_2O control for 30 min at 4°C, and distributed into 0.2 ml PCR tubes. Samples were heated in parallel for 3 min at the target temperatures (37, 41, 44, 47, 50, 53, 56, 60, 63, 67°C). After subsequent 3-min incubation at room temperature, precipitated proteins were separated from the soluble fraction by centrifugation at 17,000 g for 20 min at 4°C.

For *ex vivo* CETSA on living cells, cell medium was changed to non-serum DMEM after HT-22 cells had reached ~90% confluency, followed by drug incubation with 20 µM ketamine, 20 µM R-HNK (final concentrations) or H_2O control for 1 h at 37°C. Cells were resuspended in PBS buffer after the removal of medium and washing with cold PBS twice. Cells were aliquoted into PCR tubes and then heated in parallel for 3 min under the target temperatures (37, 41, 44, 47, 50, 53, 56, 60, 63, 67°C). After subsequent 3-min incubation at room temperature, cells were lysed and soluble fractions were collected as above.

Supernatants were reduced with 10 mM TCEP for 20 min at room temperature, followed by alkylation with 20 mM IAM for 15 min. Digestion was performed at 37°C for 16 h by adding trypsin (1:100, w/w). Peptide concentration was determined using a peptide

quantification assay to check the efficiency of digestion. Digests were labeled with 10-plex TMT reagents according to the manufacturer's protocol. Samples under the same drug treatment but various heating treatments were labeled with different TMT labels, enabling relative quantification of a broad range of 10 temperature points in a single experiment. TMT labeling was performed in 25 mM HEPES (pH 8.5) at room temperature. Reactions were quenched after 1 h incubation with 5% hydroxylamine. Labeled peptide extracts were combined into a single sample per experiment. Offline high pH reverse phase fractionation was performed on mixed samples, and 8 fractions from each experiment were collected. After being dried in a vacuum, samples were immediately frozen at -80^{o}C until being subjected to LC-MS/MS analysis.

3.3.3.4 SILAC-DARTS

SILAC-labeled HT-22 cell lysates were incubated with 20 μM ketamine, 20 μM HNKs (1:1, R:S) or H_2O control for 30 min at 4^{o}C. A label swapping strategy was applied in the drug treatment to avoid the risk of isotopic incorporation variation and other systematic technical biases. Pronase (1:100 or 1:300, w/w) was then added to digest samples for 10 min at room temperature. Digestion was quenched by addition of 1 × protease inhibitor cocktail. Samples in different SILAC labels were combined and concentrated in preconditioned filters to discard peptides and small protein fragments. Washing and concentrating were repeated 3 times.

8 M urea in 100 mM Tris-HCl (pH 8.5) was added to denature concentrated samples, followed by reduction with 10 mM TCEP for 20 min and alkylation with IAM for 15 min in darkness at room temperature. Urea was then removed by buffer displacement with 25 mM ammonium bicarbonate, repeated 3 times. Subsequently, digestion was performed with trypsin (1:100, w/w) for 16 h. Digestion was quenched by 2% formic acid and desalting with C18 desalting tips. The SILAC mixture of peptides was further prefractionated as described above. Fractionated peptides were died before being frozen at -80^{o}C.

3.3.3.5 SILAC-SIP

SILAC-labeled HT-22 cells were harvested and washed with cold PBS three times. Subsequently, cells were lysed using PBS containing 0.4% NP-40 and 1× protease inhibitor cocktail at pH 7.4 with three free-thaw cycles in liquid nitrogen and a 37^{o}C water bath. Soluble fractions were separated by centrifugation at 20,000 g for 10 min at 4^{o}C.

Cell lysates with different SILAC labels were incubated with 20 µM ketamine, 20 µM HNKs (1:1, R:S) or H_2O control for 30 min at 4°C. A label swapping strategy was applied in the drug treatment to avoid the risk of isotopic incorporation variation and other systematic technical biases. The incubated extract from each sample was divided into seven aliquots of 100 µl in new tubes followed by denaturation initiated by addition of an A.E.A. solvent mixture (acetone: ethanol: acetic acid = 50: 50: 1) to reach a final percentage of organic solvent ranging from 9% to 19%. Subsequently, the mixtures were equilibrated by rotating at 800 rpm for 20 min at 37 °C and proteins precipitated by organic solvents were separated and discarded after centrifugation at 20,000 g for 10 min at 4°C. Supernatants from different SILAC labels were combined and subjected to mass spectrometry sample preparation in the same way as described above.

3.3.3.6 LC-MS/MS analysis

The analysis of fractionated labeled peptides was performed on an Ultimate 3000 UHPLC system (Thermo) coupled with a Q-Exative-Plus mass spectrometer, controlled by Xcalibur software v4.2.47 (Thermo Fisher Scientific, Waltham, MA, USA). Briefly, 1 µg of the 0.1% formic acid (FA)-resuspended peptides from each fraction was automatically loaded onto a C18 precolumn (300 µm i.d., Thermo) at a flow rate of 10 µl/min (2% ACN/0.1% FA). The 15 cm capillary analytical column (75 µm i.d., New Objective, Inc.) was packed in-house with 1.9 µm C18 ReproSil particles (Dr. Maisch GmbH). The mobile phases used for elution of the peptides was 0.1% FA as phase A and 95% ACN/0.1% FA as phase B with a flow rate of 300 nl/min. The 160 min-gradient for TMT labeled peptides was developed as follows: a pre-equilibration phase with 95% A for 5 min; 5% - 30% B for 110 min; 30% - 60% B for 20 min; 98% B for 5 min and a post-equilibration with 96% A for 20 min. The 160 min-gradient for SILAC labeled peptides was developed as follows: a pre-equilibration phase with 98% A for 5 min; 2% - 25% B for 110 min; 25% - 60% B for 20 min; 98% B for 5 min and a post-equilibration with 98% A for 20 min.

The liquid chromatography-tandem mass spectrometry (LC-MS/MS) system was operated in data-dependent acquisition (DDA) mode. The full mass scans were acquired in the Orbitrap mass analyzer under the profile mode at a resolution of 70,000 over a range of 375 to 1400 m/z. The top 10 precursor ions were selected for HCD fragmentation with a normalized collision energy (NCE) of 32% (for TMT labeled peptides) or 27% (for

SILAC labeled peptides) and a dynamic exclusion time of 30 s. The MS/MS scans were also acquired in the Orbitrap under the centroid mode with a resolution of 35,000 (for TMT labeled peptides) or 17,500 (for SILAC labeled peptides). The AGC targets for full scan and MS/MS were set to 3×10^6 and 1×10^5, respectively. The spray voltage of the ESI ion source was 1.85 kV and the temperature of the ion transfer capillary was 250°C.

3.3.3.7 MS data interpretation

Raw files were processed with either Proteome Discoverer 2.4 (Thermo Fisher Scientific) for TMT labeled samples or MaxQuant (version 1.6.17.0) for SILAC labeled samples. The MS/MS spectra were searched against the complete Swissprot mouse protein sequence database (March 2019). Spectra selection and most other parameters were set at default settings. Trypsin was specified as the protease and up to two missed cleavages were allowed. Mass tolerance for precursor and fragment ions was set to 10 ppm and 0.02 Da. Carbamidomethyl at cysteine (C) residues was set as a static/fixed modification whereas methionine (M) oxidation was set as a variable modification. For TMT labeling, additional fixed modifications included TMT6 at the N-terminus and lysine (K). For SILAC labeling, multiplicity was set to 3, where Lys 0 & Arg 0 were light labels, Lys 4 & Arg 6 were medium labels and Lys 8 & Arg 10 were heavy labels. Posterior error probabilities (PEPs) were calculated and peptide spectrum matches (PSMs) were filtered using Percolator. False discovery rate (FDR) was estimated with q-values and controlled under 0.05. For TMT reporter ion quantification in consensus workflow, raw intensity of unique and razor peptides without normalization was calculated. For SILAC quantification, normalized SILAC ratios were used for subsequent statistical analysis.

3.3.3.8 Processing of quantification data

The quantified CESTA data exported from Proteome Discoverer 2.4 were processed with R package TPP downloaded from Bioconductor. Briefly, fold-changes were calculated by using the lowest temperature condition as the reference. Relative fold changes as a function of temperature followed a sigmoidal trend, which was fitted with the following equation derived from chemical denaturation theory:

$$f(T) = \frac{1 - \text{plateau}}{1 + e^{-\left(\frac{a}{T} - b\right)}} + plateau$$

Where *T* is the temperature and a, b, and *plateau* are constants. A heuristic normalization was performed based on the fitted curve of joint proteins in all groups. Melting curves of individual proteins were fitted after normalization. The protein whose melting curve fulfills the following criteria was selected as a potential target protein: (i) both fitted curves for the vehicle and compound treated condition had to have an R^2 greater than 0.8, which confirms the good fitting of melting curves; (ii) p-values of comparisons between two groups in both biological duplicates less than 0.1, indicating that the difference between treatments was significant; (iii) the vehicle curve had a plateau of less than 0.3 and the slope of the curve was below -0.06 to ensure that the proteins were melting during heat treatment; (iv) melting temperature difference (ΔT_m) in duplicates showed the same trends to ensure reproducibility.

The quantified DARTS data exported from Maxquant were processed with Perseus (1.6.10.43). Proteins identified only by site, by reverse sequences and potential contaminants were removed from the quantified data. Proteins identified with at least 2 peptides were kept for further analysis. The normalized M/L ratio (ketamine vs control) and H/L ratio (HNKs vs control) were presented as a log2 fold change (FC). Proteins with > 30% missing values were removed from datasets, followed by quantile normalization. Statistical analysis was performed with the student t-test to select candidates with a cutoff of protein fold change > 1.3 and adjusted p-value < 0.05. All proteins were visualized in volcano plots.

The quantified SIP data exported from Maxquant were processed with Perseus (1.6.10.43). Proteins identified only by site, by reverse sequences and potential contaminants were removed from quantified data. Proteins identified with at least 2 peptides were kept for further analysis. The normalized M/L ratio (ketamine vs control) and H/L ratio (HNKs vs control) was presented as a log2 fold change (FC). Proteins identified in only one replicate were removed from datasets, followed by quantile normalization. Scatter plots were used for both visualization and selection of candidate proteins.

3.3.3.9 Western blots

Western blots were performed according to standard procedures. HT-22 cell lysates, recombinant PKLR (rPKLR) or recombinant COMT (rCOMT) were mixed with sample loading buffer and then subjected to sodium docecylsulfate polyacrylamide gel

electrophoresis (SDS-PAGE) in a 10% acrylamide gel. Electrophoresis was performed under constant 100 V for 90 min. Subsequently, proteins were transferred from the gel to a polyvinylidene difluoride (PVDF) membrane using a standard semi-dry transfer protocol from Biorad. The membranes were blocked with TBS-Tween 20 supplemented with 5% skimmed milk (w/v) for 1 h at room temperature. Primary antibodies of relevant proteins were incubated with membranes at 4°C overnight followed by secondary antibody incubation at room temperature for 1 h. Membranes were developed with HRP-enhanced chemiluminescence reagents. ImageLab was used to visualize the protein bands on membranes and ImageJ was used to calculate the protein intensity.

3.3.3.10 Isothermal dose-response fingerprints (ITDRF)

HT-22 cell lysates were distributed into 10 PCR tubes and incubated with 10 concentrations of ketamine, R-HNK or S-HNK with (100 µM, 33 µM, 10 µM, 3.3 µM, 1 µM, 330 nM, 100 nM, 33 nM, 10 nM and 0) for 30 min at 4°C. Samples were heated in parallel for 3 min at 55°C followed by extra incubation on ice for 3 min. Precipitated proteins were separated from the soluble fraction by centrifugation at 17,000 g for 20 min at 4°C and subjected to mass spectrometry sample preparation and TMT labeling as described above.

3.3.3.11 PKLR enzymatic assay

20 ng of recombinant PKLR were incubated with 20 µM ketamine, 20 µM R-HNK, 20 µM S-HNK or H_2O control at 4°C for 30 min to allow binding. The reaction mixes including drug-bound PKLR, Pyruvate Kinase Substrate Mix and Fluorescent Peroxidase Substrate were prepared according to the manufacturer's protocol to set up the reaction. Absorbance at 570 nm was measured 10 min after the reaction stared and used to calculate the concentration of generated pyruvate and PKLR activity.

3.3.3.12 COMT enzymatic assay

COMT (enzyme) and dopamine (substrate) concentrations were optimized according to the manufacturer's protocol to obtain stable assay readouts. To study the drug effect on COMT activity, 15 ng of recombinant COMT were incubated with 20 µM ketamine, 20 µM R-HNK, 20 µM S-HNK or H_2O control at 4°C for 30 min to allow binding. A mixture comprising drug-bound COMT, 2 mM dopamine and 200 µM SAM was incubated at 37°C to trigger the reaction. Subsequently, MTase-Glo™ Reagent and Detection Solution

was added to the samples according to the manufacturer's protocol and luminescence was measured using a plate-reading luminometer.

3.3.3.13 PRM-MS

Peptides of four candidates in DARTS analysis (SF3B1, ESTD, TRM112 and STXBP1) identified with the DDA mode were selected for targeted PRM-MS analysis on a Q-Exactive Plus Mass spectrometer (Thermo Fisher). Peptide sequences and m/z with light, medium or heavy SILAC labels were used to create an inclusion list in Xcalibur v4.2.47. DARTS samples were prepared as described above.

The tryptic peptides were resuspended in 0.1% formic acid and injected onto a C18 precolumn (300 µm i.d., Thermo) at a flow rate of 10 µl/min (2% ACN/0.1% FA). The 15 cm capillary analytical column (75 µm i.d., New Objective, Inc.) was packed in-house with 1.9 µm C18 ReproSil particles (Dr. Maisch GmbH). The mobile phases used to elute the peptides comprised 0.1% FA as phase A and 95% ACN/0.1% FA as phase B with a flow rate of 300 nl/min. The 60 min-gradient was developed as follows: a pre-equilibration phase with 95% A for 3 min; 5% - 30% B for 37 min; 30% - 40% B for 8 min; 98% B for 6 min and a post-equilibration with 98% A for 6 min.

The mass spectrometer was set to collect in PRM mode using the inclusion peptide list created above. An additional full survey scan was collected to assess possible interference. The full mass scans were acquired in the Orbitrap mass analyzer under the profile mode at a resolution of 70,000 over a range of 375 to 1400 m/z with AGC targets set to 3×10^6. PRM scan settings were: resolution of 17,500, injection time of 50 ms and AGC targets of 1×10^5 and isolation width of 1.6 m/z. The spray voltage of the ESI ion source was 1.85 kV and the temperature of the ion transfer capillary was 250°C.

Proteins were identified by database searches with MaxQuant and quantification was performed based on extracted-ion chromatograms using Skyline (MacCoss Lab Software).

3.4 Results

3.4.1 Screening for drug target candidates with quantitative proteomics-based protein-drug interaction methodologies

3.4.1.1 MS-CETSA (CETSA)

To screen for direct binding partners of ketamine or HNK, MS-CETSA (or Thermal Proteome Profiling Temperature Range, TPP-TR) was first performed with HT-22 cell lysates. NP-40 was used as a mild detergent during cell lysate extraction to also capture membrane proteins. Quantitative thermal stability data for 6940 proteins across 10 temperature points were acquired. 4615, 4475, 4646 and 4633 proteins were quantified in biological duplicates for the vehicle control group, ketamine treatment group, R-HNK treatment group and S-HNK treatment group, respectively. Subsequently 3834 proteins quantified in all datasets were subjected to TPP analysis (Figure 3.11).

The heatmap represents the stability of soluble proteins in HT-22 cell lysates. For each protein, the relative concentration at the indicated temperature was compared with the lowest temperature (37^{o}C). The soluble fraction of the heated proteome decreased with increasing temperature, indicating solubilization at the initial temperatures followed by increasing aggregation and precipitation at higher temperatures. The proteins displayed a wide range of sensitivity to heat treatment. Some extremely heat resistant proteins did not exhibit aggregation or precipitation for the entire temperature range. No significant drug effect on proteome thermal stability was observed, suggesting that ketamine and its metabolites do not induce global protein stability changes in HT-22 cellular lysates.

Relative fold changes as a function of temperature followed a sigmoidal trend called "melting curves", which was fitted by a mathematical model from chemical denaturation theory (see Section 3.3). Fitted melting curves of the same subset of 77 proteins from all datasets demonstrated good correlation ($R^2 \sim 0.99$) and was further used for normalization of individual proteins. Normalization succeeded in removing the variation between different melting profiles that were initially difficult to combine into a single model with a good fit (Figure 3.11).

After normalization, melting curves were fitted for all 3834 proteins analyzed. Melting temperature (T_m), determined as the temperature where half of the protein is denatured, was calculated for each fitted protein thermal shift curve. A distribution of T_m in

comparisons between different groups or biological duplicates revealed that the majority of proteins were not affected by ketamine or HNK binding. Although more proteins showed a positive melting temperature shift indicating drug-induced stabilization, some proteins also exhibited negative shifts, which may result from drug-induced destabilization.

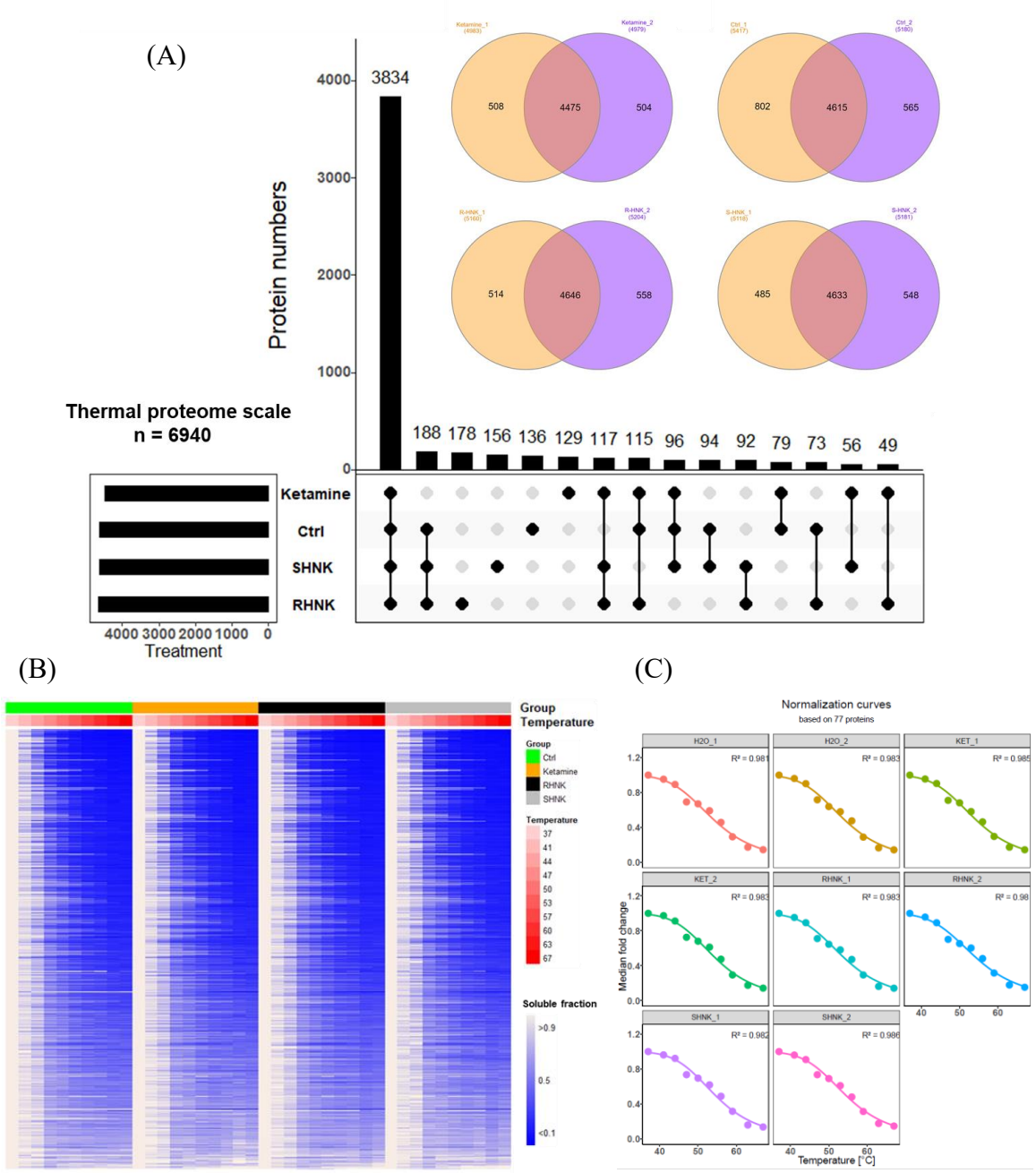

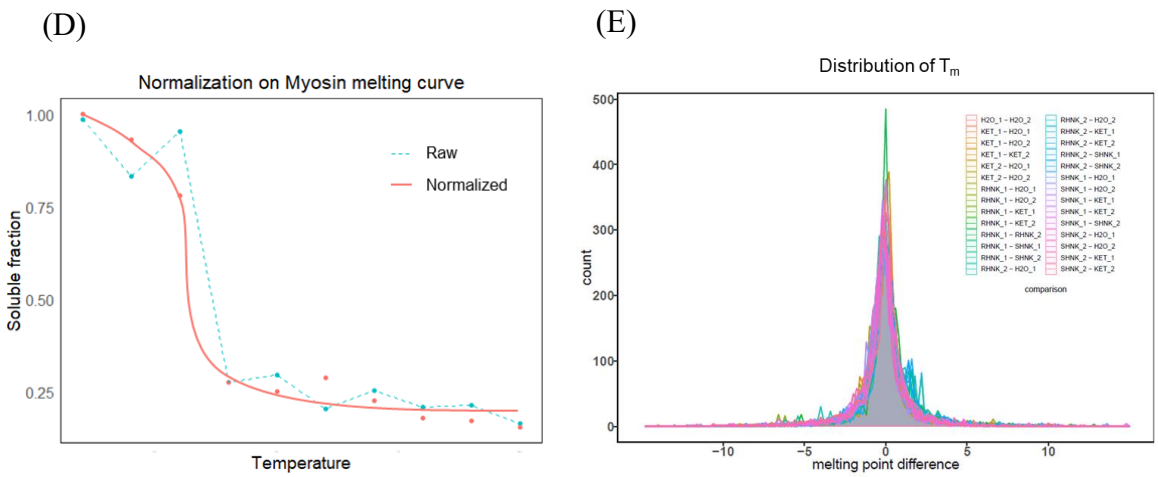

Figure 3.11 MS-CETSA (TPP) analysis of HT-22 cell lysates. (A) Scale of the HT-22 thermal proteome; (B) heatmap of the soluble fraction of heat-treated samples; (C) normalization curves; (D) an example (myosin) of a normalization step in fitting thermal shift curves; (E) ΔT_m distribution in each comparison.

To identify ketamine and HNK binding partners, a series of criteria were applied to melting curve parameters as described in Section 3.3. As a result, in the ketamine treated group, 2472 and 2396 proteins passed the filter of R^2 in biological duplicates, ~20% of the proteins were significantly affected ($p < 0.05$). 2158 and 2122 proteins in the R-HNK treated group, and 2108 and 2155 proteins in the S-HNK treated group passed the R^2 filter. In total, 45 proteins passed all criteria and displayed significantly affected thermal stability. Most of the proteins were affected by the treatment of only one drug (Figure 3.12). 21 proteins were found to bind only ketamine, 11 and 10 were identified for R-HNK and S-HNK, respectively, suggesting that ketamine has more endogenous binding targets. Polyadenylate-binding protein-interacting protein (PAIP2) and ER lumen protein-retaining receptor 1 (KDELR1) showed binding with both ketamine and S-HNK. Only one protein, pyruvate kinase L/R type (PKLR) was affected by both ketamine and R-HNK; this protein also exhibited high binding affinity for S-HNK and a large change in thermal stability. Most proteins (62.2%) were stabilized by drugs, whereas 37.8% of proteins demonstrated higher sensitivity to heat treatment upon drug binding. Proteins identified by TPP belonged to a wide range of classes and included 10 enzymes, 3 kinases, 2 phosphatases, 2 receptors and 2 translation factors. Melting curves of candidate proteins that are biologically relevant to ketamine's pharmacological effect are shown in Figure 3.12. The full list of proteins and relevant information is attached in Appendixes. Among all the candidate protein targets pyruvate kinase L/R type stood out by being affected by all three drugs and showing the greatest melting temperature difference. All three

compounds showed substantial shifts of PKLR thermal stability (ΔT_m = 7.18°C for ketamine), (ΔT_m = 8.61°C for R-HNK) and (ΔT_m = 8.97°C for S-HNK).

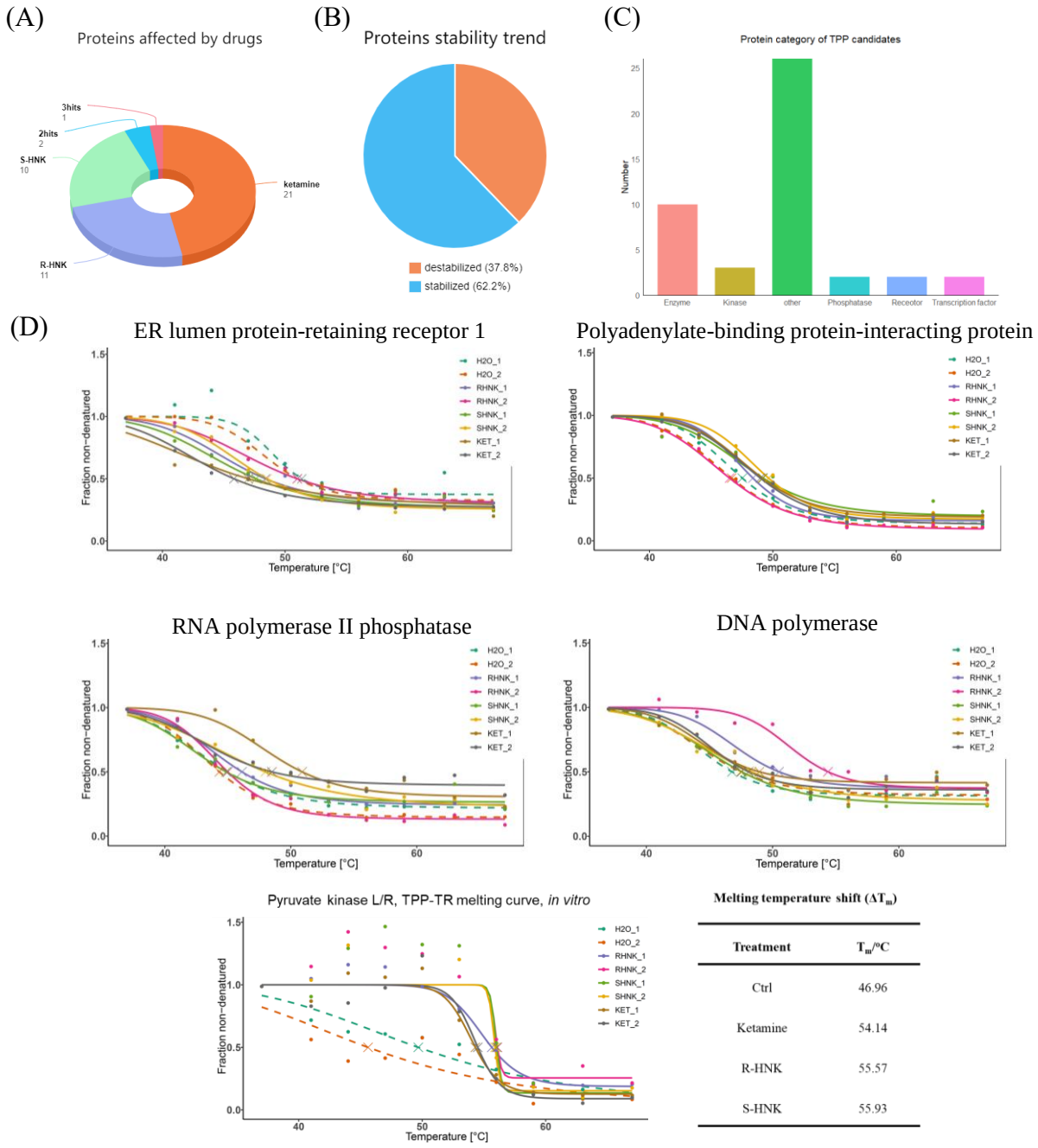

Melting temperature shift (ΔT_m)

Treatment	T_m/°C
Ctrl	46.96
Ketamine	54.14
R-HNK	55.57
S-HNK	55.93

Figure 3.12 Top hits in MS-CETSA (TPP) analysis of HT-22 cell lysates. (A) Proteins affected by different drugs; (B) protein stability trends; (C) protein categories; (D) examples of thermal shift curves for proteins affected by more than one drug.

Ex vivo MS-CETSA was also performed to screen indirect binding partners or proteins affected by ketamine or HNK (R:S = 1:1). In two separate TPP-TR experiments with living cells, 4081 and 4054 proteins were identified, of which 2072 and 2199 proteins were subjected to TPP analysis, yielding 27 *ex vivo* potential targets for ketamine and 29

for HNK, including pyruvate kinase L/R type (PKLR) and another biologically relevant protein, Catechol O-methyltransferase (COMT). Interestingly, PKLR was reproducibly identified as a target for ketamine and HNK in *ex vivo* TPP analysis, although with a relatively smaller melting temperature difference (ΔT_m = 2.36°C for ketamine) and (ΔT_m = 3.78°C for both HNKs).

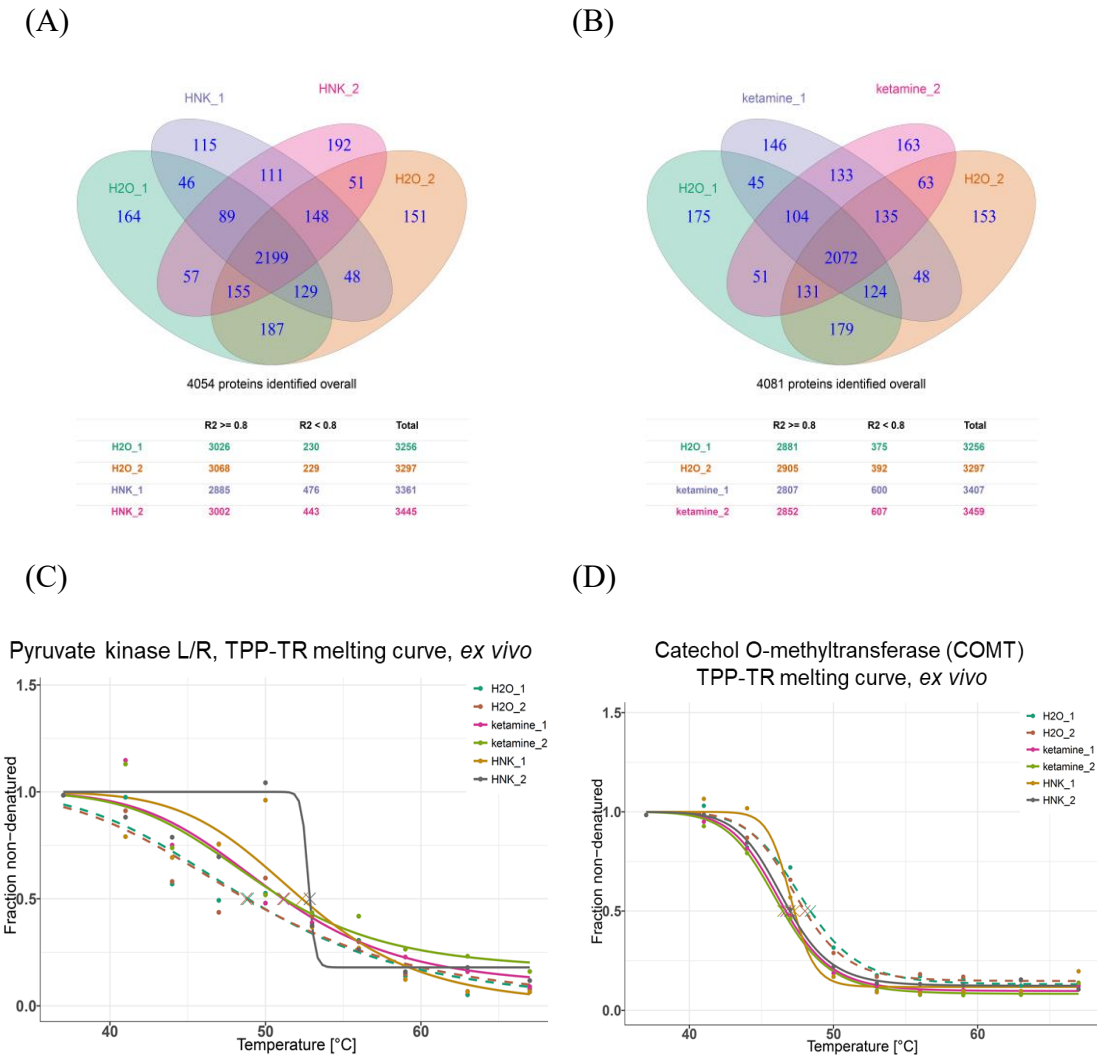

Figure 3.13 MS-CETSA (TPP) analysis of HT-22 living cells. (A) Proteins identified in a ketamine-vehicle comparison; (B) proteins identified in an HNKs-vehicle comparison; (C-D) thermal shift curves for PKLR and COMT.

3.4.1.2 DARTS

HT-22 extracts with three different SILAC labels were incubated with a vehicle control, ketamine or HNKs (R:S, 1:1). DARTS-limited proteolysis was performed at room temperature for 10 min with 1:100 and 1:300 pronase (protease: substrate, w/w) in two independent experiments. SILAC quantification was performed after combining samples

from different drug treatments and medium/light (M/L) and heavy/light (H/L) ratios were calculated (Figure 3.14). 1447 and 1321 proteins were quantified in at least 4 out of 6 replicates. Pearson correlation among independent replicates showed that proteins after DARTS proteolysis were reproducibly quantified. Histogram plots revealed that drug treatment did not affect the global susceptibility of the HT-22 proteome to pronase. Log2-transformed SILAC ratios of 6 biological replicates were visualized in volcano plots and proteins with fold changes greater than 1.3 (log2 FC > 0.378) and statistical significance p-values < 0.05 were applied as the threshold for selecting candidates. Overall, 54 proteins exhibited altered susceptibility upon drug binding. No overlap was found in the 1:300 and 1:100 pronase groups, indicating that the protective effect of drugs on target proteins is only sustained within a certain pronase concentration range, depending on the initial sensitivity of the protein to proteolysis. 4 proteins were found to be regulated after 1:300 pronase digestion under the treatment of both ketamine and HNKs. Another 5 proteins were identified in the 1:100 pronase digestion group. Interestingly, Catechol O-methyltransferase (COMT), for which the thermal shift curve also displayed potential binding between drugs in the TPP analysis, was one of the most significant candidates in the DARTS datasets.

(A)

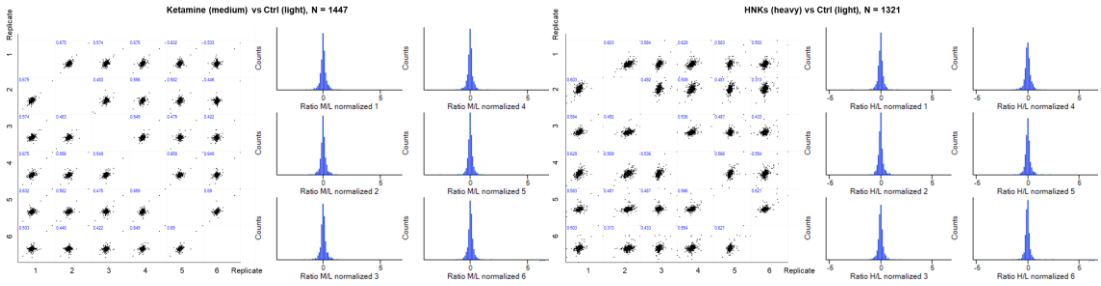

(B)

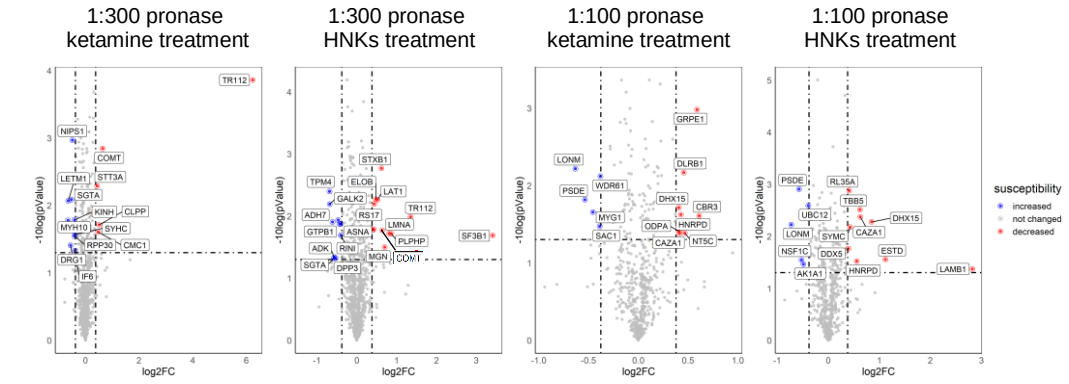

(C)

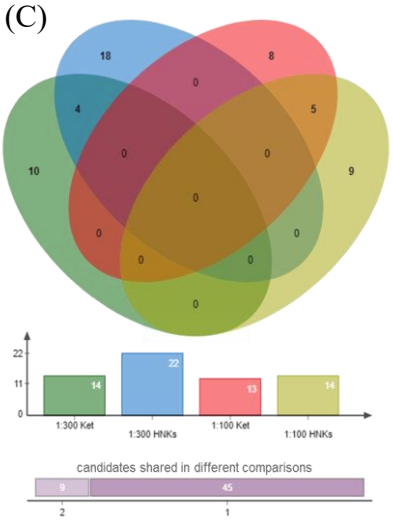

Proteins protected by both ketamine and HNKs at 1:300 pronase

Accession	Gene	Description
Q61879	MYH10	Myosin-10
Q8BJU0	SGTA	Small glutamine-rich tetratricopeptide repeat-containing protein alpha
Q9DCG9	TRMT112	Multifunctional methyltransferase subunit TRM112-like protein
O88587	COMT	Catechol O-methyltransferase

Proteins protected by both ketamine and HNKs at 1:100 pronase

Accession	Gene	Description
O35286	DHX15	Pre-mRNA-splicing factor ATP-dependent RNA helicase DHX15
O35593	PSDE	26S proteasome non-ATPase regulatory subunit 14
P47753	CAZA1	F-actin-capping protein subunit alpha-1
Q60668	HNRPD	Heterogeneous nuclear ribonucleoprotein D0
Q8CGK3	LONM	Lon protease homolog, mitochondrial

Figure 3.14 DARTS analysis of HT-22 cell lysates. (A) Proteins identified and distribution of SILAC ratios; (B) volcano plots illustrating the proteins' abundance change under DARTS treatment with 1:100 or 1:300 pronase; (C) DARTS candidate statistics.

3.4.1.3 Solvent-induced protein precipitation (SIP)

Solvent-induced protein precipitation was also applied to HT-22 cell lysates to identify ketamine or HNKs binding proteins. Proteins denature and precipitate following the addition of organic solvents due to a decrease in the dielectric constant. In contrast to DARTS where proteins are degraded by proteolysis with pronase, SIP precipitates proteins by addition of an organic solvent mixture (A.E.A, acetone: ethanol: acetic acid = 50: 50: 1). Proteins protected by drug binding were quantified and visualized in scatter plots. The number of proteins quantified in the soluble fraction decreased with increasing A.E.A. concentration (Figure 3.15). Only some proteins showed lower denaturation after drug treatment in the presence of A.E.A., while very few proteins were found changed in an original input control group when A.E.A. was not added. Most solubility changes were observed for both ketamine and HNKs treatment groups with 13 ~ 17% A.E.A. When A.E.A. was increased to 19%, most proteins denatured, suggesting that drug binding did not protect proteins from being precipitated under high concentrations of organic solvents. In summary, 77 proteins displayed a change in abundance at 13 ~ 17% A.E.A (37 for ketamine and 50 for HNKs) with 10 identical proteins found for both drugs.

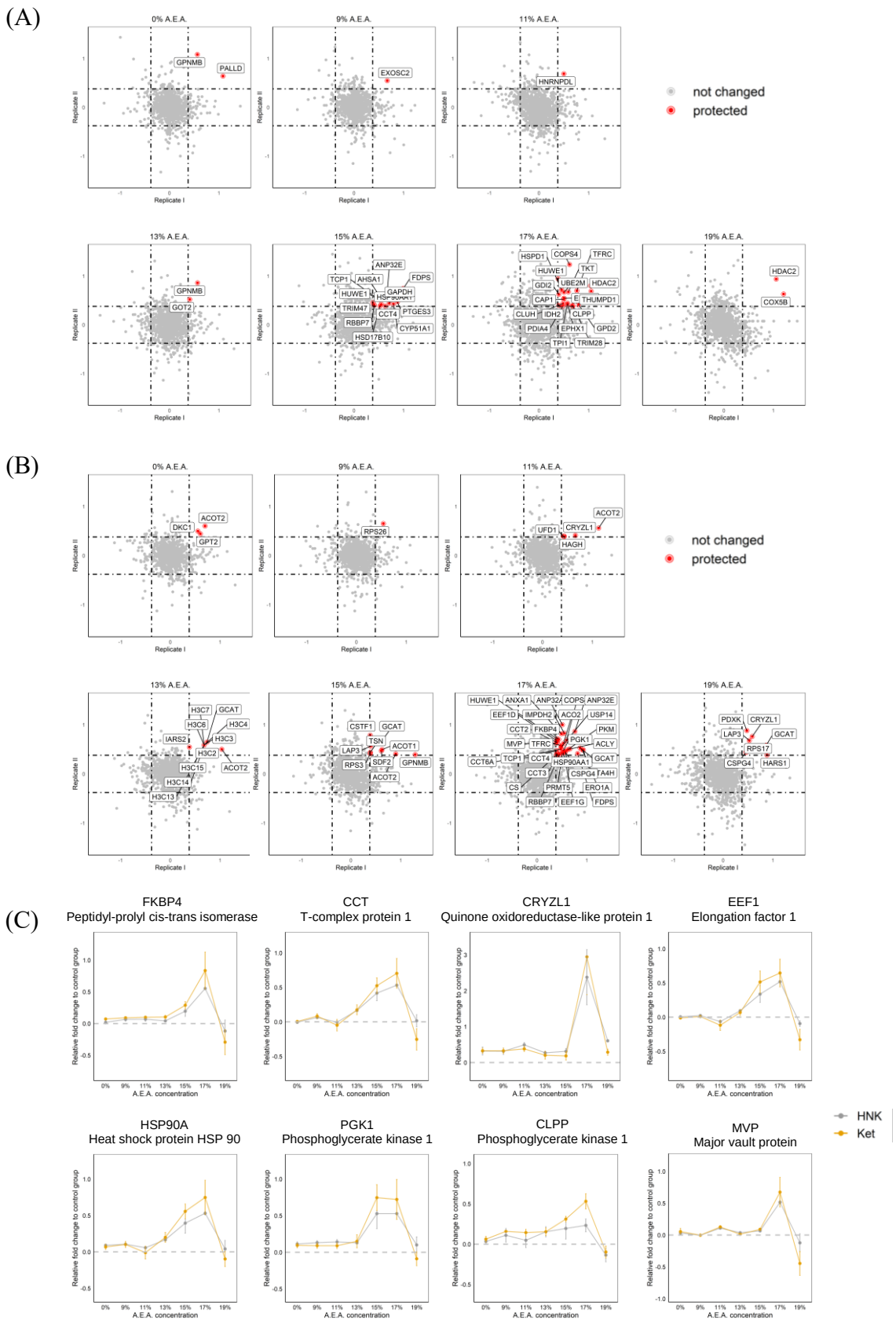

Figure 3.15 SIP analysis of HT-22 cell lysates. (A-B) scatter plots of SILAC ratios in duplicates under treatment of A.E.A. ranging from 0 to 19%; grey dots represent proteins without significant change; red dots represent proteins protected by drug binding; (A) ketamine treatment; (B) HNKs treatment; (C) protein intensity curves of SIP candidates.

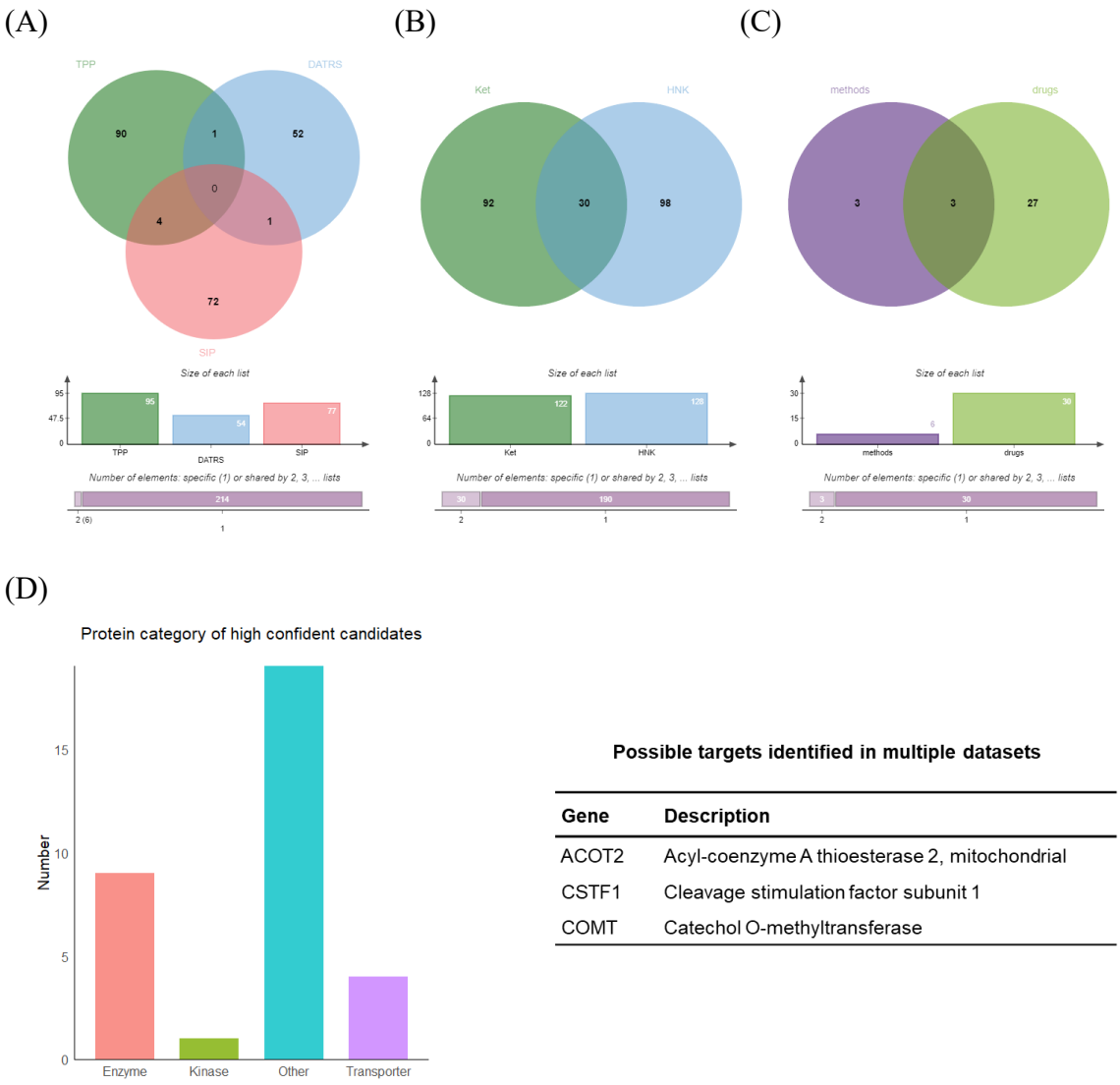

Possible targets identified in multiple datasets

Gene	Description
ACOT2	Acyl-coenzyme A thioesterase 2, mitochondrial
CSTF1	Cleavage stimulation factor subunit 1
COMT	Catechol O-methyltransferase

Figure 3.16 Classification and annotation of the 220 proteins candidates identified with MS-CETSA, DARTS and SIP. (A) Methodology comparison; (B) drug comparison; (C) summary of high-confidence candidates identified with different methodologies in response to different drugs; (D) protein categories of high-confidence candidates.

Screening of potential binding targets of ketamine and HNKs yielded 220 protein candidates with three different methodologies. A complete list of all protein candidates from *in vitro* TPP, DARTS and SIP is provided in Appendixes. Most small-molecule drugs and probes alter cell circuitry by interacting with more than one single target[223]. Several antidepressants including ketamine induce undesirable side effects, probably due to multiple binding targets in organisms that trigger various pharmacological effects. The large number of candidate protein targets resulting from the initial screens made it necessary to select the most promising for further validation. To select high confident potential targets to be validated, classification and annotation of these 220 proteins were performed. Comparison between the three methodologies and two drug treatments

revealed that 6 proteins were identified as possible targets with more than one method and 30 proteins were candidate target proteins for both ketamine and HNKs (Figure 3.16). Among these 33 high-confidence candidates, three proteins were identified in two groups with at least two different methodologies, including Catechol O-methyltransferase (COMT).

3.4.2 Validation of potential drug targets

To validate the identified drug target binding, different methods were used depending on the protein. The proteins subjected to validation include pyruvate kinase L/R type (PKLR), catechol O-methyltransferase (COMT) and Syntaxin binding protein-1 (STXBP1). PKLR is the most significant and promising candidate in MS-CETSA (TPP) analysis. COMT is a candidate identified in both MS-CETSA (TPP) and DARTS. STXBP1 is a candidate identified with DARTS that showed binding with HNKs but not ketamine. They are described separately in following sections.

3.4.2.1 Pyruvate kinase

Pyruvate kinase is the enzyme involved in the last step of glycolysis, catalyzing the transfer of a phosphate group from phosphoenolpyruvate (PEP) to adenosine diphosphate (ADP), yielding one molecule of pyruvate and one molecule of ATP.

For validation, HT-22 cell lysates with recombinant human PKLR were used in a CETSA experiment followed by Western blots. Five different temperature points were analyzed and high-affinity PKLR antibodies were used for immunoblotting to analyze and visualize the change in protein stability. Western blots confirmed that both ketamine and R-HNK, but not S-HNK (not shown), protected PKLR from unfolding and forming aggregates with increased temperatures, whereas PKLR in a vehicle treated control group displayed a sharp and instant decrease in solubility. Protection by R-HNK was stronger than that of ketamine based on Western blots, in consistence with the higher melting temperature upon R-HNK binding discovered by MS-CETSA (Figure 3.12 D).

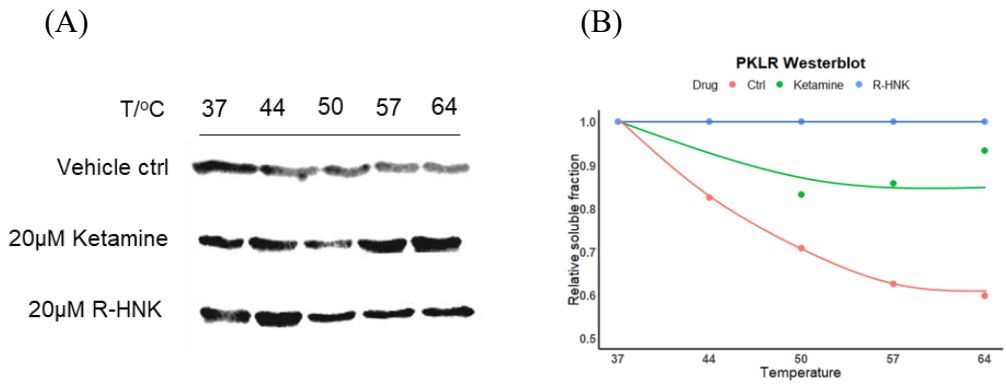

Figure 3.17 Western blot validation of binding between PKLR and ketamine/R-HNK. Five temperature points were chosen (as indicated) for CETSA heat-treatment; band density calculated as protein relative abundance with respective to the lowest temperature (37°C) was used to plot the thermal curve. (A) blots; (B) quantitation curves of bands.

After the Western blot verification of binding of ketamine and R-HNK to PKLR, an isothermal dose-response fingerprint (ITDRF) assay was performed to study the effect of drug concentration on the protection of PKLR. A change in thermal stability by ketamine but not HNKs (not shown) was drug dose dependent and the estimated EC50 value (~ 50 μM) was close to the drug dose used for TPP-TR analysis (Figure 3.17). Loss of protection by HNKs might possibly result from an irreversible transition upon heat treatment at 55°C.

As mentioned above, pyruvate kinase catalyzes the transfer of a phosphate group to generate pyruvate. Therefore, apart from binding validation, an enzyme assay was also performed to test the effect of drug binding on the kinase activity of PKLR. Pyruvate concentration was determined by a coupled enzymatic assay measuring the colorimetric product, which was proportional to pyruvate levels and indicated the activity of pyruvate kinase. Three different doses of ketamine, R-HNK and S-HNK as well as vehicle controls were incubated with recombinant PKLR followed by the enzymatic assay. The concentration of pyruvate produced in the assay was constant across the different drug treatments and drug doses, indicating that binding of the drugs does not affect the activity of PKLR (Figure 3.18).

(A) (B) (C)

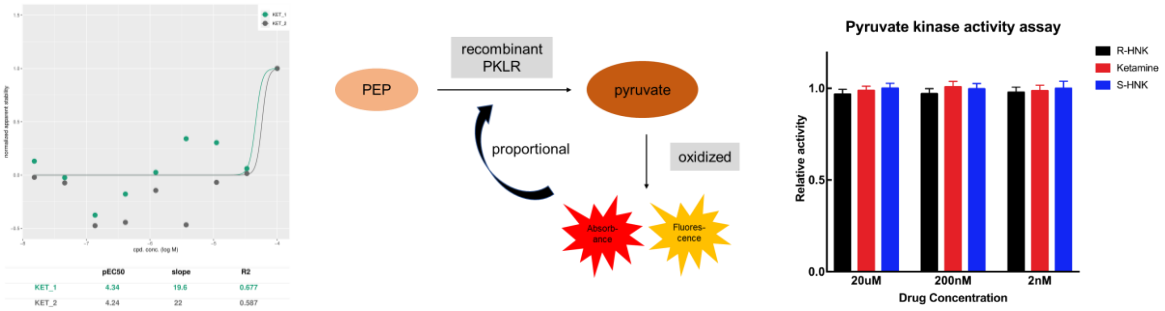

Figure 3.18 PKLR protection and activity validation with ITDRF and an enzymatic assay. (A) ITDRF binding curve of PKLR in response to ketamine; estimated EC50 ≈ 50 μM; (B) Principle of the PKLR enzymatic assay: pyruvate generated by PKLR catalyzation is oxidized to produce absorbance (570 nm) and fluorescence (Ex/Em 535/587 nm) proportional to PKLR activity; (C) PKLR activity under the treatment of drugs.

3.4.2.2 Catechol-O-methyltransferase

Catechol-O-methyltransferase (COMT) catalyzes the O-methylation, and thereby the inactivation, of catecholamine neurotransmitters and catechol hormones such as dopamine, epinephrine and norepinephrine, and has previously been implicated in depression.

To verify binding between drugs and COMT, an analogous experiment performed where HT-22 lysates were treated with drugs or a vehicle control and then subjected to limited proteolysis followed by visualization using immunoblotting. Consistent with the result from DARTS proteomic data (Section xx), COMT showed lower protease susceptibility with HNKs (1:1), confirming binding between HNKs and COMT. However, COMT exhibited a comparable non-digested fraction after ketamine treatment compared to the control.

For the sake of further verification, a bioluminescence-based assay was also designed for COMT to monitor whether drug binding modulates its activity. COMT adds a methyl group donated by S-adenosyl methionine (SAM) to catecholamine and produces S-adenosyl homocysteine (SAH). The assay applied here monitors the formation of SAH, which is converted into ADP after the methyltransferase reaction is complete. The further conversion of ADP to ATP followed by a coupled luciferase reaction measures luminescence that can be correlated with SAH concentration, reflecting the activity of COMT (Figure 3.19). Dopamine was the receiver of the methyl group, and was converted

into 3-Methoxytyramine (3-MT) in the presence of COMT. A series of pre-experiments were carried out to determine the feasibility of the enzymatic assay and optimal concentrations of COMT and dopamine. Both COMT and dopamine concentrations exhibited good correlation to luminescence in proportion to COMT activity, and 0.15 ng of COMT/100 µM dopamine gave a good luminescence readout. After incubation with vehicle control, 20 µM ketamine, 20 µM R-HNK or 20 µM S-HNK, COMT was subjected to the assay under the optimized condition. Drug binding resulted in no change in COMT activity, suggesting that drug binding to COMT does not affect its function.

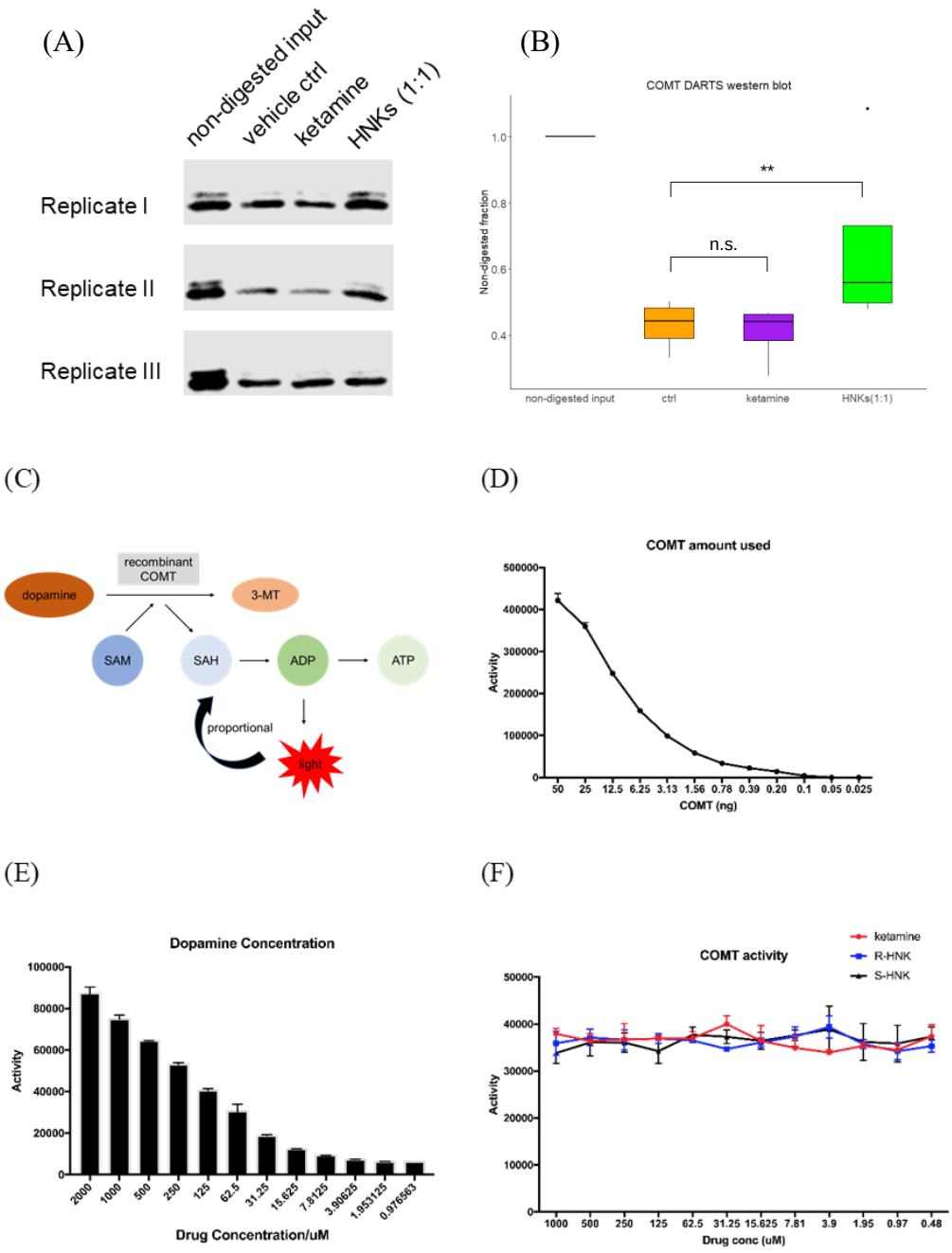

Figure 3.19 Validation of COMT binding and activity. (A-B) Western blot detection of COMT recombinant protein with anti-COMT antibody; gel band density was used to calculate protein abundance; n.s. refers to not signigicant;(C) Principle of the COMT enzymatic assay: SAM is converted into SAH by COMT, which is further converted to ADP and eventually to ATP; a coupled luciferase reaction measures the luminescence during production of ATP in proportion to SAH concentration and COMT activity; (D) COMT catalyzation curve; (E) substrate (dopamine) concentration determined in the COMT enzymatic assay; (F) COMT activity assay under the treatment of drugs.

3.4.2.3 Syntaxin-binding protein 1

Syntaxin-binding protein 1 (STXBP1) participates in the regulation of synaptic vesicle docking and fusion essential for neurotransmission via regulation of syntaxin, a transmembrane attachment protein receptor.

Parallel Reaction Monitoring-Mass Spectrometry (PRM-MS) was used to validate binding between the drugs and STXBP1. As a targeted proteomics strategy based on Q-Orbitrap, PRM-MS performs a full scan of each transition by a precursor ion and parallel monitoring of all fragments from the precursor ion, and thus is suitable for both qualification and quantification of peptides with high sensitivity and accuracy. SILAC-labeled HT-22 cell lysates were preconditioned with the DARTS protocol under the treatment of drugs or vehicle control and samples were subjected to PRM analysis. To increase the specificity, a few other candidate proteins from the DARTS dataset as well as several negative controls were also analyzed in the same MS run. Under the treatment of ketamine or HNKs, susceptibility of STXBP1 to limited proteolysis was significantly decreased due to drug protection (Figure 3.20). In contrast, ketamine and HNKs failed to show the same effect on the other candidate proteins from the DARTS assay or negative controls (randomly selected proteins).

Western blot analysis of STXBP1 was also performed to reproduce the DARTS assay and PRM analysis data. However, no significant difference in antibody-based STXBP1 protein level detection was observed after drug treatment.

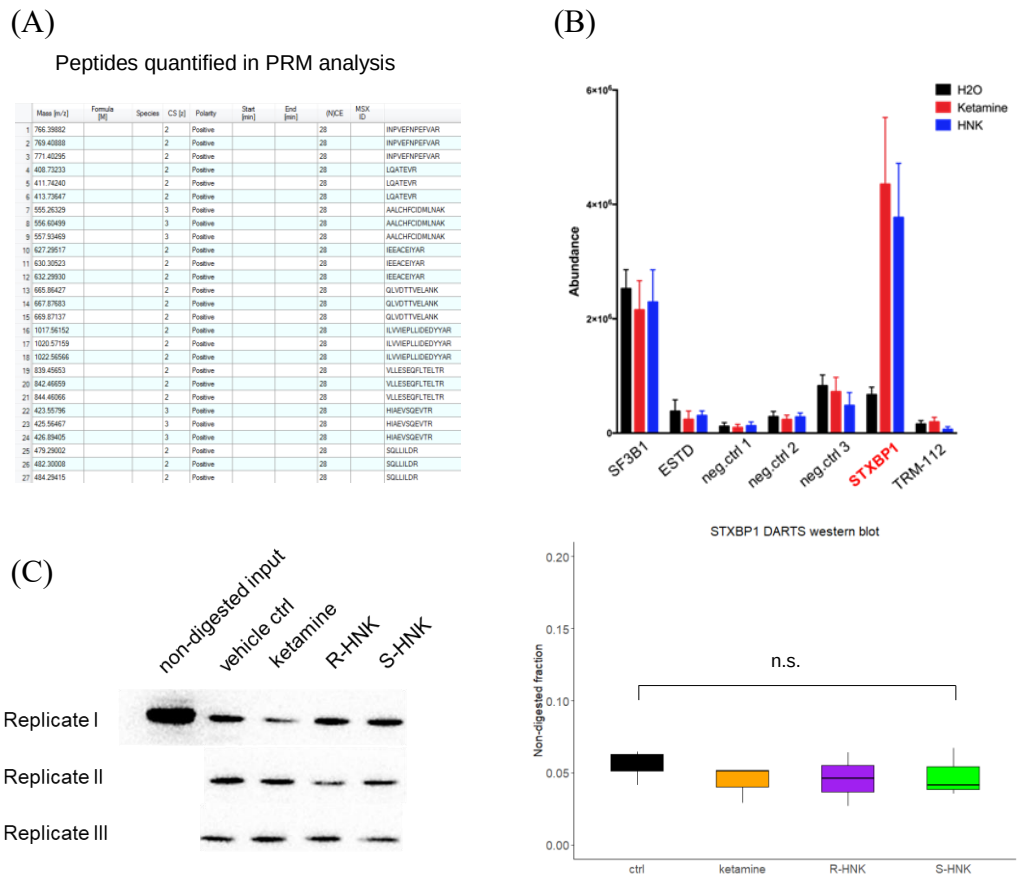

Figure 3.20 Validation of STXBP1 protection. (A) Peptides of STXBP1 and negative control proteins monitored in PRM-MS; (B) quantification of monitored proteins in PRM-MS; (C) Western blot detection with anti-STXBP1 antibody; gel band density was used to calculate protein abundance.

3.5 Discussion

Major depressive disorder (MDD) has been a heavy burden to society and affects millions of people. Despite the psychotherapy and pharmacotherapy currently applied, many patients still suffer from treatment-resistant depression (TRD) and thus show no response to clinical treatment. Side effects and other drawbacks of currently used antidepressants have limited the access to medication with significant efficacy. Ketamine, an NMDA receptor antagonist, traditionally used for starting and maintaining anesthesia, exhibits fast-acting and long-lasting antidepressant effects. However, the detailed mechanism of the mode of action of ketamine and its metabolites, HNKs, is still unknown. Unraveling the molecular target(s) of ketamine and HNK is not only fundamental for understanding their pharmacological action, but also critical to overcoming ketamine-induced adverse effects and developing novel antidepressants.

Two major strategies are usually applied for small molecule drug discovery: target-

based drug discovery and phenotype-based drug discovery. Target-based screening, which starts with selecting a known target followed by compound screening to investigate active small molecule drugs, has been largely used in drug discovery due to developments in both genomics and large-scale compound libraries. In contrast, starting with a known active drug or natural product, phenotype-based drug discovery uses an intact biological system that closely mimics clinical responses and thus increases the probability of success in drug discovery. One of the main limitations of the phenotype-based strategy is the unknown target of a drug, which necessitates the identification of proteins targets, termed "target deconvolution". Different approaches to target deconvolution have been used to discover protein targets. In this present project, taking advantage of mass spectrometry-based quantitative proteomics techniques, I applied target deconvolution to ketamine and its metabolites, HNKs, in order to identify their binding targets and uncover the mechanism of ketamine's antidepressant effect.

Chemical proteomics is widely used in protein-drug interaction studies, including labeling and label-free strategies. Label-free strategies have gained increasing attention since they require no (severe) chemical modification and thus do not affect the initial activity of the small molecules. Ketamine and its metabolites, HNKs, are small molecules with very simple structures. Chemical modification of ketamine and HNKs might induce irreversible loss of drug activity. A label-free strategy that retains the natural activity would be more suited for identifying protein targets of ketamine and HNK. The label-free strategies applied in the present work include thermal proteome profiling (TPP), drug affinity responsive target stability (DARTS) and solvent-induced protein precipitation (SIP).

In order to improve quantification accuracy, MS2-based TMT quantification and MS-based SILAC quantification were applied, depending on the samples processed in parallel. In TPP analysis where 10 temperature points were designed for each group, TMT allows the multiplexing of 10 samples. Samples in one group treated at different temperatures were labeled and combined, followed by concurrent LC-MS/MS analysis. Quantification was performed by calculating the relative intensity of reporter ions at each temperature point respective to that of the starting temperature.

In contrast to TMT labeling, SILAC quantification was lower throughput, enabling the concurrent quantification of a maximum of 3 samples. However, SILAC samples were

merged immediately after protein concentration determination, one of the earliest steps in sample preparation, thus reducing the variation from sample preparation. In DARTS and SIP analysis, SILAC was used for cell lysates incubated with a vehicle control, ketamine and a racemic mixture of R-HNK and S-HNK (HNKs). Both TMT and SILAC improved the quantification accuracy and reproducibility without obvious loss of identified protein numbers in our data.

Validation of a novel drug target involves the application of a range of techniques that aim to demonstrate not only binding between the drug and the target protein, but effects of the drug on the target protein. Early in-depth target validation increases the understanding of the relationship between target manipulation and disease efficacy, thus increasing the likelihood of success in drug development. One of the most critical tests for a novel drug target is assessing how its role changes before and after drug binding in an animal model of a specific disease[224]. However, animal models for certain diseases, including psychiatric disorders, are extremely difficult to develop due to heterogeneous syndromes resulting from multiple and varied causal factors[225]. Therefore, *in vitro* target validation is of importance for verifying drug effects especially in psychiatric illnesses.

Target deconvolution can be achieved by numerous methods including affinity chromatography, expression-cloning, protein microarray, 'reverse transfected' cell microarray, biochemical assays, and so on. As one of the most straightforward ways, biochemical assays involve the addition of a small molecule to protein extracts, which inhibits or activates an activity of interest, and where the inhibition or activation is measured using an activity assay. Biochemical assays are ideal for biologically active target proteins such as kinases, phosphatases and enzymes. In the present work, we applied both western blot and enzymatic assay on the validation of potential targets of ketamine and HNKs,

Pyruvate kinase L/R type (PKLR) was the most promising drug target candidate and its validation was attempted using different biochemical assays. The protein exhibited the most significant (melting temperature $\Delta T_m \sim 8\ ^oC$) protection effect by all 3 drugs. In addition, PKLR was identified as a possible binding target in both *in vitro* and *ex vivo* TPP analysis. As a shared target of ketamine and HNKs, PKLR binding might explain the antidepressant effects of HNKs observed in many reported studies[186, 206, 226, 227]. It

has also been reported that ketamine inhibits aerobic glycolysis[228] which involves catalyzation of pyruvate kinase. Previous studies from our laboratory have found that phosphofructokinase (PFK), another key enzyme involved in glycolysis, is stabilized by another SSRI antidepressant, paroxetine. Chronic paroxetine treatment significantly increased mouse brain PFK thermal stability and increased PFK enzymatic activity both *in vitro* and *in vivo*[229]. The binding between ketamine/HNKs and PKLR further links MDD and the antidepressant effect of ketamine with energy metabolism, which has been previously reported to be affected after the treatment of ketamine and other antidepressants[230, 231]. In our validation for PKLR, binding between PKLR and ketamine/HNKs was confirmed with a human PKLR recombinant protein (rPKLR) using immunoblotting. Similar to the thermal shift curve fitted from mass spectrometry data, stabilization of PKLR upon ketamine and HNKs binding were also observed by Western blot. Subsequently, isothermal dose-response fingerprints (ITDRF) was applied to rPKLR and further verified that binding between PKLR and the drugs was dose-dependent.

Since pyruvate kinase catalyzes the transfer of a phosphate group, an enzyme assay was then used to explore the effects of drug binding on PKLR activity. However, no significant change in PKLR activity was observed using different drug concentrations, suggesting that drug binding does not affect the overall kinase activity of PKLR. This could be explained by the non-functional binding of drugs. Binding between ligands and proteins is based on sufficient binding affinity and physical distance determined by their chemical structures. In contrast, the catalytic activity of kinases is usually determined by the binding between kinases and their endogenous substrates. In competitive inhibition, an inhibitor that resembles the normal substrate binds to the enzyme, usually at the active site, and prevents the substrate from binding. At any given moment, the enzyme may be bound to the inhibitor or the substrate (or neither), but it cannot bind both at the same time. Inhibition of PKLR activity would only become apparent when it binds to ketamine or HNKs at its active sites. The binding found here is apparently at another non-active site. Therefore, further validation with other methods, such as immunoprecipitation pull-down assays, should be applied to PKLR to explore the possible mechanism of drug modulation.

We also selected catechol-O-methyltransferase (COMT) as a biologically relevant protein target for validation. COMT, which is expressed in different tissues and degrades catecholamines including dopamine, has previously been implicated in depression. Some animal studies revealed that altered levels of dopamine and other neurotransmitters lead

to depressive-like behavior[232-234]. A pilot study of outpatients with MDD showed a significant reduction in depression severity after open treatment with tolcapone, a COMT inhibitor[235]. In our validation, the binding between COMT and HNKs was confirmed with human recombinant COMT protein (rCOMT) using immunoblotting. COMT showed decreased susceptibility to proteolysis with HNKs, a mixture of R-HNK and S-HNK in a 1:1 ratio. However, the effect of ketamine was not significant, which is probably due to the lack of co-factors for binding present in the cell extracts, but not with the recombinant protein. A bioluminescence-based assay was also designed for COMT to test modulation of its activity by drugs via measuring the concentration of 3-Methoxytyramine (3-MT) generated from the conversion of dopamine catalyzed by COMT. The drugs mediated no significant effects on COMT activity, which might also be due to binding to a non-functional COMT site. Further validation with other methods should also be applied to confirm the binding between COMT and ketamine/HNKs.

Syntaxin binding protein-1 (STXBP1), a target of HNKs but not ketamine from our data, was also subjected to validation. STXBP1 participates in the regulation of synaptic vesicle docking and fusion through interaction with GTP-binding proteins, and thus is essential for neurotransmission via binding syntaxin, a component of the synaptic vesicle fusion machinery. STXBP1 has been associated with MDD in a shotgun proteomic analysis of post-mortem dorsolateral prefrontal cortex (DLPFC) brain tissue from 24 MDD patients[236]. Other syntaxin binding proteins including STXBP3, as well as vesicle-associated protein 1 (VAMP1), were found to be downregulated in chronic unpredictable mild stress induced depression[237].

All the above-mentioned candidate targets we selected for validation have been linked with depression and an antidepressant effect, yet to our knowledge, have not been identified as drug targets of antidepressants. Parallel Reaction Monitoring-Mass Spectrometry (PRM-MS) was used to verify the DARTS data for STXBP1with higher sensitivity and quantification accuracy. In contrast to negative controls (non-target proteins) that showed no change under drug treatment in PRM analysis, STXBP1 exhibited significant changes in the peptides monitored in the parallel reaction, confirming that the abundance change of STXBP1 was a result of ketamine or HNKs binding. However, Western blots did not show any regulation of STXBP1 after drug treatment. The ambiguous results obtained from different validation methods indicated that STXBP1 might not be a true target of ketamine/HNKs.

The compatibility between label-free protein-ligand interaction methods and common protein targets of antidepressants might be one of the limitations in my PhD project. Label-free strategies for studying protein-ligand interactions have been widely used for screening protein targets, but were mainly limited to soluble proteins. For psychiatric disorders where drug targets are more likely to involve transmembrane proteins, the extraction of membrane proteins may be incompatible with drug binding. Common protocols for extracting membrane proteins use a variety of detergents which can result in deactivation and denaturation, whereas binding between a drug and target proteins require proteins in their native state. Although we attempted to overcome this problem by using milder detergents (e.g. 0.4% NP-40), which do not alter protein structures, indeed very few membrane proteins were included in our datasets. Therefore, most of the candidates we identified are cytoplasmic proteins.

In addition, poor reproducibility in the validation of STXBP1 suggests that DARTS, as well as other affinity-based protein-ligand identification methods, highly depend on the strict control of experimental conditions. Drug binding to protect a protein from denaturation or degradation only takes place within a very narrow range of denaturing conditions. Slightly higher concentrations of proteases or longer digestion times may therefore not show any drug protection effects. Moreover, selection of candidates for validation is also important because drug binding does not necessarily produce biological effects, as shown for PKLR. Our strategy was to find proteins conservatively identified using different methods. However, low overlap was found in the identification of new targets of ketamine and HNKs among the different methods. These methods are based on different principles. The thermal stability of a protein and proteolysis susceptibility may not necessarily give the same result. For that reason, choosing biologically relevant proteins or protein classes (transporter, kinases, etc.) may increase the possibility of successfully discovering a novel drug target.

In conclusion, using mass spectrometry-based proteomics methods, we identified 33 high-confidence potential binding targets of ketamine and/or its metabolite HNK. Subsequent validation revealed that pyruvate kinase (PKLR) might be a target for both ketamine and HNK with an unknown mechanism.

4 Summary and outlook

Major depressive disorder (MDD), as well as the costs of medication for its treatment impose a heavy burden on patients and society. Pharmacological treatment of MDD relies on antidepressants. The development of novel antidepressants should be aimed at reducing any drug's side effects and accelerating the mode of action.

In my PhD projects I have used mass spectrometry-based proteomics techniques to study the impulsivity-related side effects of a classic selective serotonin reuptake inhibitor, fluoxetine, and discover novel drug targets of the fast-acting antidepressant ketamine. I have found that the GABAergic synapse is involved in mechanisms underlying the increased impulsivity observed in juvenile macaques in response to chronic fluoxetine treatment. Several biomarkers were also identified, which upon validation could be used as a biosignature for impulsivity or risk of suicidality in depressed children taking fluoxetine. A number of potential protein targets of the fast-acting antidepressant ketamine and/or its metabolites, HNK, were also identified using a complete screening with several protein-drug interaction methods. Pyruvate kinase was found to be a target of ketamine and HNKs, further supporting the involvement of energy metabolism in MDD and an antidepressant mode of action.

The candidate biomarkers and drug targets in combination with the affected pathways contribute to a better understanding of the mechanisms underlying the side effects of clinically used antidepressants and pharmacological effects of novel antidepressants; both of which have been widely studied yet not completely elucidated. In addition, drug development, in this case antidepressants, also benefits from discovering novel binding targets and modes of action enabling modification or derivatization of small molecules for drug development efforts aiming for high efficacy and low side effects. The results of my project support the notion that mass spectrometry-based proteomics is a powerful tool for studying human diseases and drug development.

Appendixes

Appendix 1 Proteins associated with impulsivity behavior of fluoxetine-treated macaques

Gene	Human homology	Description
(DLPFC)		
PTGES3	Q15185	Prostaglandin E synthase 3
VPS8	Q8N3P4	Vacuolar protein sorting-associated protein 8 homolog
KIRREL3	Q8IZU9	Kin of IRRE-like protein 3
SH3BP5L	Q7L8J4	SH3 domain-binding protein 5-like
FECH	P22830	Ferrochelatase, mitochondrial
UBA1	P22314	Ubiquitin-like modifier-activating enzyme 1
IFITM10	A6NMD0	Interferon-induced transmembrane protein 10
RAB12	Q6IQ22	Ras-related protein Rab-12
RGCC	Q9H4X1	Regulator of cell cycle RGCC
CD59	P13987	CD59 glycoprotein
MRPL3	P09001	39S ribosomal protein L3, mitochondrial
DCAKD	Q8WVC6	Dephospho-CoA kinase domain-containing protein
ITGA6	P23229	Integrin alpha-6
RHOF	Q9HBH0	Rho-related GTP-binding protein RhoF
RNMT	O43148	mRNA cap guanine-N7 methyltransferase
RRAS	P10301	Ras-related protein R-Ras
ITGAV	P06756	Integrin alpha-V
ADGRB3	O60242	Adhesion G protein-coupled receptor B3
BTF3	P20290	Transcription factor BTF3
NFIA	Q12857	Nuclear factor 1 A-type
ATP5E	P56381	ATP synthase subunit epsilon, mitochondrial
(CC)		
PDZD4	Q76G19	PDZ domain-containing protein 4
SEPTIN4	O43236	Septin-4
ANLN	Q9NQW6	Anillin
NEFH	P12036	Neurofilament heavy polypeptide
OTUD7A	Q8TE49	OTU domain-containing protein 7A
CA14	Q9ULX7	Carbonic anhydrase 14
GSTO1	P78417	Glutathione S-transferase omega-1

DCTN1	Q14203	Dynactin subunit 1
MADD	Q8WXG6	MAP kinase-activating death domain protein
NOL3	O60936	Nucleolar protein 3
TRAPPC10	P48553	Trafficking protein particle complex subunit 10
LOC720791	P13489	Ribonuclease inhibitor
FOLH1	Q04609	Glutamate carboxypeptidase 2
PPP1R9B	Q96SB3	Neurabin-2
HDAC11	Q96DB2	Histone deacetylase 11
HAPLN1	P10915	Hyaluronan and proteoglycan link protein 1
CFL2	Q9Y281	Cofilin-2
KIF5A	Q12840	Kinesin heavy chain isoform 5A
LRP4	O75096	Low-density lipoprotein receptor-related protein 4
UBE4A	Q14139	Ubiquitin conjugation factor E4 A
NPEPPS	P55786	Puromycin-sensitive aminopeptidase
SPTBN1	Q01082	Spectrin beta chain, non-erythrocytic 1
VPS50	Q96JG6	Syndetin

Appendix 2 Phosphorylation sites associated with impulsivity behavior of macaques dosed by fluoxetine

Gene	Phospho Site	Description
(DLPFC)		
DPYSL2	S507/T509	Dihydropyrimidinase-related protein 2
LOC719082	T331/S333	WASH complex subunit 2C
DMTN	S201	Dematin
RAP1GAP	S584/S585	Rap1 GTPase-activating protein 1
PDE4B	S86	cAMP-specific 3',5'-cyclic phosphodiesterase 4B
PITPNM3	S295/S297	Membrane-associated phosphatidylinositol transfer protein 3
NCAM1	UC	Neural cell adhesion molecule 1
SRRM2	S992/S994/S1876 /S1878/T1880	Serine/arginine repetitive matrix protein 2
MAPT	S311/T314	Microtubule-associated protein tau
SLC7A11	S39	Cystine/glutamate transporter

SEC62	T337	Translocation protein SEC62
MAPT	S61	Microtubule-associated protein tau
MAP1A	S853	Microtubule-associated protein 1A
SLC39A3	S125/UC	Zinc transporter ZIP3
SRCIN1	S229	SRC kinase signaling inhibitor 1
RTN3	S372	Reticulon-3
MAP1B	S1260/S1262/ S1265/S1443/UC	Microtubule-associated protein 1B
SPP1	S303/S308/S310	Osteopontin
ANK2	S1455	Ankyrin-2
MAP2K4	T391/UC	Dual specificity mitogen-activated protein kinase kinase 4
PAK1	T219	Serine/threonine-protein kinase PAK 1
NCL	S28/S41/S42	Nucleolin
COX7B	T30	Cytochrome c oxidase subunit 7B, mitochondrial
(CC)		
DPYSL2	S507/T509	Dihydropyrimidinase-related protein 2
TCEA1	S79	Transcription elongation factor A protein 1
STK39	S375/S376	STE20/SPS1-related proline-alanine-rich protein kinase
MBP	T232/UC	Myelin basic protein
GAS7	S152	Growth arrest-specific protein 7
KIF21A	S1258/S1262	Kinesin-like protein KIF21A
BIN1	UC	Myc box-dependent-interacting protein 1
ACAP2	S373	Arf-GAP with coiled-coil, ANK repeat and PH domain-containing protein 2
RANGAP1	S441/UC	Ran GTPase-activating protein 1
NEFH	T765/T900	Neurofilament heavy polypeptide
TMEM163	S38	Transmembrane protein 163
GBF1	UC	Golgi-specific brefeldin A-resistance guanine nucleotide exchange factor 1
OXR1	S526	Oxidation resistance protein 1
CHGB	S292/UC	Secretogranin-1
SLC29A1	S608	Equilibrative nucleoside transporter 1
IWS1	S315	Protein IWS1 homolog

MADD	S818/S820	MAP kinase-activating death domain protein
TCP11L1	S42/UC	T-complex protein 11-like protein 1
CAMK2A	T409/S412	Calcium/calmodulin-dependent protein kinase type II subunit alpha
MPHOSPH10	S164/S168/S172	U3 small nucleolar ribonucleoprotein protein MPP10
MAP1A	S2851	Microtubule-associated protein 1A
NEFM	S44	Neurofilament medium polypeptide
HNRNPD	S83	Heterogeneous nuclear ribonucleoprotein D0
SH3PXD2A	S487/T488	SH3 and PX domain-containing protein 2A
MAP1B	S1144/UC	Microtubule-associated protein 1B
ANK2	S2820	Ankyrin-2
BSN	S2578/S2581	Protein bassoon
HSF1	S303/S307	Heat shock factor protein 1
SNW1	S220/S228	SNW domain-containing protein 1
PDE4D	S132	cAMP-specific 3',5'-cyclic phosphodiesterase 4D
PDHA1	S293/S300	Pyruvate dehydrogenase E1 component subunit alpha, somatic form, mitochondrial
SPTAN1	S1180	Spectrin alpha chain, non-erythrocytic 1
PRAG1	UC	Inactive tyrosine-protein kinase PRAG1
MFAP1	T267	Microfibrillar-associated protein 1
RAB1A	T195	Ras-related protein Rab-1A
BCAS3	S570	Breast carcinoma-amplified sequence 3
SIRT2	UC	NAD-dependent protein deacetylase sirtuin-2
CNP	S22/S312	2',3'-cyclic-nucleotide 3'-phosphodiesterase

* UC = uncertain

Appendix 3 Drug target candidates

MS-CETSA (TPP) (N = 45)

Gene	Description	ΔTm (°C)		
		Ket	R-HNK	S-HNK
DDI2	Protein DDI1 homolog 2	2.5	-	-
TLK2	Serine/threonine-protein kinase 2	-	-	3.7
H2BC14	Histone H2B type 1-M	3.9	-	-

RPL12	60S ribosomal protein L12	-	-	-2.5
CREBBP	Histone lysine acetyltransferase CREBBP	-	-	4.3
PKLR	Pyruvate kinase PKLR	7.0	8.5	8.4
YWHAQ	14-3-3 protein theta	-	-	2.0
SMPD1	Sphingomyelin phosphodiesterase	-	-	2.0
ACOT6	Acyl-coenzyme A thioesterase 6	-3.4	-	-
RAB26	Ras-related protein Rab-26	-	-3.2	-
P4HA2	Prolyl 4-hydroxylase subunit alpha-2	-	-	-1.6
MAP2K2	Dual specificity mitogen-activated protein kinase kinase 2	2.3	-	-
H2BC9	Histone H2B type 1-H	3.9	-	-
MARS1	Methionine--tRNA ligase, cytoplasmic	3.1	-	-
INPPL1	Phosphatidylinositol 3,4,5-trisphosphate 5-phosphatase 2	-	2.5	-
ACOT5	Acyl-coenzyme A thioesterase 5	-3.4	-	-
CFAP94	Dynein intermediate chain CFAP94, axonemal	-	-2.2	-
H2BC4	Histone H2B type 1-C/E/G	3.9	-	-
ECI3	Enoyl-CoA delta isomerase 3, peroxisomal	-1.9	-	-
CTDP1	RNA polymerase II subunit A C-terminal domain phosphatase	4.9	-	-
EHD2	EH domain-containing protein 2	-2.9	-	-
PSMD5	26S proteasome non-ATPase	-2.4	-	-
ACOT4	Peroxisomal succinyl-coenzyme A thioesterase	-3.4	-	-
RAE1	mRNA export factor	-	1.3	-
RAB43	Ras-related protein Rab-43	-	-3.2	-
AIMP2	Aminoacyl tRNA synthase complex-interacting multifunctional protein 2	2.9	-	-
CACUL1	CDK2-associated and cullin domain-containing protein 1	-	-	4.3
NUDCD3	NudC domain-containing protein 3	-	1.2	-
PANK3	Pantothenate kinase 3	-	-	2.8
RBM42	RNA-binding protein 42	2.8	-	-
PAIP2B	Polyadenylate-binding protein-interacting protein 2B	1.9	-	2.4

CSDE1	Cold shock domain-containing protein E1	-	-	2.9
RAB30	Ras-related protein Rab-30	-	-3.1	-
KDELR1	ER lumen protein-retaining receptor 1	-4.7	-	-3.0
IGF2BP3	Insulin-like growth factor 2 mRNA-binding protein 3	-2.9	-	-
POLE4	DNA polymerase epsilon subunit 4	-	5.2	-
CAP2	Adenylyl cyclase-associated protein 2	-1.5	-	-
OLA1	Obg-like ATPase 1	1.3	-	-
TAX1BP3	Tax1-binding protein 3	1.6	-	-
GABARAP	Gamma-aminobutyric acid receptor-associated protein	-	-	3.6
GTF2I	General transcription factor II-I	-	1.7	-
RAB37	Ras-related protein Rab-37	-	-3.2	-
CYHR1	Cysteine and histidine-rich protein 1	2.7	-	-
ACOT3	Acyl-coenzyme A thioesterase 3	-3.4	-	-
TSC22D3	TSC22 domain family protein 3	-	4.5	-

DARTS (N = 54)

Gene	Description
GTPBP1	GTP-binding protein 1
HDAC1	Histone deacetylase 1
GET3	ATPase GET3
LMNA	Prelamin-A/C
ADK	Adenosine kinase
MAGOH	Protein mago nashi homolog
ELOB	Elongin-B
RPS17	40S ribosomal protein S17
MYH10	Myosin-10
ADH7	All-trans-retinol dehydrogenase [NAD
GALK2	N-acetylgalactosamine kinase
TPM4	Tropomyosin alpha-4 chain
SGTA	Small glutamine-rich tetratricopeptide repeat-containing protein alpha
RNH1	Ribonuclease inhibitor
DPP3	Dipeptidyl peptidase 3
SF3B1	Splicing factor 3B subunit 1
RPL22L1	60S ribosomal protein L22-like 1

TRMT112	Multifunctional methyltransferase subunit TRM112-like protein
SLC7A5	Large neutral amino acids transporter small subunit 1
PLPBP	Pyridoxal phosphate homeostasis protein
NIPSNAP1	Protein NipSnap homolog 1
EIF6	Eukaryotic translation initiation factor 6
CLPP	ATP-dependent Clp protease proteolytic subunit, mitochondrial
RPP30	Ribonuclease P protein subunit p30
DRG1	Developmentally-regulated GTP-binding protein 1
STT3A	Dolichyl-diphosphooligosaccharide--protein glycosyltransferase
HARS1	Histidine--tRNA ligase, cytoplasmic
KIF5B	Kinesin-1 heavy chain
SLC25A12	Calcium-binding mitochondrial carrier protein Aralar1
LETM1	Mitochondrial proton/calcium exchanger protein
DHX15	Pre-mRNA-splicing factor ATP-dependent RNA helicase DHX15
PSDE	26S proteasome non-ATPase regulatory subunit 14
PDHA1	Pyruvate dehydrogenase E1 component subunit alpha
CAZA1	F-actin-capping protein subunit alpha-1
DYNLRB1	Dynein light chain roadblock-type 1
HNRPD	Heterogeneous nuclear ribonucleoprotein D0
LONM	Lon protease homolog, mitochondrial
CBR3	Carbonyl reductase [NADPH] 3
GRPEL1	GrpE protein homolog 1, mitochondrial
SACM1L	Phosphatidylinositol-3-phosphatase SAC1
WDR61	WD repeat-containing protein 61
MYG1	MYG1 exonuclease
NT5C	5'(3')-deoxyribonucleotidase, cytosolic type
RPL35A	60S ribosomal protein L35a
LAMB1	Laminin subunit beta-1
UBE2M	NEDD8-conjugating enzyme Ubc12
TUBB5	Tubulin beta-5 chain
DDX5	Probable ATP-dependent RNA helicase DDX5
MARS1	Methionine--tRNA ligase, cytoplasmic
NSFL1C	NSFL1 cofactor p47
AKR1A1	Aldo-keto reductase family 1 member A1
ESD	S-formylglutathione hydrolase
STXBP1	Syntaxin-binding protein 1

COMT	Catechol O-methyltransferase

SIP (N = 77)

Gene	Description
GPT2	Alanine aminotransferase 2
DKC1	H/ACA ribonucleoprotein complex subunit DKC1
ACOT2	Acyl-coenzyme A thioesterase 2, mitochondrial
RPS26	40S ribosomal protein S26
UFD1	Ubiquitin recognition factor in ER-associated degradation protein 1
CRYZL1	Quinone oxidoreductase-like protein 1
HAGH	Hydroxyacylglutathione hydrolase, mitochondrial
GCAT	2-amino-3-ketobutyrate coenzyme A ligase, mitochondrial
H3C2	Histone H3.2
IARS2	Isoleucine--tRNA ligase, mitochondrial
ACOT1	Acyl-coenzyme A thioesterase 1
RPS3	40S ribosomal protein S3
TSN	Translin
CSTF1	Cleavage stimulation factor subunit 1
GPNMB	Transmembrane glycoprotein NMB
LAP3	Cytosol aminopeptidase
SDF2	Stromal cell-derived factor 2
ANP32A	Acidic leucine-rich nuclear phosphoprotein 32 family member A
UGDH	UDP-glucose 6-dehydrogenase
COPS4	COP9 signalosome complex subunit 4
HSP90AA1	Heat shock protein HSP 90-alpha
PGK1	Phosphoglycerate kinase 1
ANXA1	Annexin A1
TCP1	T-complex protein 1 subunit alpha
LTA4H	Leukotriene A-4 hydrolase
IMPDH2	Inosine-5'-monophosphate dehydrogenase 2
FKBP4	Peptidyl-prolyl cis-trans isomerase FKBP4
PKM	Pyruvate kinase PKM
EEF1D	Elongation factor 1-delta
CCT2	T-complex protein 1 subunit beta
CCT4	T-complex protein 1 subunit delta

CCT6A	T-complex protein 1 subunit zeta
CCT3	T-complex protein 1 subunit gamma
ANP32E	Acidic leucine-rich nuclear phosphoprotein 32 family member E
RBBP7	Histone-binding protein RBBP7
TFRC	Transferrin receptor protein 1
HUWE1	E3 ubiquitin-protein ligase HUWE1
PRMT5	Protein arginine N-methyltransferase 5
ERO1A	ERO1-like protein alpha
CSPG4	Chondroitin sulfate proteoglycan 4
ACLY	ATP-citrate synthase
FDPS	Farnesyl pyrophosphate synthase
ACO2	Aconitate hydratase, mitochondrial
CS	Citrate synthase, mitochondrial
EEF1G	Elongation factor 1-gamma
MVP	Major vault protein
USP14	Ubiquitin carboxyl-terminal hydrolase 14
RPS17	40S ribosomal protein S17
HARS1	Histidine--tRNA ligase, cytoplasmic
PDXK	Pyridoxal kinase
PALLD	Palladin
EXOSC2	Exosome complex component RRP4
HNRNPDL	Heterogeneous nuclear ribonucleoprotein D-like
GOT2	Aspartate aminotransferase, mitochondrial
HSD17B10	3-hydroxyacyl-CoA dehydrogenase type-2
GAPDH	Glyceraldehyde-3-phosphate dehydrogenase
AHSA1	Activator of 90 kDa heat shock protein ATPase homolog 1
TRIM47	E3 ubiquitin-protein ligase TRIM47
CYP51A1	Lanosterol 14-alpha demethylase
PTGES3	Prostaglandin E synthase 3
CLPP	ATP-dependent Clp protease proteolytic subunit, mitochondrial
PDIA4	Protein disulfide-isomerase A4
TPI1	Triosephosphate isomerase
CAP1	Adenylyl cyclase-associated protein 1
TKT	Discoidin domain-containing receptor 2
IDH2	Isocitrate dehydrogenase [NADP], mitochondrial
ERP29	Endoplasmic reticulum resident protein 29

UBE2M	NEDD8-conjugating enzyme Ubc12
HSPD1	60 kDa heat shock protein, mitochondrial
HDAC2	Histone deacetylase 2
CLUH	Clustered mitochondria protein homolog
GDI2	Rab GDP dissociation inhibitor beta
TRIM28	Transcription intermediary factor 1-beta
GPD2	Glycerol-3-phosphate dehydrogenase, mitochondrial
THUMPD1	THUMP domain-containing protein 1
EPHX1	Epoxide hydrolase 1
COX5B	Cytochrome c oxidase subunit 5B, mitochondrial

References

1. Otte, C., et al., *Major depressive disorder.* Nat Rev Dis Primers, 2016. **2**: p. 16065.
2. WHO. *Depression*. 2020; Available from: https://www.who.int/news-room/fact-sheets/detail/depression.
3. Edition, F., *Diagnostic and statistical manual of mental disorders.* Am Psychiatric Assoc, 2013.
4. Seedat, S., et al., *Cross-national associations between gender and mental disorders in the World Health Organization World Mental Health Surveys.* Arch Gen Psychiatry, 2009. **66**(7): p. 785-95.
5. Bromet, E., et al., *Cross-national epidemiology of DSM-IV major depressive episode.* BMC medicine, 2011. **9**(1): p. 90.
6. WHO, *Suicide.* 2016.
7. Chesney, E., G.M. Goodwin, and S. Fazel, *Risks of all‐cause and suicide mortality in mental disorders: a meta‐review.* World psychiatry, 2014. **13**(2): p. 153-160.
8. Olesen, J., et al., *The economic cost of brain disorders in Europe.* Eur J Neurol, 2012. **19**(1): p. 155-62.
9. Belmaker, R. and G. Agam, *Major depressive disorder.* New England Journal of Medicine, 2008. **358**(1): p. 55-68.
10. Kendler, K.S., C.O. Gardner, and C.A. Prescott, *Clinical characteristics of major depression that predict risk of depression in relatives.* Archives of general psychiatry, 1999. **56**(4): p. 322-327.
11. Schildkraut, J.J., *The catecholamine hypothesis of affective disorders: a review of supporting evidence.* American journal of Psychiatry, 1965. **122**(5): p. 509-522.
12. Von Knorring, A.L., et al., *Platelet MAO activity as a biological marker in subgroups of alcoholism.* Acta Psychiatrica Scandinavica, 1985. **72**(1): p. 51-58.
13. Meyer, J.H., et al., *Elevated monoamine oxidase a levels in the brain: an explanation for the monoamine imbalance of major depression.* Archives of general psychiatry, 2006. **63**(11): p. 1209-1216.
14. Buznikov, G.A., W.H. Lambert, and J.M. Lauder, *Serotonin and serotonin-like substances as regulators of early embryogenesis and morphogenesis.* Cell and tissue research, 2001. **305**(2): p. 177-186.
15. Johnson, S., et al., *The reduction of R1, a novel repressor protein for monoamine oxidase A, in major depressive disorder.* Neuropsychopharmacology, 2011. **36**(10): p. 2139-2148.
16. McEwen, B.S., *Protective and damaging effects of stress mediators.* New England journal of medicine, 1998. **338**(3): p. 171-179.
17. Merali, Z., et al., *Dysregulation in the suicide brain: mRNA expression of corticotropin-releasing hormone receptors and GABAA receptor subunits in frontal cortical brain region.* Journal of Neuroscience, 2004. **24**(6): p. 1478-1485.
18. MacMaster, F.P., et al., *Pituitary volume in treatment-naive pediatric major depressive disorder.* Biological psychiatry, 2006. **60**(8): p. 862-866.
19. Burke, H.M., et al., *Depression and cortisol responses to psychological stress: a meta-analysis.* Psychoneuroendocrinology, 2005. **30**(9): p. 846-856.
20. Carroll, B., et al., *Pathophysiology of hypercortisolism in depression.* Acta Psychiatrica Scandinavica, 2007. **115**: p. 90-103.
21. Boyle, M.P., et al., *Acquired deficit of forebrain glucocorticoid receptor produces depression-like changes in adrenal axis regulation and behavior.* Proceedings of

the National Academy of Sciences, 2005. **102**(2): p. 473-478.
22. Kozlovsky, N., et al., *Long-term down-regulation of BDNF mRNA in rat hippocampal CA1 subregion correlates with PTSD-like behavioural stress response.* International Journal of Neuropsychopharmacology, 2007. **10**(6): p. 741-758.
23. Angelucci, F., S. Brene, and A. Mathe, *BDNF in schizophrenia, depression and corresponding animal models.* Molecular psychiatry, 2005. **10**(4): p. 345-352.
24. Hasler, G., et al., *Reduced prefrontal glutamate/glutamine and γ-aminobutyric acid levels in major depression determined using proton magnetic resonance spectroscopy.* Archives of general psychiatry, 2007. **64**(2): p. 193-200.
25. Zarate, C.A., et al., *A randomized trial of an N-methyl-D-aspartate antagonist in treatment-resistant major depression.* Archives of general psychiatry, 2006. **63**(8): p. 856-864.
26. Bhagwagar, Z., et al., *Reduction in occipital cortex γ-aminobutyric acid concentrations in medication-free recovered unipolar depressed and bipolar subjects.* Biological psychiatry, 2007. **61**(6): p. 806-812.
27. Sanacora, G., et al., *Subtype-specific alterations of γ-aminobutyric acid and glutamatein patients with major depression.* Archives of general psychiatry, 2004. **61**(7): p. 705-713.
28. Brambilla, P., et al., *GABAergic dysfunction in mood disorders.* Molecular psychiatry, 2003. **8**(8): p. 721-737.
29. Rajkowska, G., et al., *GABAergic neurons immunoreactive for calcium binding proteins are reduced in the prefrontal cortex in major depression.* Neuropsychopharmacology, 2007. **32**(2): p. 471-482.
30. Felger, J.C. and F.E. Lotrich, *Inflammatory cytokines in depression: neurobiological mechanisms and therapeutic implications.* Neuroscience, 2013. **246**: p. 199-229.
31. Lewy, A.J., et al., *The circadian basis of winter depression.* Proceedings of the National Academy of Sciences, 2006. **103**(19): p. 7414-7419.
32. Beasley, C.L., et al., *Reductions in cholesterol and synaptic markers in association cortex in mood disorders.* Bipolar disorders, 2005. **7**(5): p. 449-455.
33. Torregrossa, M.M., et al., *Peptidic delta opioid receptor agonists produce antidepressant-like effects in the forced swim test and regulate BDNF mRNA expression in rats.* Brain research, 2006. **1069**(1): p. 172-181.
34. Janowsky, D.S. and D.H. Overstreet, *Cholinergic-muscarinic dysfunction in mood disorders.* MEDICAL PSYCHIATRY, 2007. **35**: p. 67.
35. Sullivan, G.M., et al., *Low cerebrospinal fluid transthyretin levels in depression: correlations with suicidal ideation and low serotonin function.* Biological psychiatry, 2006. **60**(5): p. 500-506.
36. Mayberg, H.S., et al., *Deep brain stimulation for treatment-resistant depression.* Neuron, 2005. **45**(5): p. 651-660.
37. Hillhouse, T.M. and J.H. Porter, *A brief history of the development of antidepressant drugs: from monoamines to glutamate.* Exp Clin Psychopharmacol, 2015. **23**(1): p. 1-21.
38. American, A.D.A.o. *Clinical Practice Review for Major Depressive Disorder*. 2020; Available from: https://adaa.org/resources-professionals/practice-guidelines-mdd#First-Line%20Treatments:%20Pharmacotherapy.
39. BN, N.A., *STAR* D: revising conventional wisdom.* CNS Drugs, 2009. **23**: p. 627647Schlattner.
40. Crown, W.H. and J.M. Russell, *The impact of treatment-resistant depression on*

health care utilization and costs. The Journal of clinical psychiatry, 2002. **63**(11): p. 963-971.
41. Lespérance, F., et al., *Five-year risk of cardiac mortality in relation to initial severity and one-year changes in depression symptoms after myocardial infarction.* Circulation, 2002. **105**(9): p. 1049-1053.
42. Mezuk, B., et al., *Depression and type 2 diabetes over the lifespan: a meta-analysis.* Diabetes care, 2008. **31**(12): p. 2383-2390.
43. Lader, M., *Limitations of current medical treatments for depression: disturbed circadian rhythms as a possible therapeutic target.* European neuropsychopharmacology, 2007. **17**(12): p. 743-755.
44. Yang, C., et al., *Molecular and cellular mechanisms underlying the antidepressant effects of ketamine enantiomers and its metabolites.* Translational Psychiatry, 2019. **9**(1).
45. NHS. *Side effects - Antidepressants*. 2018 [cited 2018 Aug. 16]; Available from: https://www.nhs.uk/mental-health/talking-therapies-medicine-treatments/medicines-and-psychiatry/antidepressants/side-effects/.
46. Wilkins, M.R., et al., *Progress with proteome projects: why all proteins expressed by a genome should be identified and how to do it.* Biotechnol Genet Eng Rev, 1996. **13**: p. 19-50.
47. Zhang, Y., et al., *Protein analysis by shotgun/bottom-up proteomics.* Chem Rev, 2013. **113**(4): p. 2343-94.
48. Jungbauer, A. and R. Hahn, *Chapter 22 Ion-Exchange Chromatography.* 2009. **463**: p. 349-371.
49. Voedisch, B. and H. Thie, *Size exclusion chromatography*, in *Antibody Engineering*. 2010, Springer. p. 607-612.
50. Hage, D.S., et al., *Pharmaceutical and biomedical applications of affinity chromatography: recent trends and developments.* J Pharm Biomed Anal, 2012. **69**: p. 93-105.
51. Aslam, B., et al., *Proteomics: Technologies and Their Applications.* J Chromatogr Sci, 2017. **55**(2): p. 182-196.
52. Issaq, H. and T. Veenstra, *Two-dimensional polyacrylamide gel electrophoresis (2D-PAGE): advances and perspectives.* Biotechniques, 2008. **44**(5): p. 697-8, 700.
53. Marouga, R., S. David, and E. Hawkins, *The development of the DIGE system: 2D fluorescence difference gel analysis technology.* Anal Bioanal Chem, 2005. **382**(3): p. 669-78.
54. Sutandy, F.X., et al., *Overview of protein microarrays.* Curr Protoc Protein Sci, 2013. **Chapter 27**: p. Unit 27 1.
55. Aebersold, R. and M. Mann, *Mass spectrometry-based proteomics.* Nature, 2003. **422**(6928): p. 198-207.
56. Yates III, J.R., *Mass spectrometry and the age of the proteome.* Journal of Mass Spectrometry, 1998. **33**(1): p. 1-19.
57. Schaffer, L.V., et al., *Identification and quantification of murine mitochondrial proteoforms using an integrated top-down and intact-mass strategy.* Journal of proteome research, 2018. **17**(10): p. 3526-3536.
58. Venable, J.D., et al., *Automated approach for quantitative analysis of complex peptide mixtures from tandem mass spectra.* Nature methods, 2004. **1**(1): p. 39-45.
59. Gerber, S.A., et al., *Absolute quantification of proteins and phosphoproteins from cell lysates by tandem MS.* Proceedings of the National Academy of Sciences,

2003. **100**(12): p. 6940-6945.
60. Washburn, M.P., D. Wolters, and J.R. Yates, *Large-scale analysis of the yeast proteome by multidimensional protein identification technology.* Nature biotechnology, 2001. **19**(3): p. 242-247.
61. Bantscheff, M., et al., *Quantitative mass spectrometry in proteomics: a critical review.* Analytical and bioanalytical chemistry, 2007. **389**(4): p. 1017-1031.
62. Gygi, S.P., et al., *Quantitative analysis of complex protein mixtures using isotope-coded affinity tags.* Nature biotechnology, 1999. **17**(10): p. 994-999.
63. Hsu, J.-L., et al., *Stable-isotope dimethyl labeling for quantitative proteomics.* Analytical chemistry, 2003. **75**(24): p. 6843-6852.
64. Reynolds, K.J., X. Yao, and C. Fenselau, *Proteolytic 18O labeling for comparative proteomics: evaluation of endoprotease Glu-C as the catalytic agent.* Journal of proteome research, 2002. **1**(1): p. 27-33.
65. Ong, S.-E., et al., *Stable isotope labeling by amino acids in cell culture, SILAC, as a simple and accurate approach to expression proteomics.* Molecular & cellular proteomics, 2002. **1**(5): p. 376-386.
66. Ross, P.L., et al., *Multiplexed protein quantitation in Saccharomyces cerevisiae using amine-reactive isobaric tagging reagents.* Molecular & cellular proteomics, 2004. **3**(12): p. 1154-1169.
67. Rifai, N., M.A. Gillette, and S.A. Carr, *Protein biomarker discovery and validation: the long and uncertain path to clinical utility.* Nat Biotechnol, 2006. **24**(8): p. 971-83.
68. Zhou, W., E.F. Petricoin, and C. Longo, *Mass spectrometry-based biomarker discovery*, in *Molecular Profiling*. 2017, Springer. p. 297-311.
69. Nasca, C., et al., *Acetyl-l-carnitine deficiency in patients with major depressive disorder.* Proc Natl Acad Sci U S A, 2018. **115**(34): p. 8627-8632.
70. Kennis, M., et al., *Prospective biomarkers of major depressive disorder: a systematic review and meta-analysis.* Mol Psychiatry, 2020. **25**(2): p. 321-338.
71. Fuller, R.W., K.W. Perry, and B.B. Molloy, *Effect of an uptake inhibitor on serotonin metabolism in rat brain: Studies with 3-(p-trifluoromethylphenoxy)-n-methyl-3-phenylpropylamine (Lilly 110140).* Life Sciences, 1974. **15**(6): p. 1161-1171.
72. *A selective inhibitor of serotonin uptake: Lilly 110140, 3-(p-Trifluoromethylphenoxy)-n-methyl-3-phenylpropylamine.*
73. Wong, D.T., K.W. Perry, and F.P. Bymaster, *Case history: the discovery of fluoxetine hydrochloride (Prozac).* Nat Rev Drug Discov, 2005. **4**(9): p. 764-74.
74. Emslie, G.J., et al., *A double-blind, randomized, placebo-controlled trial of fluoxetine in children and adolescents with depression.* Archives of General Psychiatry, 1997. **54**(11): p. 1031-1037.
75. Mulrow, C.D., et al., *Efficacy of newer medications for treating depression in primary care patients.* The American journal of medicine, 2000. **108**(1): p. 54-64.
76. Fleming, J.E. and D.R. Offord, *Epidemiology of childhood depressive disorders: A critical review.* Journal of the American Academy of Child & Adolescent Psychiatry, 1990. **29**(4): p. 571-580.
77. Costello, E.J., et al., *Prevalence and development of psychiatric disorders in childhood and adolescence.* Archives of general psychiatry, 2003. **60**(8): p. 837-844.
78. Lewinsohn, P.M., P. Rohde, and J.R. Seeley, *Major depressive disorder in older adolescents: prevalence, risk factors, and clinical implications.* Clinical psychology review, 1998. **18**(7): p. 765-794.

79. Kessler, R.C. and E.E. Walters, *Epidemiology of DSM‐III‐R major depression and minor depression among adolescents and young adults in the national comorbidity survey.* Depression and anxiety, 1998. **7**(1): p. 3-14.
80. NIMH. *Major depression*. 2018 [cited 2018 December 13]; Available from: https://www.nimh.nih.gov/health/statistics/major-depression.shtml#part_155031.
81. Williamson, D.E., et al., *A case-control family history study of depression in adolescents.* Journal of the American Academy of Child & Adolescent Psychiatry, 1995. **34**(12): p. 1596-1607.
82. Puig-Antich, J., et al., *A controlled family history study of prepubertal major depressive disorder.* Archives of General Psychiatry, 1989. **46**(5): p. 406-418.
83. Neuman, R.J., et al., *Increased prevalence and earlier onset of mood disorders among relatives of prepubertal versus adult probands.* Journal of the American Academy of Child & Adolescent Psychiatry, 1997. **36**(4): p. 466-473.
84. Jaffee, S.R., et al., *Differences in early childhood risk factors for juvenile-onset and adult-onset depression.* Archives of general psychiatry, 2002. **59**(3): p. 215-222.
85. Ryan, N.D., *Treatment of depression in children and adolescents.* The Lancet, 2005. **366**(9489): p. 933-940.
86. Simeon, J.G., et al., *Adolescent depression: a placebo-controlled fluoxetine treatment study and follow-up.* Progress in Neuro-Psychopharmacology and Biological Psychiatry, 1990. **14**(5): p. 791-795.
87. Emslie, G.J., et al., *Fluoxetine for acute treatment of depression in children and adolescents: a placebo-controlled, randomized clinical trial.* Journal of the American Academy of Child & Adolescent Psychiatry, 2002. **41**(10): p. 1205-1215.
88. Sohel, A.J., M.C. Shutter, and M. Molla, *Fluoxetine.* StatPearls [Internet], 2019.
89. Laje, G., et al., *Genetic markers of suicidal ideation emerging during citalopram treatment of major depression*

Am J Psychiatry, 2007. **164**(10): p. 1530-8.
90. U.S.FDA. *Suicidality in children and adolescents being treated with antidepressant medications.* 2019 [cited 2019 August 12]; Available from: https://www.fda.gov/drugs/postmarket-drug-safety-information-patients-and-providers/suicidality-children-and-adolescents-being-treated-antidepressant-medications.
91. Reeves, R.R. and M.E. Ladner, *Antidepressant-induced suicidality: an update.* CNS Neurosci Ther, 2010. **16**(4): p. 227-34.
92. Goodman, W.K., T.K. Murphy, and E.A. Storch, *Risk of adverse behavioral effects with pediatric use of antidepressants.* Psychopharmacology, 2007. **191**(1): p. 87-96.
93. Erhardt, S., et al., *Connecting inflammation with glutamate agonism in suicidality.* Neuropsychopharmacology, 2013. **38**(5): p. 743-52.
94. Gross, C., et al., *Serotonin 1A receptor acts during development to establish normal anxiety-like behaviour in the adult.* Nature, 2002. **416**(6879): p. 396-400.
95. Tsai, S.-J., *Possible involvement of the BDNF-dependent pathway in treatment-emergent suicidality or decreased response to antidepressants.* Medical hypotheses, 2005. **65**(5): p. 942-946.
96. Amitai, M., et al., *Increased circulatory IL-6 during 8-week fluoxetine treatment is a risk factor for suicidal behaviors in youth.* Brain Behav Immun, 2020. **87**: p. 301-308.

97. Amitai, M., et al., *An increase in IL-6 levels at 6-month follow-up visit is associated with SSRI-emergent suicidality in high-risk children and adolescents treated with fluoxetine.* Eur Neuropsychopharmacol, 2020. **40**: p. 61-69.
98. Wikipedia. *Impulsivity*. 2021; Available from: https://en.wikipedia.org/wiki/Impulsivity.
99. Suicidology, A.A.o. *Risk factors for suicide and suicidal behaviors I*. 2013 [cited 2015 June 26]; Available from: http://suicidology.org/Portals/14/docs/Resources/FactSheets/Risk-Factors_2013.pdf.
100. Bryan, C.J. and M.D. Rudd, *Advances in the assessment of suicide risk.* Journal of clinical psychology, 2006. **62**(2): p. 185-200.
101. Williams, C.L., J.A. Davidson, and I. Montgomery, *Impulsive suicidal behavior.* Journal of Clinical Psychology, 1980. **36**(1): p. 90-94.
102. Brent, D.A. and N. Melhem, *Familial transmission of suicidal behavior.* Psychiatric Clinics of North America, 2008. **31**(2): p. 157-177.
103. Diaconu, G. and G. Turecki, *Family history of suicidal behavior predicts impulsive–aggressive behavior levels in psychiatric outpatients.* Journal of affective disorders, 2009. **113**(1-2): p. 172-178.
104. Gvion, Y. and A. Apter, *Aggression, impulsivity, and suicide behavior: a review of the literature.* Archives of suicide research, 2011. **15**(2): p. 93-112.
105. Kim, B. and H.I. Im, *The role of the dorsal striatum in choice impulsivity.* Annals of the New York Academy of Sciences, 2019. **1451**(1): p. 92-111.
106. Cho, S.S., et al., *Continuous theta burst stimulation of right dorsolateral prefrontal cortex induces changes in impulsivity level.* Brain stimulation, 2010. **3**(3): p. 170-176.
107. Steinbeis, N., B.C. Bernhardt, and T. Singer, *Impulse control and underlying functions of the left DLPFC mediate age-related and age-independent individual differences in strategic social behavior.* Neuron, 2012. **73**(5): p. 1040-1051.
108. Banfield, J.F., et al., *The cognitive neuroscience of self-regulation.* 2004.
109. Kiehl, K.A., P.F. Liddle, and J.B. Hopfinger, *Error processing and the rostral anterior cingulate: An event‐related fMRI study.* Psychophysiology, 2000. **37**(2): p. 216-223.
110. Carter, C.S. and V. Van Veen, *Anterior cingulate cortex and conflict detection: an update of theory and data.* Cognitive, Affective, & Behavioral Neuroscience, 2007. **7**(4): p. 367-379.
111. Worlein, J.M., *Nonhuman primate models of depression: effects of early experience and stress.* ILAR J, 2014. **55**(2): p. 259-73.
112. Reite, M. and R. Short, *Maternal separation studies: rationale and methodological considerations.* Progress in clinical and biological research, 1983. **131**: p. 219-253.
113. Golub, M.S., et al., *Bone growth in juvenile rhesus monkeys is influenced by 5HTTLPR polymorphisms and interactions between 5HTTLPR polymorphisms and fluoxetine.* Bone, 2015. **79**: p. 162-9.
114. He, Y., et al., *Identifying individual differences of fluoxetine response in juvenile rhesus monkeys by metabolite profiling.* Transl Psychiatry, 2014. **4**: p. e478.
115. Su, S.Y., et al., *Peripheral fibroblast metabolic pathway alterations in juvenile rhesus monkeys undergoing long-term fluoxetine administration.* Eur Neuropsychopharmacol, 2016. **26**(7): p. 1110-8.
116. Golub, M.S., C.E. Hogrefe, and A.M. Bulleri, *Regulation of emotional response in juvenile monkeys treated with fluoxetine: MAOA interactions.* Eur

Neuropsychopharmacol, 2016. **26**(12): p. 1920-1929.
117. Paxinos, G., X.-F. Huang, and A.W. Toga, *The rhesus monkey brain in stereotaxic coordinates.* 2000.
118. Plubell, D.L., et al., *Extended multiplexing of tandem mass tags (TMT) labeling reveals age and high fat diet specific proteome changes in mouse epididymal adipose tissue.* Molecular & Cellular Proteomics, 2017. **16**(5): p. 873-890.
119. Johnson, W.E., C. Li, and A. Rabinovic, *Adjusting batch effects in microarray expression data using empirical Bayes methods.* Biostatistics, 2007. **8**(1): p. 118-127.
120. Ritchie, M.E., et al., *limma powers differential expression analyses for RNA-sequencing and microarray studies.* Nucleic acids research, 2015. **43**(7): p. e47-e47.
121. Johnson, E.C., et al., *Large-scale proteomic analysis of Alzheimer's disease brain and cerebrospinal fluid reveals early changes in energy metabolism associated with microglia and astrocyte activation.* Nature medicine, 2020. **26**(5): p. 769-780.
122. Blume-Jensen, P. and T. Hunter, *Oncogenic kinase signalling.* Nature, 2001. **411**(6835): p. 355-365.
123. Rikova, K., et al., *Global survey of phosphotyrosine signaling identifies oncogenic kinases in lung cancer.* Cell, 2007. **131**(6): p. 1190-1203.
124. Zanivan, S., et al., *In vivo SILAC-based proteomics reveals phosphoproteome changes during mouse skin carcinogenesis.* Cell reports, 2013. **3**(2): p. 552-566.
125. Eidenmüller, J., et al., *Phosphorylation-mimicking glutamate clusters in the proline-rich region are sufficient to simulate the functional deficiencies of hyperphosphorylated tau protein.* Biochemical Journal, 2001. **357**(3): p. 759-767.
126. Danielsson, A., et al., *Attenuation of insulin-stimulated insulin receptor substrate-1 serine 307 phosphorylation in insulin resistance of type 2 diabetes.* Journal of biological chemistry, 2005. **280**(41): p. 34389-34392.
127. Pajer, K., et al., *Discovery of blood transcriptomic markers for depression in animal models and pilot validation in subjects with early-onset major depression.* Transl Psychiatry, 2012. **2**: p. e101.
128. Simanshu, D.K., D.V. Nissley, and F. McCormick, *RAS proteins and their regulators in human disease.* Cell, 2017. **170**(1): p. 17-33.
129. Khawaja, X., et al., *Proteomic analysis of protein changes developing in rat hippocampus after chronic antidepressant treatment: implications for depressive disorders and future therapies.* Journal of neuroscience research, 2004. **75**(4): p. 451-460.
130. Dwivedi, Y., et al., *Differential and brain region–specific regulation of Rap-1 and Epac in depressed suicide victims.* Archives of general psychiatry, 2006. **63**(6): p. 639-648.
131. Zheng, S., et al., *NMDA-induced neuronal survival is mediated through nuclear factor IA in mice.* The Journal of clinical investigation, 2010. **120**(7): p. 2446-2456.
132. Nagase, T., et al., *Prediction of the coding sequences of unidentified human genes. XVI. The complete sequences of 150 new cDNA clones from brain which code for large proteins in vitro.* DNA research, 2000. **7**(1): p. 65-73.
133. Mikhail, F.M., et al., *Clinically relevant single gene or intragenic deletions encompassing critical neurodevelopmental genes in patients with developmental delay, mental retardation, and/or autism spectrum disorders.* American journal of medical genetics Part A, 2011. **155**(10): p. 2386-2396.
134. Sun, Y., et al., *Cofilin 2 in serum as a novel biomarker for Alzheimer's disease in*

Han Chinese. Frontiers in aging neuroscience, 2019. **11**: p. 214.
135. Yamada, M. and T. Higuchi, *Functional genomics and depression research: Beyond the monoamine hypothesis.* European neuropsychopharmacology, 2002. **12**(3): p. 235-244.
136. Hensley, K., et al., *Collapsin response mediator protein-2: an emerging pathologic feature and therapeutic target for neurodisease indications.* Molecular neurobiology, 2011. **43**(3): p. 180-191.
137. Piubelli, C., et al., *Escitalopram modulates neuron-remodelling proteins in a rat gene–environment interaction model of depression as revealed by proteomics. Part I: genetic background.* International Journal of Neuropsychopharmacology, 2011. **14**(6): p. 796-833.
138. Sokolowski, M., J. Wasserman, and D. Wasserman, *An overview of the neurobiology of suicidal behaviors as one meta-system.* Molecular psychiatry, 2015. **20**(1): p. 56-71.
139. Kekesi, K.A., et al., *Altered functional protein networks in the prefrontal cortex and amygdala of victims of suicide.* PloS one, 2012. **7**(12): p. e50532.
140. Yang, Y., et al., *Proteomics reveals energy and glutathione metabolic dysregulation in the prefrontal cortex of a rat model of depression.* Neuroscience, 2013. **247**: p. 191-200.
141. PhosphoSitePlus. *Thr509 of CRMP-2(human).* 2021; Available from: https://www.phosphosite.org/siteAction.action?id=3198.
142. Wen, G., et al., *Regulation of tau protein on the antidepressant effects of ketamine in the chronic unpredictable mild stress model.* Frontiers in psychiatry, 2019. **10**: p. 287.
143. Dixit, R., et al., *Differential regulation of dynein and kinesin motor proteins by tau.* Science, 2008. **319**(5866): p. 1086-1089.
144. Lopes, S., et al., *Tau protein is essential for stress-induced brain pathology.* Proceedings of the National Academy of Sciences, 2016. **113**(26): p. E3755-E3763.
145. Yang, C., et al., *Changes in tau phosphorylation levels in the hippocampus and frontal cortex following chronic stress.* Brazilian Journal of Medical and Biological Research, 2014. **47**(3): p. 237-244.
146. Mertins, P., et al., *Proteogenomics connects somatic mutations to signalling in breast cancer.* Nature, 2016. **534**(7605): p. 55-62.
147. Zhou, B., et al., *Oligodendrocyte lineage cells and depression.* Molecular psychiatry, 2020: p. 1-15.
148. Pantazatos, S.P., et al., *Whole-transcriptome brain expression and exon-usage profiling in major depression and suicide: evidence for altered glial, endothelial and ATPase activity.* Molecular psychiatry, 2017. **22**(5): p. 760-773.
149. Hagemeyer, N., et al., *A myelin gene causative of a catatonia‐depression syndrome upon aging.* EMBO molecular medicine, 2012. **4**(6): p. 528-539.
150. Mann, J.J., et al., *Anxiety in major depression and cerebrospinal fluid free gamma‐aminobutyric acid.* Depression and anxiety, 2014. **31**(10): p. 814-821.
151. Kertes, D.A., et al., *Neurotransmitter and neuromodulator genes associated with a history of depressive symptoms in individuals with alcohol dependence.* Alcoholism: Clinical and Experimental Research, 2011. **35**(3): p. 496-505.
152. Murphy, T.M., et al., *Risk and protective genetic variants in suicidal behaviour: association with SLC1A2, SLC1A3, 5-HTR1B & NTRK2 polymorphisms.* Behavioral and Brain Functions, 2011. **7**(1): p. 1-9.
153. Yin, H., et al., *A pilot integrative genomics study of GABA and glutamate*

neurotransmitter systems in suicide, suicidal behavior, and major depressive disorder. American Journal of Medical Genetics Part B: Neuropsychiatric Genetics, 2016. **171**(3): p. 414-426.
154. Lee, R., F. Petty, and E.F. Coccaro, *Cerebrospinal fluid GABA concentration: relationship with impulsivity and history of suicidal behavior, but not aggression, in human subjects.* J Psychiatr Res, 2009. **43**(4): p. 353-9.
155. Baldessarini, R.J., L. Tondo, and J. Hennen, *Lithium treatment and suicide risk in major affective disorders: update and new findings.* Database of Abstracts of Reviews of Effects (DARE): Quality-assessed Reviews [Internet], 2003.
156. Bjork, J.M., et al., *Plasma GABA levels correlate with aggressiveness in relatives of patients with unipolar depressive disorder.* Psychiatry research, 2001. **101**(2): p. 131-136.
157. Choudary, P.V., et al., *Altered cortical glutamatergic and GABAergic signal transmission with glial involvement in depression.* Proceedings of the National Academy of Sciences, 2005. **102**(43): p. 15653-15658.
158. Kim, J.H. and R. Richardson, *A developmental dissociation of context and GABA effects on extinguished fear in rats.* Behavioral neuroscience, 2007. **121**(1): p. 131.
159. Tochigi, M., et al., *Gene expression profiling of major depression and suicide in the prefrontal cortex of postmortem brains.* Neuroscience research, 2008. **60**(2): p. 184-191.
160. Sequeira, A., et al., *Global brain gene expression analysis links glutamatergic and GABAergic alterations to suicide and major depression.* PloS one, 2009. **4**(8): p. e6585.
161. Callery, P.S. and L.A. Geelhaar, *1‐Piperideine as an In Vivo Precursor of the γ‐Aminobutyric Acid Homologue 5‐Aminopentanoic Acid.* Journal of neurochemistry, 1985. **45**(3): p. 946-948.
162. Gören, M.Z., et al., *Fluoxetine partly exerts its actions through GABA: a neurochemical evidence.* Neurochemical research, 2007. **32**(9): p. 1559-1565.
163. Nosengo, N., *New tricks for old drugs.* Nature, 2016. **534**(7607): p. 314-316.
164. Pushpakom, S., et al., *Drug repurposing: progress, challenges and recommendations.* Nat Rev Drug Discov, 2019. **18**(1): p. 41-58.
165. Paoletti, P. and J. Neyton, *NMDA receptor subunits: function and pharmacology.* Curr Opin Pharmacol, 2007. **7**(1): p. 39-47.
166. Anis, N.A., et al., *The dissociative anaesthetics, ketamine and phencyclidine, selectively reduce excitation of central mammalian neurones by N-methyl-aspartate.* Br J Pharmacol, 1983. **79**(2): p. 565-75.
167. Domino, E.F. and D.S. Warner, *Taming the ketamine tiger.* The Journal of the American Society of Anesthesiologists, 2010. **113**(3): p. 678-684.
168. Ebert, B., et al., *Norketamine, the main metabolite of ketamine, is a non-competitive NMDA receptor antagonist in the rat cortex and spinal cord.* European Journal of Pharmacology, 1997. **333**(1): p. 99-104.
169. Sofia, R. and J. Harakal, *Evaluation of ketamine HCl for anti-depressant activity.* Archives internationales de pharmacodynamie et de therapie, 1975. **214**(1): p. 68.
170. Autry, A.E., et al., *NMDA receptor blockade at rest triggers rapid behavioural antidepressant responses.* Nature, 2011. **475**(7354): p. 91-95.
171. Wedzony, K., V. Klimek, and G. Nowak, *Rapid down-regulation of beta-adrenergic receptors evoked by combined forced swimming test and CGP 37849--a competitive antagonist of NMDA receptors.* Polish journal of pharmacology, 1995. **47**(6): p. 537-540.
172. Layer, R.T., et al., *Antidepressant-like actions of the polyamine site NMDA*

antagonist, eliprodil (SL-82.0715). Pharmacology Biochemistry and Behavior, 1995. **52**(3): p. 621-627.
173. Papp, M. and E. Moryl, *Antidepressant activity of non-competitive and competitive NMDA receptor antagonists in a chronic mild stress model of depression.* European journal of pharmacology, 1994. **263**(1-2): p. 1-7.
174. Papp, M. and E. Moryl, *New evidence for the antidepressant activity of MK-801, a non-competitive antagonist of NMDA receptors.* Polish journal of pharmacology, 1993. **45**(5-6): p. 549.
175. Maj, J., et al., *Effects of MK-801 and antidepressant drugs in the forced swimming test in rats.* European Neuropsychopharmacology, 1992. **2**(1): p. 37-41.
176. Trullas, R. and P. Skolnick, *Functional antagonists at the NMDA receptor complex exhibit antidepressant actions.* European journal of pharmacology, 1990. **185**(1): p. 1-10.
177. Berman, R.M., et al., *Antidepressant effects of ketamine in depressed patients.* Biological psychiatry, 2000. **47**(4): p. 351-354.
178. Zarate, C.A., Jr., et al., *A randomized trial of an N-methyl-D-aspartate antagonist in treatment-resistant major depression.* Arch Gen Psychiatry, 2006. **63**(8): p. 856-64.
179. Price, R.B., et al., *Effects of intravenous ketamine on explicit and implicit measures of suicidality in treatment-resistant depression.* Biol Psychiatry, 2009. **66**(5): p. 522-6.
180. Murrough, J.W., et al., *Ketamine for rapid reduction of suicidal ideation: a randomized controlled trial.* Psychological Medicine, 2015. **45**(16): p. 3571-3580.
181. Newport, D.J., et al., *Ketamine and Other NMDA Antagonists: Early Clinical Trials and Possible Mechanisms in Depression.* Am J Psychiatry, 2015. **172**(10): p. 950-66.
182. Kishimoto, T., et al., *Single-dose infusion ketamine and non-ketamine N-methyl-d-aspartate receptor antagonists for unipolar and bipolar depression: a meta-analysis of efficacy, safety and time trajectories.* Psychol Med, 2016. **46**(7): p. 1459-72.
183. Grunebaum, M.F., et al., *Ketamine for Rapid Reduction of Suicidal Thoughts in Major Depression: A Midazolam-Controlled Randomized Clinical Trial.* Am J Psychiatry, 2018. **175**(4): p. 327-335.
184. Zhang, J.C., S.X. Li, and K. Hashimoto, *R (-)-ketamine shows greater potency and longer lasting antidepressant effects than S (+)-ketamine.* Pharmacol Biochem Behav, 2014. **116**: p. 137-41.
185. Yang, C., et al., *R-ketamine: a rapid-onset and sustained antidepressant without psychotomimetic side effects.* Transl Psychiatry, 2015. **5**: p. e632.
186. Zanos, P., et al., *NMDAR inhibition-independent antidepressant actions of ketamine metabolites.* Nature, 2016. **533**(7604): p. 481-6.
187. Fukumoto, K., et al., *Antidepressant Potential of (R)-Ketamine in Rodent Models: Comparison with (S)-Ketamine.* J Pharmacol Exp Ther, 2017. **361**(1): p. 9-16.
188. Yang, C., et al., *Loss of parvalbumin-immunoreactivity in mouse brain regions after repeated intermittent administration of esketamine, but not R-ketamine.* Psychiatry Res, 2016. **239**: p. 281-3.
189. Tian, Z., et al., *Expression of heat shock protein HSP-70 in the retrosplenial cortex of rat brain after administration of (R,S)-ketamine and (S)-ketamine, but not (R)-ketamine.* Pharmacol Biochem Behav, 2018. **172**: p. 17-21.
190. Chang, L., et al., *Comparison of antidepressant and side effects in mice after intranasal administration of (R,S)-ketamine, (R)-ketamine, and (S)-ketamine.*

Pharmacol Biochem Behav, 2019. **181**: p. 53-59.
191. Zanos, P., et al., *Ketamine and Ketamine Metabolite Pharmacology: Insights into Therapeutic Mechanisms.* Pharmacol Rev, 2018. **70**(3): p. 621-660.
192. Hashimoto, K., *Rapid‐acting antidepressant ketamine, its metabolites and other candidates: A historical overview and future perspective.* Psychiatry and Clinical Neurosciences, 2019. **73**(10): p. 613-627.
193. Pham, T.H., et al., *Common neurotransmission recruited in (R, S)-ketamine and (2R, 6R)-hydroxynorketamine–induced sustained antidepressant-like effects.* Biological Psychiatry, 2018. **84**(1): p. e3-e6.
194. Fukumoto, K., et al., *Activity-dependent brain-derived neurotrophic factor signaling is required for the antidepressant actions of (2R,6R)-hydroxynorketamine.* Proc Natl Acad Sci U S A, 2019. **116**(1): p. 297-302.
195. Yao, N., et al., *Ketamine and its metabolite (2R,6R)-hydroxynorketamine induce lasting alterations in glutamatergic synaptic plasticity in the mesolimbic circuit.* Mol Psychiatry, 2018. **23**(10): p. 2066-2077.
196. Shaffer, C.L., et al., *Pharmacological evaluation of clinically relevant concentrations of (2R, 6R)-hydroxynorketamine.* Neuropharmacology, 2019. **153**: p. 73-81.
197. Nations, K.R., et al., *Examination of Org 26576, an AMPA receptor positive allosteric modulator, in patients diagnosed with major depressive disorder: an exploratory, randomized, double-blind, placebo-controlled trial.* Journal of Psychopharmacology, 2012. **26**(12): p. 1525-1539.
198. Suzuki, K., et al., *Effects of a ketamine metabolite on synaptic NMDAR function.* Nature, 2017. **546**(7659): p. E1-E3.
199. Zanos, P., et al., *(2R,6R)-hydroxynorketamine exerts mGlu2 receptor-dependent antidepressant actions.* Proc Natl Acad Sci U S A, 2019. **116**(13): p. 6441-6450.
200. Wray, N.H., et al., *NMDAR-independent, cAMP-dependent antidepressant actions of ketamine.* Mol Psychiatry, 2019. **24**(12): p. 1833-1843.
201. Yang, C., et al., *(R)-Ketamine Shows Greater Potency and Longer Lasting Antidepressant Effects Than Its Metabolite (2R,6R)-Hydroxynorketamine.* Biol Psychiatry, 2017. **82**(5): p. e43-e44.
202. Shirayama, Y. and K. Hashimoto, *Lack of Antidepressant Effects of (2R,6R)-Hydroxynorketamine in a Rat Learned Helplessness Model: Comparison with (R)-Ketamine.* Int J Neuropsychopharmacol, 2018. **21**(1): p. 84-88.
203. Xiong, Z., et al., *Beneficial effects of (R)-ketamine, but not its metabolite (2R, 6R)-hydroxynorketamine, in the depression-like phenotype, inflammatory bone markers, and bone mineral density in a chronic social defeat stress model.* Behavioural brain research, 2019. **368**: p. 111904.
204. Zanos, P., et al., *(R)-Ketamine exerts antidepressant actions partly via conversion to (2R,6R)-hydroxynorketamine, while causing adverse effects at sub-anaesthetic doses.* Br J Pharmacol, 2019. **176**(14): p. 2573-2592.
205. Shirayama, Y. and K. Hashimoto, *Effects of a single bilateral infusion of R-ketamine in the rat brain regions of a learned helplessness model of depression.* European archives of psychiatry and clinical neuroscience, 2017. **267**(2): p. 177-182.
206. Chaki, S. and J.I. Yamaguchi, *Now is the time for (2R,6R)-hydroxynorketamine to be viewed independently from its parent drug.* Pharmacol Biochem Behav, 2018. **175**: p. 24-26.
207. Speers, A.E. and B.F. Cravatt, *Chemical strategies for activity-based proteomics.* Chembiochem, 2004. **5**(1): p. 41-7.

208. Wang, S., et al., *Advanced Activity-Based Protein Profiling Application Strategies for Drug Development.* Front Pharmacol, 2018. **9**: p. 353.
209. Xu, J., et al., *Applications of Activity-Based Protein Profiling (ABPP) and Bioimaging in Drug Discovery.* Chem Asian J, 2020. **15**(1): p. 34-41.
210. Krysiak, J. and R. Breinbauer, *Activity-based protein profiling for natural product target discovery*, in *Activity-Based Protein Profiling*. 2011, Springer. p. 43-84.
211. Lomenick, B., et al., *Target identification using drug affinity responsive target stability (DARTS).* Proc Natl Acad Sci U S A, 2009. **106**(51): p. 21984-9.
212. Lomenick, B., et al., *Target identification using drug affinity responsive target stability (DARTS).* Curr Protoc Chem Biol, 2011. **3**(4): p. 163-180.
213. Pai, M.Y., et al., *Drug affinity responsive target stability (DARTS) for small-molecule target identification.* Methods Mol Biol, 2015. **1263**: p. 287-98.
214. Chang, J., Y. Kim, and H.J. Kwon, *Advances in identification and validation of protein targets of natural products without chemical modification.* Nat Prod Rep, 2016. **33**(5): p. 719-30.
215. West, G.M., et al., *Quantitative proteomics approach for identifying protein-drug interactions in complex mixtures using protein stability measurements.* Proc Natl Acad Sci U S A, 2010. **107**(20): p. 9078-82.
216. Meng, H., R. Ma, and M.C. Fitzgerald, *Chemical Denaturation and Protein Precipitation Approach for Discovery and Quantitation of Protein-Drug Interactions.* Anal Chem, 2018. **90**(15): p. 9249-9255.
217. Zhang, X., et al., *Solvent-Induced Protein Precipitation for Drug Target Discovery on the Proteomic Scale.* Anal Chem, 2020. **92**(1): p. 1363-1371.
218. Martinez Molina, D., et al., *Monitoring drug target engagement in cells and tissues using the cellular thermal shift assay.* Science, 2013. **341**(6141): p. 84-7.
219. Savitski, M.M., et al., *Tracking cancer drugs in living cells by thermal profiling of the proteome.* Science, 2014. **346**(6205): p. 1255784.
220. Ball, K.A., et al., *An isothermal shift assay for proteome scale drug-target identification.* Commun Biol, 2020. **3**(1): p. 75.
221. Nagasawa, I., et al., *Identification of a Small Compound Targeting PKM2-Regulated Signaling Using 2D Gel Electrophoresis-Based Proteome-wide CETSA.* Cell Chem Biol, 2020. **27**(2): p. 186-196 e4.
222. Feng, Y., et al., *Global analysis of protein structural changes in complex proteomes.* Nat Biotechnol, 2014. **32**(10): p. 1036-44.
223. Ong, S.-E., et al., *Identifying the proteins to which small-molecule probes and drugs bind in cells.* Proceedings of the National Academy of Sciences, 2009. **106**(12): p. 4617-4622.
224. Smith, C., *Drug target validation: Hitting the target.* Nature, 2003. **422**(6929): p. 342-345.
225. Salgado, J.V. and G. Sandner, *A critical overview of animal models of psychiatric disorders: challenges and perspectives.* Brazilian Journal of Psychiatry, 2013. **35**: p. S77-S81.
226. Aleksandrova, L.R., Y.T. Wang, and A.G. Phillips, *Hydroxynorketamine: Implications for the NMDA Receptor Hypothesis of Ketamine's Antidepressant Action.* Chronic Stress (Thousand Oaks), 2017. **1**.
227. Kavalali, E.T. and L.M. Monteggia, *The Ketamine Metabolite 2R,6R-Hydroxynorketamine Blocks NMDA Receptors and Impacts Downstream Signaling Linked to Antidepressant Effects.* Neuropsychopharmacology, 2018. **43**(1): p. 221-222.
228. Hu, J., W. Duan, and Y. Liu, *Ketamine inhibits aerobic glycolysis in colorectal*

cancer cells by blocking the NMDA receptor ‐ CaMK II ‐ c ‐ Myc pathway. Clinical and Experimental Pharmacology and Physiology, 2020. **47**(5): p. 848-856.
229. Park, D.I., et al., *Paroxetine binding and activation of phosphofructokinase implicates energy metabolism in antidepressant mode of action.* J Psychiatr Res, 2020. **129**: p. 8-14.
230. Weckmann, K., et al., *Ketamine's antidepressant effect is mediated by energy metabolism and antioxidant defense system.* Scientific reports, 2017. **7**(1): p. 1-11.
231. Z Reus, G., et al., *Ketamine treatment partly reverses alterations in brain derived-neurotrophic factor, oxidative stress and energy metabolism parameters induced by an animal model of depression.* Current neurovascular research, 2015. **12**(1): p. 73-84.
232. Almas, A., et al., *Association of Catechol-O-methyltransferase (COMT Val 158 Met) with future risk of cardiovascular disease in depressed individuals-a Swedish population-based cohort study.* BMC medical genetics, 2018. **19**(1): p. 1-7.
233. Di Chiara, G., et al., *Dopamine and drug addiction: the nucleus accumbens shell connection.* Neuropharmacology, 2004. **47**: p. 227-241.
234. Tunbridge, E.M., P.J. Harrison, and D.R. Weinberger, *Catechol-o-methyltransferase, cognition, and psychosis: Val158Met and beyond.* Biological psychiatry, 2006. **60**(2): p. 141-151.
235. Fava, M., et al., *Open study of the catechol-O-methyltransferase inhibitor tolcapone in major depressive disorder.* Journal of clinical psychopharmacology, 1999. **19**(4): p. 329-335.
236. Martins-de-Souza, D., et al., *Identification of proteomic signatures associated with depression and psychotic depression in post-mortem brains from major depression patients.* Translational psychiatry, 2012. **2**(3): p. e87-e87.
237. Guo, L., et al., *microRNA-15b contributes to depression-like behavior in mice by affecting synaptic protein levels and function in the nucleus accumbens.* Journal of Biological Chemistry, 2020. **295**(20): p. 6831-6848.

Acknowledgements

Throughout conducting the PhD projects as well as writing this dissertation I have received a great deal of support and assistance.

First of all, I would like to thank my supervisor, Prof. Dr. Christoph Turck, for offering me the valuable opportunity to pursue my PhD degree at the Max Planck Institute of Psychiatry and enlightening me with insightful advice and invaluable experience during the 4-year academic journey. It would be totally unrealistic for me to overcome all the difficulties encountered all the way without his continuous support and the greatest patience. I also profoundly appreciate his guidance in non-scientific field that really helps me adapt to life in Germany.

My gratitude extends to my thesis advisory committee members, Dr. Yaoyang Zhang from Chinese Academy of Sciences, Prof. Dr. Dr. Walter Zieglgänsberger from Max Planck Institute of Psychiatry and Dr. Dietmar Martin from Department of Biochemistry at LMU, for their inspiring feedback during the entire process of my PhD study. Special thanks to Dr. Mari Golub for providing me with the macaque brain tissue and behavior data.

I am also very grateful for the support by Dr. Dongmei Zhang from the LMU International Office responsible for the coordination of LMU-CSC program.

Additionally, I would express my gratitude to all my colleagues and all the staff of Max Planck Institute of Psychiatry for the long-term company and assistance. @Giuseppina: I really enjoy having discussions with her about both academic questions and life. I am glad to become a friend of Edward, her smart and cute son. @Bozo: thanks for all support and convenience he provided in both work and life. Whenever I have trouble, I always tell myself “better call Bozo!”. @Karin: people in our lab come and go but we two have been always here together. She is like my younger sister and I am so grateful for receiving so much assistance and encouragement from her. @Jinqiu: my little brother, I would thank him without reservation for assisting me with my lab work and sharing with me some life experience of being a Chinese living in Germany. @Dongik: special thanks to him for his guide when I was fresh at Max Planck Institute of Psychiatry that helped me quickly initiate my work and life. I have been so appreciative about his pioneering work prior to my thesis projects including CETSA setup and macaque sample collection. @Frederik:

apart from the assistance from the lab side, I would especially thank him for setting a good example for a talented, precise and strict research scientist. @All my dear colleagues who worked in our lab for a short time since I arrived including Michaela, Yijing, Christina, Anton, Ezgi and Cristina: I would express my special gratitude to them for their support and thank them for bringing light to my life and I feel so honored to be able to work with them.

There is nothing to express my infinite gratitude but a sincere “thank you” to my housemates and friends I met in Munich as well as those keeping in touch with me remotely in Berlin and China. Their company has granted me a feeling of being at home. I really appreciate for meeting them, which infuses a gleam of brilliance to my tough scientific research work.

Last but not least, I would like to thank my family including my parents and my girlfriend, for their remote support and great patience. I would not have got to where I am now without them. They are the source of motivation that keeps improving myself and makes me become better and better.

Finally, I would love to thank everyone who has been part of my life including people mentioned above. I cannot wait anymore to move forward to explore new challenges with all their expectations.